UNIVERSITÀ DEGLI STUDI DI SALERNO

DIFARMA

UNIVERSITÀ DEGLI STUDI DI SALERNO

Dipartimento di Farmacia

PhD Program

in **Drug Discovery and Development**

XXXV Cycle — Academic Year 2022/2023

PhD Thesis in

A multi-disciplinary approach based on mass spectrometry to disclose the potential of phytoextracts as natural cosmetics

Candidate

Sara Ceccacci

Tutor

Prof. *Maria Chiara Monti*

PhD Program Coordinator: Prof. Dr. *Gianluca Sbardella*

Firmato digitalmente da: GIANLUCA SBARDELLA
Luogo: Fisciano
Data: 07/02/2023 13:17:23

The PhD scholarship was co-financed with resources from Programma Operativo Complementare Ricerca e Innovazione 2014-2020, Asse I "Capitale Umano", Azione I.1 "Dottorati Innovativi con caratterizzazione Industriale".

Table of contents

Abstract

Plant cells represent a valid source of cosmetic ingredients since their extracts can be considered bio-sustainable, contaminant-free and standardized secondary metabolites mixtures (Barbulova et al., 2014). This PhD project has met the interest of Arterra Bioscience S.p.A in performing a broad chemical and biological characterization of some plant cell extracts in the prospective to exploit them as cosmetic ingredients. In particular, we focused on the hydrophilic extract of *Oenothera biennis* cells (ObHEx) and on the hydroethanolic extract of *Jasminum sambac* cells (JasHEx). The mass spectrometry-based chemical characterization was performed using Global Natural Products Social Molecular Networking (GNPS)(M. Wang et al., 2016) as bioinformatics tool for data organization and annotation. The biological activity of the extracts was evaluated by a panel of *in vitro* (global proteomics analysis and cell-based assays) and *ex vivo* experiments.

Interesting secondary metabolites were identified in ObHEx: they belong to lignans (salvadoraside and liriodendrin) and triterpenes (myrianthic acid, arjunolic acid, asiatic acid and hederagenin), some of which previously associated with pro-collagen I production in human fibroblasts (Bonte et al., 1994; Farwick et al., 2014). Indeed, bioassays revealed that ObHEx is able, by increasing Myosin light chain kinase (MYLK) gene expression, to promote matrix collagen contraction, actin polymerization and the production of extracellular matrix proteins (Ceccacci et al., 2021). Moreover, global proteomics experiments, performed during my period as visiting PhD student at the Proteomics Platform of the INSERM US24, proved a pro-mitotic mechanism of action of ObHEx on senescent human dermal fibroblasts: it

stimulates the re-entry into cell cycle of senescent cells via increase of mitotic protein expression (Ceccacci et al., 2022b).

JasHEx is principally composed by phenolic acid derivatives, lignans (secoisolariciresinol, nortrachelogenin and matairesinol) and triterpenes (arjunolic acid, asiatic acid, maslinic acid, oleanolic acid and ursolic acid) (Ceccacci et al., 2022a). Biological experiments, carried out during my research period at Arterra Bioscience SpA, proved that JasHEx is able to reduce cytosolic reactive oxygen species production in stressed keratinocytes. It also showed anti-glycation activity and an extracellular matrix booster effect, by increasing collagen type I synthesis. In particular, the antioxidant properties of JasHEx were related not only to its free radical scavenging and metal chelating activities, but also to the enhancement of Nrf2/ARE pathway. This latter also explains JasHEx anti-inflammatory activity which decreased nitric oxide levels in LPS stimulated macrophages.

Thus, on the basis of these results, both extracts can be considered as powerful cosmetic bioactive ingredients to counteract skin aging.

SECTION 1

INTRODUCTION

Section 1 – Chapter 1

Plant cell cultures as source of bioactive cosmetic ingredients

1.1.1 Natural Products (NPs) in cosmetics

Plants synthesize an array of Natural Products (NPs), termed secondary metabolites, in order to defend themselves against exogenous (a)biotic stresses and to fulfil important physiological tasks (Guerriero et al., 2018). Many of these compounds show a broad spectrum of biological activities in humans: secondary metabolites, in fact, exhibiting a wide range of pharmacophores and a high degree of stereochemistry, have multi-ligandable properties and trigger many biological effects (Harvey et al., 2015). Recently, the demand for NPs, especially phytochemicals, is growing in cosmetics: companies are replacing synthetic chemicals with natural ingredients, partly because of a move towards sustainable raw materials, partly because of the requirements of consumers that perceive NPs as healthier, organic and ecological (Antignac et al., 2011). Consequently, this is leading to an increased pressure on the production of these molecules and particularly of plant extracts, which often are more effective than isolated compounds, due to the synergy between the different constituents (Caesar and Cech, 2019).

1.1.2 Advantages of plant cell cultures for NPs synthesis

Extraction from plants is the typical strategy to obtain many NPs (Ochoa-Villarreal et al., 2015). However, the cultivation on an industrial scale together with the difficulty to optimize the cropping techniques and the extraction methods makes the whole process economically unsustainable (Barbulova et al., 2014). A valid alternative to plants as source of bioactive cosmetic ingredients, is represented by plant cell cultures that, in fact, offer several advantages: i) high sustainability of the production process, since no agricultural land is needed; ii) continuous supply of NPs without geographical, season and plant reproductive cycle dependence; iii) no risks of contamination by pathogens, environmental pollutants and agrochemical residues; iv) standardized growing conditions that allow to obtain higher and more reproducible rates of biomass and metabolite yield; v) high versatility, since the concentration of compounds can be optimized by changing culturing conditions; vi) easier and less time consuming extraction protocols, reducing the need of aggressive solvents. Thus, to date, different types of cosmetic active ingredients have been developed and produced from plant cell cultures, such as the whole lysate of *Malus domesticus* cell suspension culture, able to revert senescence signs in fibroblasts, the cell wall preparation of *Nicotiana sylvestris* with strong anti-ageing properties by increasing collagen I levels, and the hydrosoluble cell culture extract of *Rubus ideaus*, endowed with high anti-inflammatory activity (Barbulova et al., 2014).

1.1.3 Dedifferentiated plant cells (DDCs) cultures

Only plant stem cells, localized in specialized regions (meristems) present at the tip of roots, shoots and in the vascular tissue, are capable of cell division in *planta* (Ochoa-

Villarreal et al., 2015). Mitotically active planta cell cultures have most frequently depended upon a process of dedifferentiation (Figure 1.1) (Partap et al., 2022). It is a process by which mature or specialized cells lose their differentiate character and acquire a 'stem cell-like' state that confers totipotency. Plant cell culture is initiated from plant explant (Fehér, 2019). As a result of wounding, the cells on the surface of the explant expand their volume, start to divide and form a callus of dedifferentiated cells (DDCs). This is, then, transferred to a liquid medium to create suspension cultures which are subsequently incubated under agitation and controlled temperature to produce the desired NPs (Barbulova et al., 2014; Ochoa-Villarreal et al., 2015; Partap et al., 2022).

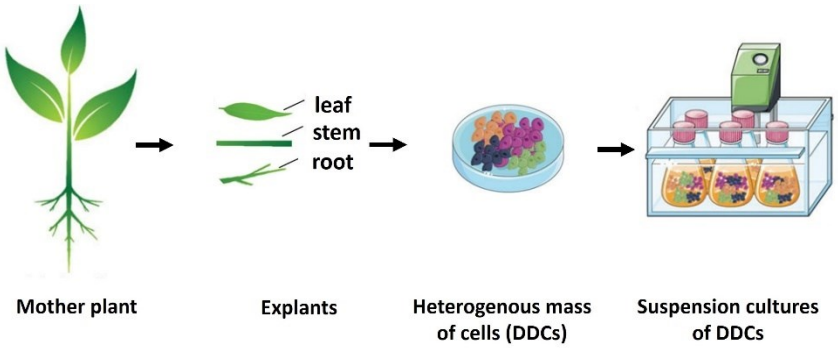

Figure 1.1 *Schematic representation of bioprocess development for dedifferentiated cells (DDCs) cultures (Adapted from Partap et al., 2022).*

Although DDCs cultures certainly represent a valuable source of extracts with proven cosmetic efficacy, however, this approach suffers from some significant limitations: i) poor growth rates and inconsistent yield properties, due to deleterious genetic and epigenetic modifications that occur during the dedifferentiation; ii) lack of homogenous cell type and variability in product accumulation: suspension cultures of DDCs form large cellular aggregates, leading to heterogeneous microenvironments

and, therefore, to differences in cell physiology and metabolism. Recent evidence has showed that cambial meristematic cell (CMC) cultures could overcome some previously reported limitations associated with DCCs cultures (Barbulova et al., 2014; Ochoa-Villarreal et al., 2015; Partap et al., 2022).

Section 1 – Chapter 2

Mass spectrometry in "Omics" era

1.2.1 Classification of Omics Research

"Omics" is a form of high-throughput systems science. On the basis of the information level examined, we can discern: genomics, epigenomics, transcriptomics, miRNomics/ncRNomics, proteomics, metabolomics, lipidomics, glycomics, interactomics, phenomics, environmental omics and pharmacogenomics (Pirih and Kunej, 2018, 2017).

Genomics focuses on the information at the DNA level. In particular, whole genome sequencing (WGS) determinates the entire DNA sequence of an organism genome and next generation sequencing (NGS) technology is frequently used to identify single-nucleotide polymorphisms (SNPs), indels and copy number and/or structural variations, as well as to discriminate between different individuals or species (Bick and Dimmock, 2011; El-Metwally et al., 2013; Pareek et al., 2011; Zhou et al., 2010). GWAS (whole genome association study) tries to associate genetic variants, usually SNPs, to a particular phenotypic trait or disease (Bush and Moore, 2012).

Epigenomics analyses epigenetic marks which are often DNA methylation and histone modifications including methylation, phosphorylation, acetylation, ubiquitylation, and SUMOylation. These modifications can affect gene expression by directly altering chromatin structure or by providing binding sites for the recruitment of other nonhistone proteins to chromatin (Flanagan, 2015; Zhang et al., 2015).

Transcriptomics studies the information at the RNA level. The aim of whole transcriptome analysis (WTA) is to capture coding and noncoding RNA (ncRNA), mainly to identify heterogeneous gene expression profiles of cells/ tissues/organisms (Jiang et al., 2015).

miRNomics and ncRNomics focuse on microRNA (miRNA) and non-coding RNAs (ncRNAs) that are functional RNAs involved in silencing or activation of specific target genes (Kunej et al., 2012).

Proteomics purposes to study the levels, the post-translational modifications (PTMs) and the interactors of all the expressed proteins, as well described in paragraph 1.2.4 of this section.

Interactomics investigates DNA–DNA, DNA–protein, RNA–protein, and protein–protein interactions. The first three interactions are important to understand the variability of gene expression, whereas the last one is crucial to investigate functions of proteins, focusing on the biological mechanism of proteins, protein complexes, and their molecular interactions (Lv et al., 2015).

Metabolomics is the study of the metabolic spectrum and metabolites quantities of a biological system. The so called metabotype represents a link between genetic variants and visible phenotypes and, therefore, metabolites can be considered as biomarkers for the prediction of the traits (Gieger et al., 2008). Lipidomics has been described as a subsection of metabolomics dedicated to lipid analysis (Monnerie et al., 2020).

Glycomics aims to profile all the glycans including glycoproteins, proteoglycans, glycolipids and free or unconjugated glycans, that a cell, tissue or organism produces

under specified conditions of time, location, and environment. Since the glycome is influenced by both genetic and environmental factors, the comparison between glycome profiles obtained from different biological systems can shed light on intra- and inter-species variations, including providing indicators of disease that can be used for diagnosis and for monitoring the efficacy of drugs (Rudd et al., 2015).

Phenomics investigates the association between SNPs and a wide spectrum of phenotypes, known as phenome. It is a ‘‘reverse GWAS’’: GWAS uses a phenotype-to-genotype approach, whereas the phenomic wide association study (PheWAS) the reverse genotype-to-phenotype strategy (Pendergrass et al., 2012).

Environmental omics allow to better understand the effect of environmental and genetic factors and of their interactions on complex phenotypic traits (Morrison et al., 2006).

Pharmacogenomics identifies binding sites for small molecules across the genome in order to improve their selectivity, resulting in an increased therapeutic index and reduced off-target effects (Pirih and Kunej, 2017).

1.2.2 Mass Spectrometry (MS): Principles and Advances

Mass spectrometry (MS) is one of the key analytical technology used by ‘‘omics’’ sciences. “The basic principle of mass spectrometry (MS) is to generate ions from either inorganic or organic compounds by any suitable method, to separate these ions by their mass-to-charge ratio (m/z) and to detect them qualitatively and quantitatively by their respective m/z and abundance” (Gross, 2017a). Basically, a mass spectrometer consists of an ion source, a mass analyser and a detector.

1.2.2.1 Electrospray Ionization

One of the most largely used ionization technique in the field of the analytic chemistry applied to biology and biochemistry is the electrospray ionization (ESI). It is defined as a soft ionization technique that allows the transfer of ions from solution to the gas phase, starting at atmospheric pressure and incrementally proceeding into the high vacuum of the mass analyser (Fenn et al., 1990; Gross, 2017b; Smith et al., 1990). The passage of the ions into the mass analyser is guaranteed by a differential pumping. Indeed, the sample solution flows through a hypodermic needle, the spray capillary, kept at a potential of 3–4 kV relative to a surrounding cylindrical electrode. At the end of the capillary, the emerging liquid is exposed to an electric field (10^6 V/m), causing the charge separation in the electrolytic solution and the deformation of the meniscus. The curvature of the meniscus, in turn, contributes to increasing the strength of the electric field. As soon as the field strength reaches a critical value, the so-called Taylor cone forms and, when electrostatic forces overcome the surface tension, it starts injecting a fine jet of liquid from its apex to the counter electrode (Taylor, 1964; Wilm and Mann, 1994; Zeleny, 1917). This jet, ending with the so-named “plume” of the electrospray, is not stable and breaks up into smaller droplets (Nemes et al., 2007). The electrospray expands into a counter-current stream of inert gas that helps its focus and favours the evaporation of the solvent. This increases the same-sign-charge density on the surface of the droplets, until reaching the Rayleigh limit. At this point, the electrostatic repulsion overcomes the surface tension force and the disintegration of the droplets in smaller microdroplets occurs (Rayleigh, 1882). There are two theories about the liberation mechanism of the nude ions in the gas phase from the charged droplets: according to the charge-residue model (CRM) (Dole et al., 1968; Felitsyn et al., 2002; Mack et al., 1970), solvent molecules are gradually lost

and the charge is transferred to the unique macromolecule of analyte present in the final droplet before the complete desolvatation; contrary, the ion evaporation model (IEM) describes the formation of nude ions as direct evaporation from the surface of highly charged microdroplets (Iribarne and Thomson, 1976; Labowsky et al., 2000; Thomson and Iribarne, 1979).

Modern ESI interfaces are equipped with a nebulizer gas o a sheath gas enclosing the spray capillary, that allows for higher liquid flow. Moreover, they may also use a stream of hot nitrogen as auxiliary gas to enforce the evaporation of the solvent (e. g. ThermoFisher HESI-II Electrospray Probe with ION MAX API Source). In addition to this, modern interfaces employ spraying at an angle to the vacuum entrance. This rearrangement has the advantage to reduce possible contamination, by preventing the clogging of capillaries and skimmers (e. g. in case of buffer salts or organic material present in blood and urine samples) (Gross, 2017b).

The electrospray gradual process, resulting into a marked softness of the ionization, and the capability to generate multicharged ions in case of high mass analytes, that shift in m/z ranges accessible for the mass analysers, make ESI “the wings for molecular elephants” (Fenn, 2003; Heck and van den Heuvel, 2004). Furthermore, it offers the possibility to scale down to the nano range. Derived from the nanoliter-flow, the term nanoelectrospray (nanoESI) has become established for this technique. Different nanoelectrospay interfaces have been developed to deliver optimum performance. For example, Bruker CaptiveSpray Ion Source provides a vortex gas that sweeps around the emitter spray tip to desolvate and focus the Taylor cone into the MS inlet capillary. Moreover, the direct connection to the inlet capillary eliminates the need for any source adjustment.

1.2.2.2 Mass analyzers

Ions generated are separated according to their m/z by mass analyzers before reaching the detector. The most common used mass analyzers are: linear quadrupoles, ion traps, time-of-flight (TOF) analyzers and orbitrap analyzers (Gross, 2017c).

Generally, linear quadrupoles and ion traps, although offer low resolving power, are commonly used in MS laboratories for their high speed scan, compactness and low-price (Gross, 2017c). Ion traps are more sensitive than quadrupoles, but are not well suited for quantitative analysis due to the possibility of space-charge effects which reduce the analyzer dynamic range (Thomas, 2019). They can also perform tandem mass spectrometry experiments in order to obtain structural information from fragmentation patterns. Tandem mass spectrometry, abbreviated MS/MS, is any general method involving at least two stages of mass analysis (McLafferty, 1981). Basically, a tandem mass spectrometry experiment can be performed in time or space (Johnson et al., 1990; Murray et al., 2013). In the first case, a single analyzer (e.g. linear ion trap, quadrupole ion trap) executes the steps of precursor ion mass selection, fragmentation and product ion analysis in the very same place but sequentially in time; contrary, in the second case, precursor ions are selected in a first mass analyzer, dissociated in an intermediate region and the generated fragment ions transmitted to a second mass spectrometer for the analysis. Generally, a low-resolution MS1 unit is combined with a high-resolution MS2. Tandem-in-time instrumentation is much more compact, usually very cost effective, and allows for MS^n, whereas tandem-in-space is less prone to overload effects, and thus better suited when quantitation is a major issue (Gross, 2017c).

The principle of TOF is that ions of different m/z are separated in time during their flight along a field-free drift path of given length. If all the ions start their journey at the same time and with the same kinetic energy, the lighter ones will arrive earlier at the detector than the heavier ones (Gross, 2017c). TOF requires the ions to be produced in bundles and is thus especially well-suited for pulsed ion source like matrix-assisted laser desorption ionization (MALDI). The introduction of the reflector, that acts as an ion mirror by deflecting the ions and sending them back through the flight tube, has improved the resolving power of the early TOF analyzers. Indeed, it corrects the kinetic energy dispersion of the ions leaving the source with the same m/z ratio and increases the flight path without increasing the dimensions of the mass spectrometer (Cotter, 1992; Guilhaus, 1995; Hoffmann and Stroobant, 2007; Ioanoviciu, 1995). Orthogonal-acceleration (oaTOF) analyzers, where package of ions are extracted orthogonally from a continuous ion beam, offer suitability for each ionization method and a further improvement in sensitivity (due to good duty cycle and high transmission), spectral acquisition rate (spectra per second) and mass-resolving power (Coles and Guilhaus, 1993; Dawson and Guilhaus, 1989; Guilhaus et al., 2000; Mirgorodskaya et al., 1994; Selby et al., 2001). oaTOFs are also well-suited for combination with other mass-analyzing devices (e.g. quadrupole) into hybrid instruments (Allen and McWhinney, 2019). Hybrid mass spectrometers aim at attaining highest resolving power and accuracy, enhancing speed and sensitivity and realizing a versatile multi-purpose instrument (Gross, 2017c).

An impressive advancement in mass spectrometry has been possible by the invention of the orbitrap mass analyser for its high resolution and mass accuracy (Makarov, 2000; Perry et al., 2008; Scigelova and Makarov, 2006). Ions, injected with kinetic energy in the orbitrap analyzer, start to oscillate in intricate spirals around a

spindle-like-shaped central electrode that creates an axial field gradient. Proper ion injection in terms of kinetic energy, timing and spatial focusing is achieved by radial ejection of ion bunches from a C-shaped radiofrequency (RF)-only quadrupole, called C-trap (Olsen et al., 2005). The image current induced by moving ions is detected by a differential amplifier connected to a barrel-shaped outer electrode, split in half by an insulating ceramic ring. The m/z of the different ions can be determined by their frequencies of oscillation after a Fourier transform (FT). Orbitrap mass spectrometers can efficiently be combined with different types of mass analyzers and ion-guiding devices into hybrid instruments that can also perform tandem mass experiments (Amy et al., 1990; Futrell, 2000). The most common fragmentation mechanisms performed is the collision-induced dissociation (CID), in which ion fragmentation is realized through collision with neutral gas atoms or molecules set to a pressure considerably above that of the surrounding high vacuum (Levsen and Schwarz, 1976; McLafferty et al., 1973). One approach towards harsher CID is the higher-energy C-trap dissociation (HCD) in which the C-trap is used as a collision cell simply by raising the RF voltage. An increase in RF voltage of the C-trap unfortunately leads to a decreased trapping efficiency in the low mass range. This disadvantage can be overcome by attaching an RF-only octopole collision cell (supplied with a radiofrequency voltage and pressurized with nitrogen) at the end of the C-trap (Olsen et al., 2007). An example of hybrid instrument is the Q Exactive mass spectrometer (Thermo Fisher Scientific) (Figure 1.2), that we used for our metabolomics analysis. In its architecture a bent flatapole transmits ions from the source to a quadrupole. Then, ions are transferred into a C-trap and injected into an Orbitrap analyzer where mass spectra are acquired by image current detection. For MS/MS fragmentation, ions pass through the C-Trap

into the HCD cell. After the ions have been fragmented, they are transferred back from the HCD cell into the C-Trap from where they are injected into the Orbitrap analyzer.

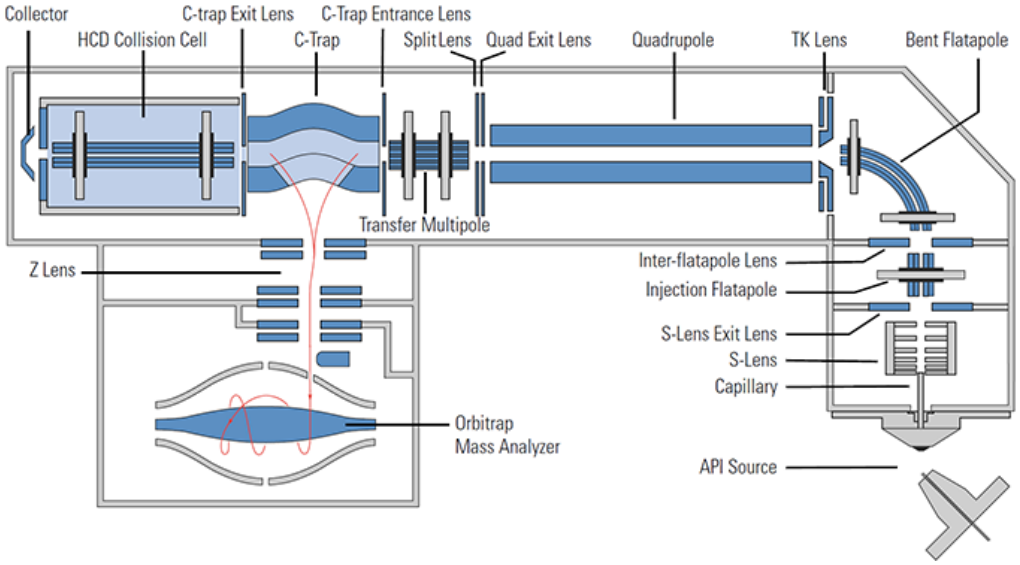

Figure 1.2 *Schematic of Q-Exactive (Thermo Fisher Scientific).*

1.2.2.3 Mass data acquisition modes

Most of applications use conventional data-dependent acquisition (DDA) or targeted methods such as multiple reaction monitoring (MRM) or its newest version, parallel reaction monitoring (PRM). Advances in mass spectrometer design and bioinformatics algorithms have allowed the development of another acquisition strategy called data independent acquisition (DIA), that approaches the identification breadth of DDA and the reproducible quantification of MRM/PRM (Figure 1.3) (Hu et al., 2016; Li et al., 2021).

In DDA, the top n most abundant precursor ions are selected based on a survey scan (MS1) and fragmented in sequential MS2 scan. The stochastic nature of precursor ion

selection prior to the fragmentation decreases the level of reproducibility and prevents the measurement of low-abundance ions. Additionally, to survey as many ions as possible, DDA deliberately samples each precursor ion only once or twice, preventing precise quantification.

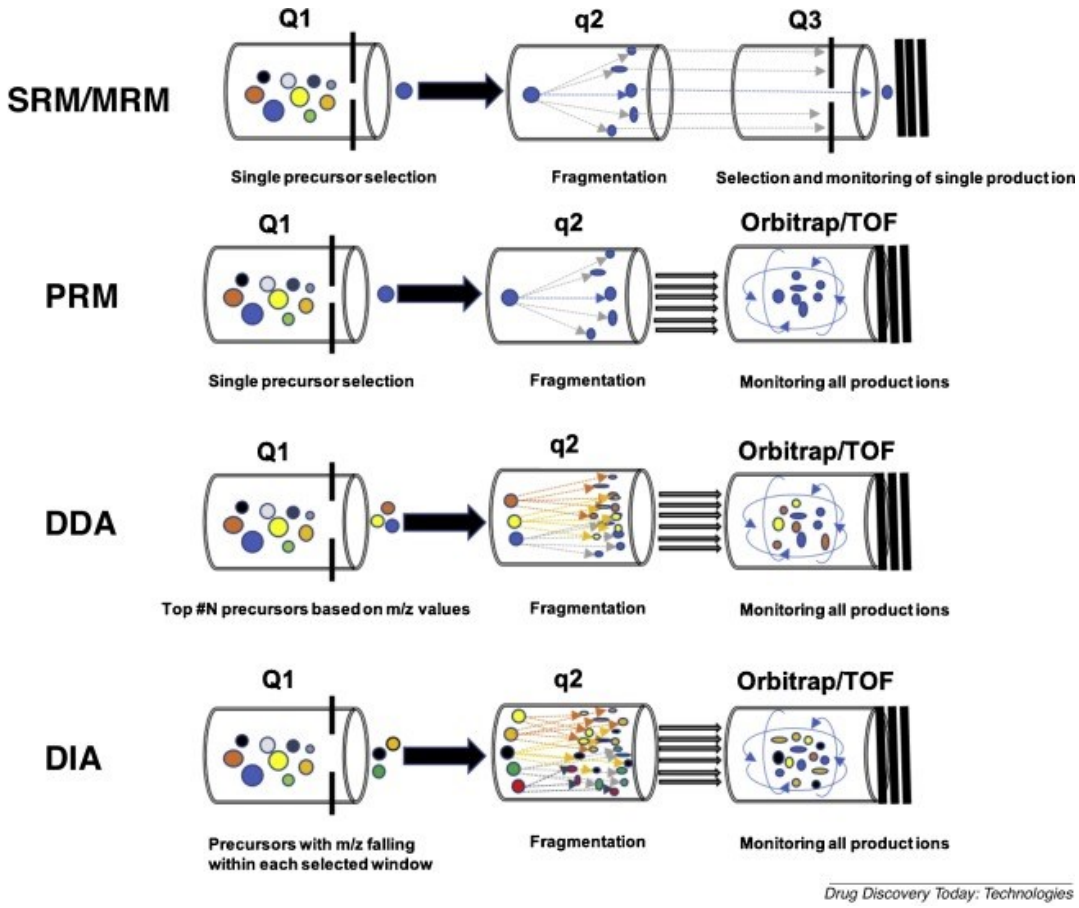

Figure 1.3 *Schematic diagrams of SRM/MRM, PRM, DDA, and DIA mode. (Adapted from Li et al., 2021)*

The targeted methods MRM and PRM are more precise and reproducible than DDA as they focus MS2 scans on only a small set of predetermined and previously identified precursor ions. In particular, for each MS1 scan, in MRM only a subset of fragment ions is measured in the subsequent MS2 scan, whereas in PRM all of the fragment ions

are measured. In both methods, the same precursors are selected and fragmented multiple times, allowing a more precise quantification in comparison with DDA.

In DIA, pre-defined wide isolation windows span the whole MS1 m/z range and all precursor ions, within each isolation window, are fragmented in MS2. Therefore, the reproducibility and sensitivity of DIA are superior to DDA (Krasny and Huang, 2021). The selectivity and sensitivity of DIA are slightly inferior to MRM/PRM, but it samples repeatedly the same precursor ion for more precise quantification, too (Hu et al., 2016).

Rapid improvements in DIA-MS sensitivity and speed have also been achieved by dia-parallel accumulation-serial fragmentation (dia-PASEF). This method is enabled by the recent development of trapped ion mobility spectrometry (TIMS) coupled to QTOF mass analysis (Krasny and Huang, 2021).

Ion mobility effects separation of ions based on their different velocities in an inert gas under the influence of an electric field (Gross, 2017c). In the classical drift tube IMS, ions are accelerated by a uniform electric field in presence of a counter current inert gas. Larger ions, having a larger collisional cross section (CCS), have more collisions with the gas than smaller ones and thus they arrive later at the detector. In particular, the ion mobility constant K is defined as the ratio of the steady state drift velocity adopted by the ion to the applied electric field, and it is convention to calculate the reduced ion mobility K0 at standard pressure and temperature and to report the inverse 1/K0. TIMS is an inverted drift tube IMS wherein ion motion is directed towards the MS by gas flow in opposition to the applied electric field strength. Ions enter in the TIMS tunnel and rest at an axial position at which the drag force on the ions from the gas flow is counterbalanced by the force from the analytical field.

Therefore, low mobility ions, requiring higher field strength to counterbalance the drag from the gas, are trapped further into the TIMS tunnel than high mobility ions. Stored ions are then eluted according to their mobility by progressively lowering the field strength. TIMS scanning operation increases sensitivity and ion duty cycle (Dodds and Baker, 2019; Meier et al., 2021).

Interfacing IMS with LC-MS adds an additional dimension of separation to the standard MS spectra. Since TIMS requires only 100 ms to analyze a wide ion mobility range, it is advantageous to integrate it with high scan rate mass analyzers such as TOF analyzers. In timsTOF mass spectrometer (Bruker) (Figure 1.4), that we used for our proteomics analysis (see paragraph 3.4.5), two TIMS regions are employed. The first TIMS region (TIMS1) is used for the accumulation of the precursor ions which are later released into the second TIMS region (TIMS2) to be motility analyzed. In parallel to the ion separation in TIMS2, TIMS1 accumulates the next batch of ions and thus this dual TIMS configuration gives 100% duty cycle. Eluted ions are transferred to a quadrupole that isolates precursor ions for the optional subsequent fragmentation in the collision cell. They are then accelerated by an orthogonal deflection unit into a time of flight with two stage reflectron, before reaching the detector (Meier et al., 2021, 2018, 2015).

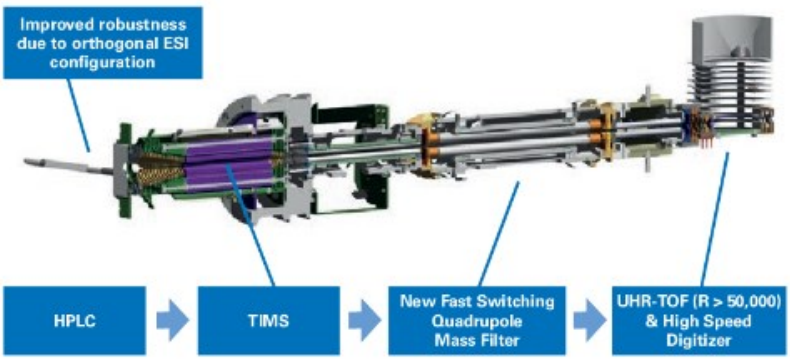

Figure 1.4 *Schematic of timsTOF mass spectrometer (Bruker, Adapted from Meier et al., 2015)*

In PASEF method (Figure 1.5) the precursor selection in the quadrupole is synchronized with the elution of mobility-separated ions from the TIMS device, allowing the fragmentation of many precursors for TIMS scan and increasing speed and sensitivity (Meier et al., 2021, 2018, 2015).

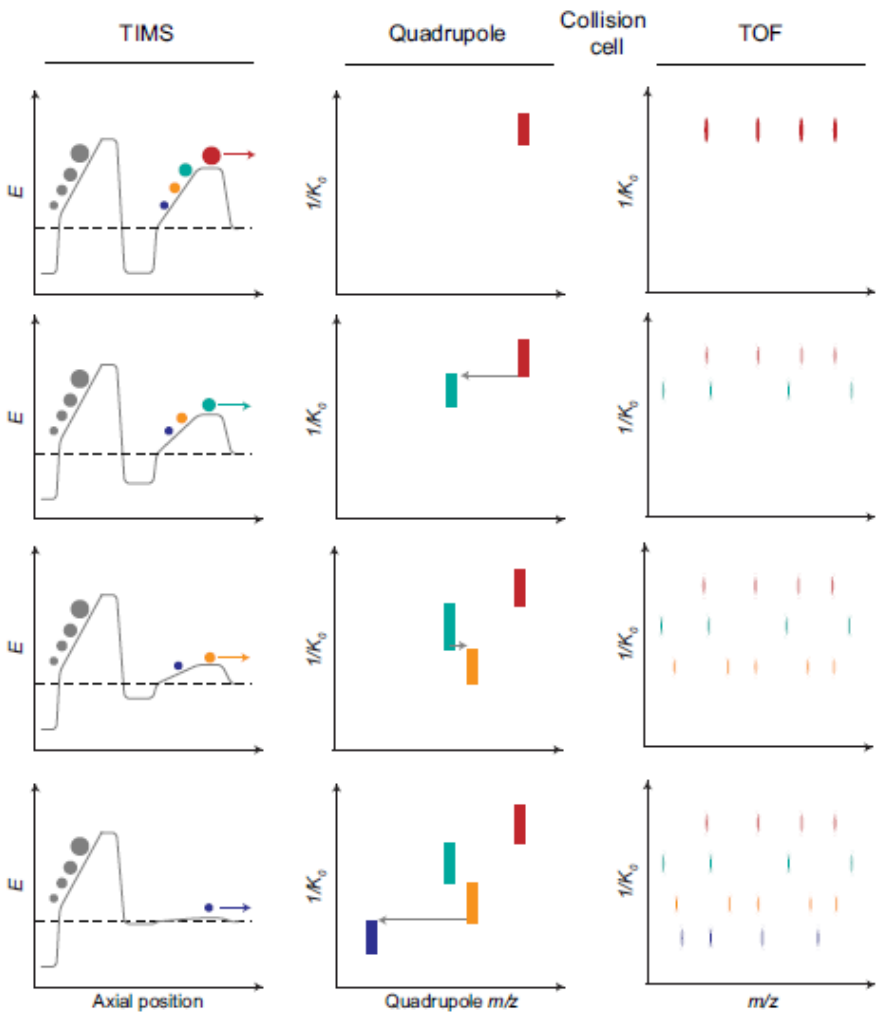

Figure 1.5 *Parallel accumulation–serial fragmentation (PASEF) (Adapted from Meier et al., 2021).*

dia-PASEF combines the advantages of DIA acquisition method with the inherent ion efficiency of PASEF and it results both more selective and sensitive. In this case, the quadrupole isolation windows are dynamically positioned as a function of TIMS ramp time, covering the vast majority of precursors of the 2^+ and 3^+ charge states (Figure1.6) (Meier et al., 2020).

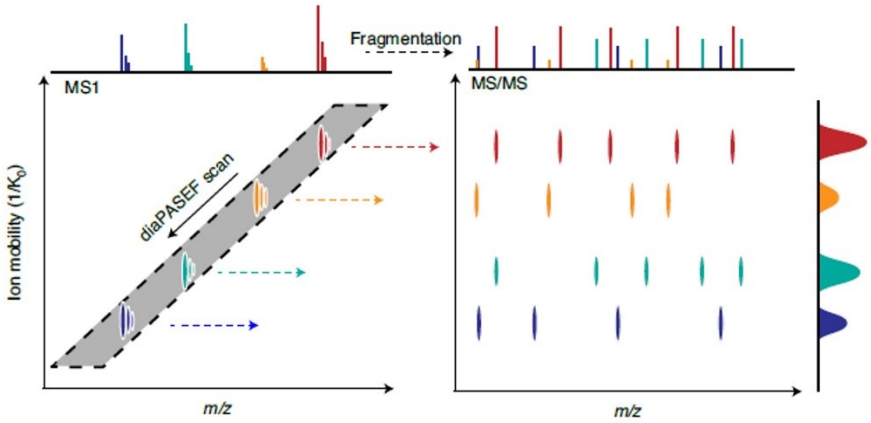

Figure 1.6 *The dia-PASEF acquisition method.(Adapted from Meier et al., 2020)*

Although the introduction of ion mobility as additional separation dimension and the application of PASEF method reduce the complexity of MS2 spectra, DIA data analysis is still challenging. Therefore, there is a high demand of computational algorithms to further improve the deconvolution of complex DIA spectra and increase their identification and quantification efficiency (Hu et al., 2016; Krasny and Huang, 2021).

1.2.3 MS-based Metabolomics

Metabolomics, by providing a holistic survey of natural extract composition, plays an important role in NPs research. For a pertinent chemical characterization, the first key step is to generate high-quality metabolite profiling data. Liquid chromatography (LC) coupled to mass spectrometry (MS) currently is the most versatile and commonly used approach for profiling extracts. The hyphenation of ultrahigh-pressure liquid chromatography (UHPLC) with high-resolution mass spectrometry (HRMS) has made possible to obtain high peak capacities with shorter analysis time and MS and MS/MS spectra with high sensitivity, mass resolution and accuracy. Today, in fact, the bottleneck lies not in the acquisition of high-quality spectral data but in the annotation of their information and, therefore, in the unambiguous identification of the highlighted chemicals. Data sets are too large for manual analysis and, thus, there is a pressing need for metabolomics data repositories and associated data analysis tools, which allow data to be shared, re-analysed and re-annotated in an automated manner (Allard et al., 2017; Chaleckis et al., 2019).

1.2.3.1 Global Natural Products Molecular Networking (GNPS)

Although several NPs databases (Dictionary of Natural Products, AntiBase, and MarinLit) assist in dereplication (identification of known compounds), they are not freely available and do not process MS data. On the other hand, MS databases like MassBank, Metlin, mzCloud, and ReSpect limit data analyses to several individual spectra or a limited amount of LC–MS files. Moreover, the reference libraries of NIST/EPA/NIH and of the free online search engines mzCloud and XCMS are not available for download. In this scenario, Global Natural Products Social Molecular

Networking (GNPS) has been developed by the University of California San Diego (UCSD) Center for Computational Mass Spectrometry. GNPS, that we exploited for our metabolomics analysis, is a data-driven platform that allows annotation (the process of attributing a putative chemical structure to a detected molecule), community sharing and collaborative curation of fragmentation mass spectrometry data (MS/MS)(M. Wang et al., 2016).

Indeed, it enables online dereplication by querying experimental MS/MS spectra against all the accumulated reference spectra in GNPS spectral libraries. They include both third-party libraries, such as MassBank, ReSpect and NIST, as well as well as spectral libraries created for GNPS (GNPS-Collections) and spectra from the NP community (GNPS-Community). GNPS also allows variable dereplication, the detection of significant matches to spectra of related molecules (analogous or compounds belonging to the same class of molecules)(M. Wang et al., 2016).

GNPS can be also used for molecular networking (MN) that, beyond spectral matching against reference spectra, allows to align experimental spectra against one another and connects related molecules by their spectral similarity. Indeed, it relies on the fundamental observation that structurally related molecules share fragment ion patterns when subjected to MS2 fragmentation methods (Aron et al., 2020). Since its introduction, MN has become a key method to explore chemical space in non-targeted mass spectrometry data. Based on the success of the 'classical' MN, GNPS has introduced Feature Based Molecular Networking (FBMN, Figure 1.7). It combines MN with feature detection tools (e.g. MZmine) and thus also incorporates MS1 information, retention time and ion mobility separation, when performed. Therefore, FBMN enables to distinguish isomers producing similar MS2 spectra that are resolved

by chromatographic or ion mobility separation. Moreover, it facilitates annotation and incorporates more accurate relative quantitative information, not using the spectral count or the summed precursor ion count, but LC–MS feature abundance (peak area or peak height). However, although FBMN offers an improvement upon many aspects, classical MN remains convenient for the analysis of large datasets, since the difficult scalability of the most feature detection and alignment software tools (Nothias et al., 2020). In the visualization of molecular networks (MNs), each node represents a MS2 spectrum and each edge (connection) between nodes a spectrum-to-spectrum alignment. Edges are defined by a cosine score that determines the similarity of two MS/MS spectra, considering precursor ion, fragment ions, and peak intensities. It ranges from 0 (no similarity at all) and 1 (identical spectra).

Each node is also queried against GNPS spectral libraries to assign putative known molecules within a molecular network and the annotation can be propagated to unknown nodes using chemical rationale (Aron et al., 2020; M. Wang et al., 2016). MNs can be visualized online in-browser or exported for third-party visualization software such as Cytoscape (Shannon et al., 2003).

1.2.3.2 MZmine: a user-friendly tool for mass spectrometry data pre-processing

The modular framework MZmine is one of the most popular and user-friendly feature detection tools. Indeed, its graphical interface is intuitive and critical data-processing steps are linked to visualization modules that provide online preview during parameter setup. Moreover, after each step, the original data are not removed and, therefore, the user can return back to previous results at any stage of data processing (Olivon et al., 2017; Pluskal et al., 2010).

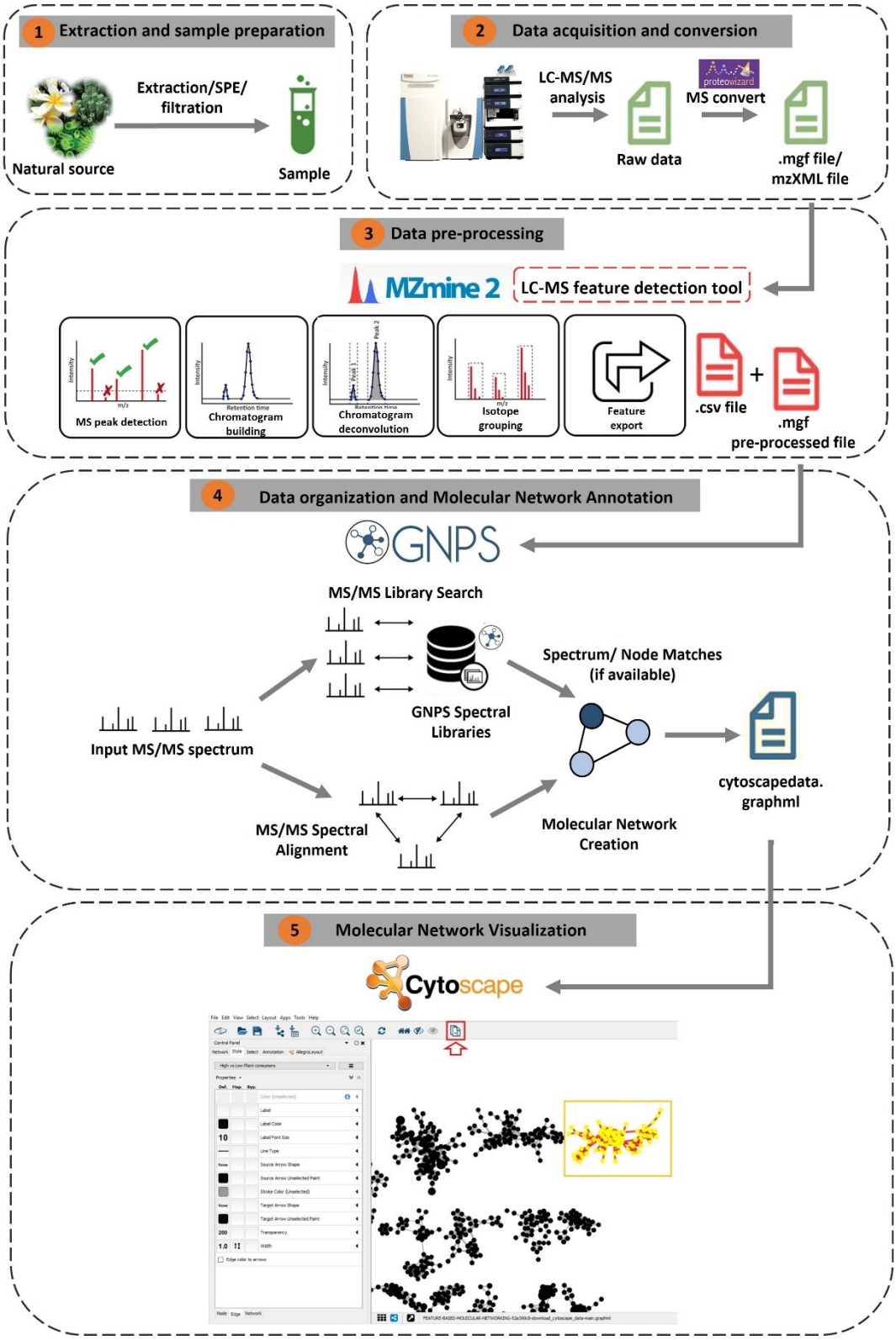

Figure 1. 7 *Schematic workflow for a GNPS based chemical characterization pipeline (Adapted from Ramos et al., 2019)*

In the MZmine framework, Automated Data Analysis Pipeline (ADAP) is incorporated. It includes: raw data import (in the supported file format .mzXML), mass detection, chromatogram building, chromatogram deconvolution, isotope grouping, feature alignment and processed data export (Figure 1.7) (Du et al., 2020).

During the mass detection step, a list of masses for each scan in the raw data file is generated. Then, the "Chromatogram Builder" connects all consecutive m/z values spanning over multiple scans and converts them into extracted ion chromatograms (EICs). The following step is the detection of chromatographic peaks (boundaries and apex) using the continuous wavelet transform (CWT). Finally, the "Isotopic Peak Grouper" module assembles peaks forming an isotopic pattern within a single feature. When comparing several samples, the RT alignment step is required to identify corresponding peaks across samples. Once data are processed, MZmine provides a MS/MS spectral summary (.mgf file), with a representative MS/MS spectrum per LC-MS feature, and a feature quantification table (.csv file) with LC-MS feature intensities. These resulting files are submitted to GNPS to launch a FBMN job (Du et al., 2020; Olivon et al., 2017; Pluskal et al., 2010).

1.2.4 MS-based proteomics

1.2.4.1 MS-based proteomics: general overview

The term proteome was proposed for the first time in 1996 by Marc Wilkins (Wilkins et al., 1996) to denote the PROTEin complement of a genOME, definition that has been soon expanded embracing all the protein isoforms and modifications, their interactomes and their structural and high-order complexes features.

Proteomics can be divided into three main groups: i) global proteomics, focusing on the alterations of proteomes or their PTMs upon different physio-pathological conditions, different internal/external stimuli or different drug treatments (Domon and Aebersold, 2010; Hsu and Chen, 2016; Lee et al., 2008); ii) compound centric chemical proteomics (CCCP), aiming to identify cellular interactomes of bioactive small molecules; (iii) active-based protein profiling (ABPP) purposing to profile proteins on the basis of their activities (Rix and Superti-Furga, 2009).

Therefore, proteomics represents a large-scale systematic study of the proteome, that unlike the genome, is subjected to spatial and temporal dynamicity in the living systems both due to intracellular and extracellular stimuli. Hence, it must handle several problems intrinsically bound to the nature of the sample material that is variable, limited, subjected to degradation, showing a vast dynamic range and a plethora of post-translational modifications (Tyers and Mann, 2003). A mass-spectrometry-based approach, thanks to its comprehensiveness and versatility, tackled most of these challenges, thus representing a key technique in the proteomics field (Aebersold and Mann, 2003).

Basically, two types of MS-based approaches can be adopted in proteomics investigations: “top-down” (McLafferty et al., 2007; Tran et al., 2011) and “bottom-up” (Figure 1.8) (Chait, 2006; Yates et al., 2009). The first is based on the fragmentation of intact proteins by tandem mass spectrometry, whereas the second on a previous enzymatic digestion of the proteins and tandem mass spectrometric analysis of the complex peptide mixtures. The “bottom up” approach is more largely employed since the fractionation, ionization and fragmentation efficiency of the peptides is easier in comparison to intact proteins.

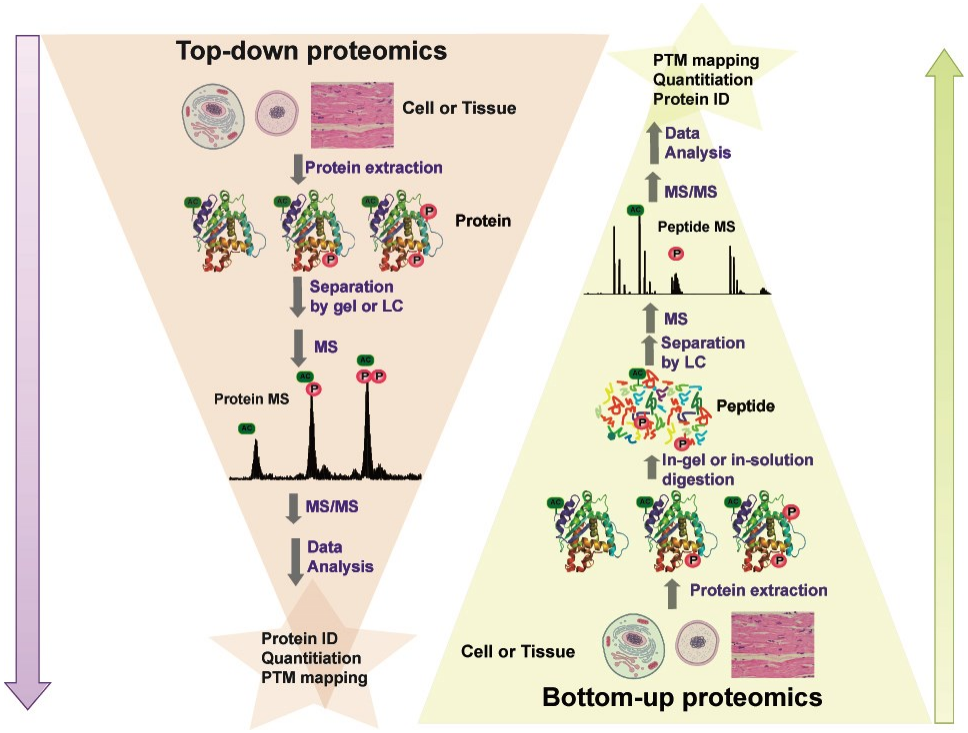

Figure 1.8 *Schematic view of "top-down" and "bottom-up" proteomics approaches.*

In the "bottom-up" workflow, the selection of a proper fractionation strategy is crucial to simplify the complex mixture of peptides. One of the first strategies relies on the separation of protein sample by means of 2D gel electrophoresis (2D-PAGE) (Klose, 1975; O'Farrell, 1975). In 2D-PAGE proteins are separated firstly by their isoelectric point (pI) and then by their molecular weight. In the first step, called isoelectric focusing (IEF), proteins are loaded onto IEF polyacrylamide gels or pH gradient strips (IPG) and by the application of an electric field they migrate through the pH gradient until they reach their pI. The subsequent SDS treatment confers to each protein a charge proportional to its molecular weight that allows their separation into a polyacrylamide gel when an electric field is applied. Protein spots can be detected by using staining techniques (e.g. Silver staining, Coomassie Blue, fluorescent dyes) and digested *in situ*. Despite the good resolving power, 2D-PAGE is

time consuming and requires large sample amount (Abdallah et al., 2012; López, 2007). Moreover, in case of many samples to run, additional problems related to the gel-to-gel variability can emerge. To overcome this drawback, the two-dimensional difference gel electrophoresis (2D-DIGE) has been developed. In this case, proteins from different experimental conditions are first tagged with different fluorescent dyes (CyDye technology), then run on the same gel and finally quantified by detecting dyes intensities at different wavelengths (Larbi and Jefferies, 2009; Timms and Cramer, 2008; Viswanathan et al., 2006).

A less both sample- and time- consuming gel-based method is the 1D-PAGE in which proteins are separated only according to their molecular weight (Laemmli, 1970). In this case, proteins are digested *in situ* (Shevchenko et al., 2006) and the obtained peptide mixture is subjected, before mass spectrometry analysis, to an additional liquid chromatography step. In order to improve sensitivity, it is performed in the nanoflow scale, using column with a particle size in the range of 1 μm interfaced with nano-electrospray sources (Wilm and Mann, 1996).

Despite gel-based methods are largely used, they suffer of some limitation, mainly the loss of sample due to an incomplete peptide extraction from gel. Therefore, during the last years, many efforts were oriented to develop gel-free methods. The Multi-Dimensional Protein Identification Technology (MuDPIT) (Washburn et al., 2001), also known as “shotgun proteomics”, uses a two-dimensional liquid chromatography (2D-LC) to resolve complex peptide mixtures with high efficiency and to improve the dynamic range of the MS identifications (Issaq et al., 2005; Vollmer et al., 2004). The second chromatographic dimension is usually a reversed-phase LC (RP-LC) step, whereas the first dimension takes advantage of a different principles such as high pH

fractionation (HpH-RP) (Wang et al., 2015), strong cation exchange (SCX) (Dormeyer et al., 2007; Taouatas et al., 2009), strong anion exchange (SAX) (Dai et al., 2009) and hydrophilic interaction liquid chromatography (HILIC) (Alpert, 1990; Boersema et al., 2009).

The obtained peptides are submitted to mass spectrometry analysis and the identification of proteins can be retrieved by two approaches: peptide mass fingerprint (PMF)(Henzel et al., 2003) or tandem mass spectrometry (Olsen and Mann, 2004).

In the PMF approach, proteins are identified by matching MS1 experimental spectra against spectra obtained by *in silico* digestion of protein sequences from a protein data bank. It is suitable for extensively simplified peptide mixtures (such as from 2D-PAGE or 2D-DIGE experiments), being limited to the analysis at the peptide level. Therefore, the more informative tandem MS experiments are becoming widespread, especially after the crucial advancements in the hybrid mass spectrometer technologies that allow the ultra-high-resolution analysis of both parent ions and their fragments. The choice of the fragmentation strategy affects the type of the information reachable from a tandem experiment. CID induces peptide fragmentation in a “mild” fashion, causing the breakage of the amide bond (mostly y and b ions are produced) (Lau et al., 2009). HCD enables the detection of fragment ions of low m/z in the cell and it is useful in isobaric tags-based quantitative investigation (Mischerikow et al., 2010; Zhang et al., 2010). Electron transfer dissociation (ETD) induces random fragmentation along the peptide backbone (even if a highly occurrence of z and c ions is detectable) and it is preferred in case of peptides with higher charge (Syka et al., 2004). CID, ETD and HCD provide complementary information and thus they can be combined to obtain better sequence coverage of proteins and peptides (Frese et al., 2011).

Once the full MS and the MSMS spectra have been generated, the empirical fragmentation peptide profiles are matched with theoretical ones, contained in protein data banks, exploiting search algorithms.

1.2.4.2 MS-based global proteomics approaches

Here, we focused on global proteomics since we adopted this approach, as described later in paragraph 3.2.1.

The drawbacks affecting gel-based approaches, together with the advancements of mass-spectrometry and liquid chromatography techniques, led to a rapid spread of gel-free methods, that can be divided into label-based and label-free approaches (Figure 1.9) (Bakalarski and Kirkpatrick, 2016).

In label-based strategies, labelled tags are used to distinguish the same analyte in different samples so that they can be mixed and analyzed in a single LC-MS run. This removes the sample-to-sample variability issue. The label-based approaches can be grouped in metabolic labelling (e.g. SILAC) and chemical labelling techniques (e.g. ICAT, dimethyl labelling and isobaric mass tags).

The most exploited metabolic labelling technique is Stable Isotope Labelling by Amino acids in Cell culture (SILAC). It employs *in vivo* incorporation of stable isotopes: cells cultured in a medium enriched with essential auxotrophic isotope-labelled amino acids (containing e.g. ^{2}H, ^{13}C, ^{15}N) are able to capture and incorporate them in newly synthesized proteins (Ong et al., 2003, 2002; Ong and Mann, 2007, 2006). In a typical SILAC experiment, two cell populations are cultivated in presence of natural or isotopically labelled amino acids and, after several cell divisions, one

population is treated with the drug. Subsequently, proteins are extracted from both the treated and un-treated cells and mixed prior to the enzymatic digestion and 2D-LC-MS/MS analysis. Same peptides coming from different samples are quantified exploiting the mass-shift of the relating peaks due to the different incorporated tags. SILAC has several limitations, requiring long incubation times for *in vivo* incorporation of labels and being very expensive.

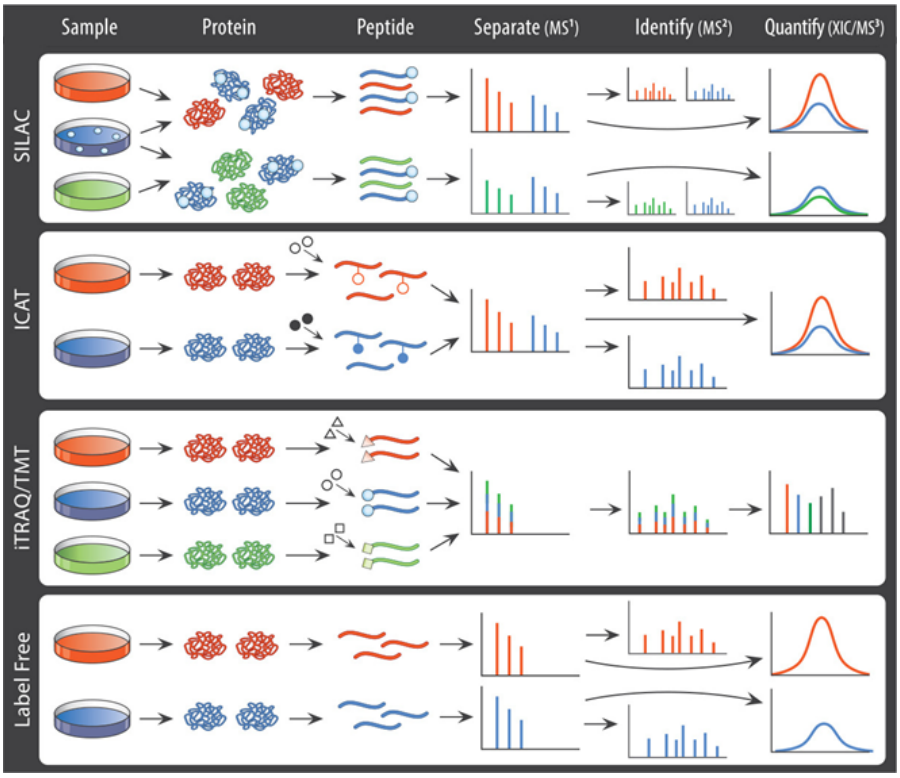

Figure 1.9 *Label-based and label-free MS-based global proteomics approaches. Adapted from (Bakalarski and Kirkpatrick, 2016)*

Chemical labelling techniques employ chemical reactions to insert an isotopically labelled tag at protein (ICAT) or peptide level (e.g. dimethyl labelling and isobaric mass tags).

The Isotope-Coated Affinity Tag (ICAT) uses probes including three elements: an affinity tag (e.g. biotin), required for the isolation of ICAT peptides, a deuterated (heavy probe) or not deuterated (light probe) oxyethylene linker and an iodoacetyl moiety, responsible for the reaction with the cysteines into protein sequences (Shiio and Aebersold, 2006) (Figure 1.10). Proteins from two different samples are differently labelled with the heavy or light probe at cysteines level, mixed and subjected to digestion. Tagged peptides are enriched by an additional affinity purification step and analysed by LC-MS/MS. Each pair of heavy and light labelled peptides are chemically identical and co-fractionate, but they present a mass-shift signature which is exploited for the relative quantification step, where the ratio of peptide pairs signal intensities is determined.

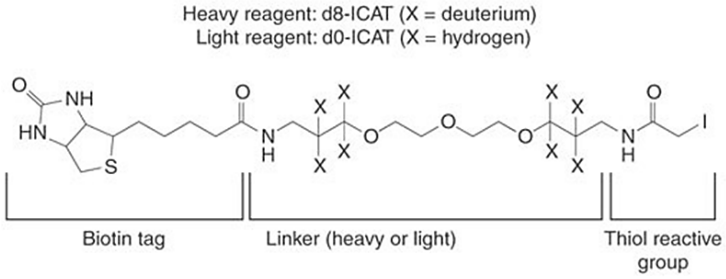

Figure 1.10 *Structure of the ICAT reagent. Adapted from (Shiio and Aebersold, 2006).*

In the attempt to increase the number of samples that can be pooled together before the MS analysis, the dimethyl labelling and, particularly, the isobaric tags (iTRAQ and TMT reagents) have been developed.

The stable-isotope dimethyl labelling (SIDL) allows to combine up to three different samples exploiting the reaction of primary amine groups (e.g. N-termini and lysine ε-amino groups) with formaldehyde to form a Schiff base, then reduced to a

secondary amine by cyanoborohydride (Figure 1.11) (Boersema et al., 2009, 2008). The combination of regular formaldehyde and cyanoborohydride generates N,N dimethyl-amine peptides with a mass increment of 28 Da (light label). Using deuterated formaldehyde and cyanoborohydride a mass increase of 32 Da (intermediate label) is obtained, whereas the treatment of peptide mixtures with ^{13}C labelled formaldehyde and cyanoborodeuteride leads to a mass increment of 36 Da (heavy label).

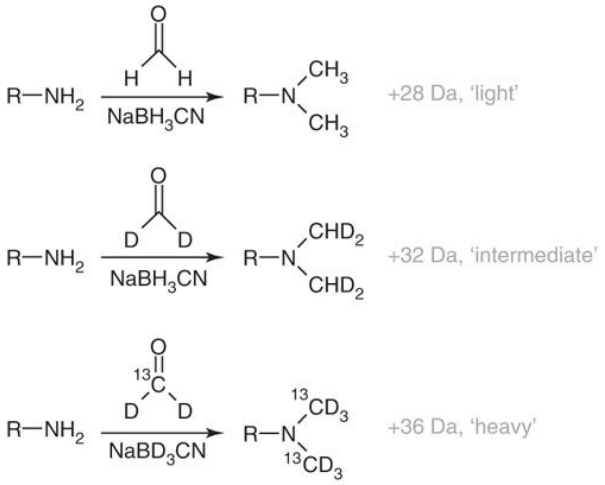

Figure 1.11 *Labelling chemes of triplex stable isotope dimethyl labelling. Adapted from (Boersema et al., 2009).*

Briefly, after protein extraction and digestion, peptides are differently labelled and pooled together for the LC-MS/MS analysis. The quantification of the same peptides coming from different samples exploits the mass-shift of the relating peaks due to the different labels introduced at the peptide level. In comparison to the other label-based approaches, SIDL is faster and less expensive.

Isobaric-Tagging for Relative and Absolute Quantification (iTRAQ) and Tandem-Mass Tags (TMT) exploit isotopomers consisting of a hydroxyl succinimide ester

moiety, that reacts with N-termini and lysine ε-amino groups, a mass normalizer spacer group and a N-methylpiperazine, that represents the mass reporter responsible for the quantification (Domon and Aebersold, 2006; Ross et al., 2004; Thompson et al., 2003). Therefore, same peptides from different samples are isobaric, have the same chromatographic elution profile and yield a unique MS1 peak, but after fragmentation, they release their reporter ions having different mass. The different mass reporter ions abundance reflects the amount of the same peptide in the different experimental conditions. Briefly, different proteomes are subjected to proteolysis, differently tagged at the peptide level and mixed prior to 2D-LC-MS/MS analysis. The commercially available kits allow the multiplexing up to 11 experimental conditions. Moreover, quantification at MS2 level gives a higher signal/noise ratio and there is a gain in sensitivity due to the isobaricity of the tags. However, the economic costs of iTRAQ reagents and the need of a mass spectrometer equipped with the opportune fragmentation source, such as HCD, limit the use of this technique (Bantscheff et al., 2012; Karp et al., 2010; Mahoney et al., 2011).

In label-free methods, each sample is disjointly prepared and subjected to LC-MS/MS analysis. Protein quantification is deduced or by counting and comparing the number of MS/MS spectra or from the intensity of the intact proteolytic peptides. In the latter case, peak area integration of a set of peptides per protein provides relative quantitative information among multiple samples. This procedure is more accurate, but has several limitations: firstly, the alignment of chromatographic elution profiles between different runs is mandatory for the evaluation of the intensities of the same peptide in different samples; moreover, a right balance between survey spectra and fragmentation spectra is pivotal to obtain an accurate protein quantification without affecting the identification. The main advantages of label free methods are the virtual

endless number of samples that can be compared and the higher dynamic range of quantification.

1.2.4.3 Bioinformatics

We focused on MaxQuant and DIA-NN software, that we used for DDA and DIA data analysis, respectively (see paragraph 3.4.6).

MaxQuant is one of the most frequently used platforms for mass-spectrometry-based proteomics data analysis (Tyanova et al., 2016a). It integrates a multitude of advanced algorithms that allows very high peptide identification rates and high-accuracy protein quantification for several thousand proteins in complex proteomes (Cox and Mann, 2008). In particular, for the identification, MaxQuant uses its own peptide database search engine, called Andromeda.

First of all, mass and intensity of the peptide peaks in a MS spectra are detected and assembled into three-dimensional (3D) peak hills over the m/z retention time plane. High mass accuracy is achieved by using a subset of high confidence peptide identifications from a first peptide database search to determine mass and time recalibration curves and to subtract the determined systematic mass error from the measured mass of each MS isotope pattern (Cox et al., 2011). After that, the main search is performed and to control the extent of false positive identifications a target-decoy-based false discovery rate (FDR) approach is utilized. Indeed, by default, MaxQuant uses a reverse database of the original search database consisting of all protein sequences read from the end to the beginning. Peptide spectrum match (PSM) is scored by posterior error probability (PEP) that is the probability of a peptide to be a false hit, given the Andromeda score plus multiple peptide properties, such as length,

charge and number of modifications. PSMs, from the forward and the reverse database, are sorted by their PEP and matches are accepted until the proportion of hits coming from the reverse database reaches the desired fraction of false positives.

Moreover, MaxQuant can identify more than one peptide from each MS/MS spectrum, as it performs a 'second peptide' search specifically looking for signals resulting from co-fragmentation of additional precursors.

In addition to this, given the partially stochastic nature of DDA, MaxQuant offers the 'Match between runs' option that allows to transfer peptide identification from an LC–MS run, in which the peptide has been identified by MS/MS, to another LC–MS run, in which no MS/MS data for this peptide were acquired or no peptide was assigned. The transfer of identifications is based on retention time, accurate mass calculation and the individual mass tolerances of peptide features. This option greatly increases the number of features available for quantification and data completeness.

The assembly of peptide hits into protein hits to identify proteins is the next step. If the set of identified peptides in one protein is equal to or contained in the set of identified peptides of another protein, these two proteins are joined in a protein group. Contrary, when two protein groups are identified with distinct peptides, except for one that is shared between the two, they cannot be combined. The shared peptide will be used for quantification (unique + razor peptides) or not (unique peptides only). A PEP is assigned to each protein group, by multiplying the individual PEPs of the peptides of the protein group. Similarly, protein PEP is used for a second level of FDR control on the list of reported protein groups.

Peptide intensities are taken at the peak maximum over the elution profile and include all isotopic peaks. Protein intensity is the sum of all identified peptide intensities for the group.

Data can be subjected to downstream statistical and functional analysis by using the bioinformatics platform Perseus (Tyanova et al., 2016b).

Data Independent Acquisition by Neural Networks (DIA-NN) is a software suite for the processing of DIA proteomics experiments (Demichev et al., 2020). It allows two types of analysis: library-based or library free. In the first case, the spectral library can be based on DDA (additional acquisitions) or DIA data. In the second case, DIA-NN automatically generates a spectral library *in silico* from a protein sequence database, using fragmentation, retention time and ion mobility predictors. In both cases, a collection of ion precursors (with several fragment ions from each precursor annotated) is obtained for the match with the experimental DIA-MS dataset. DIA-NN also generates a library of decoy precursors (Figure 1.12).

Chromatograms are extracted for each precursor ion and all its fragment ions. Each elution peak is then scored and the best peak is selected. In particular, DIA-NN calculates a set of 73 scores that reflect peak characteristics, including co-elution of fragment ions, mass accuracy and similarity between observed and reference spectra. Interfering peptides are removed through the calculation of q-values (target decoy-based approach) using an ensemble of Deep Neural Networks (DNNs).

DIA-NN allows cross-run precursor ion quantification. Each fragment is assigned a correlation score of its elution profile with the respective reference profile. For each precursor (with q-value above a given threshold), the three fragments with the highest correlation scores are selected in a cross-run manner. Their intensities are then

summed in each acquisition to obtain the precursor ion intensity. After that, sums of the intensities of these precursors are calculated and utilized for normalization. A top1 method is then used for protein quantification.

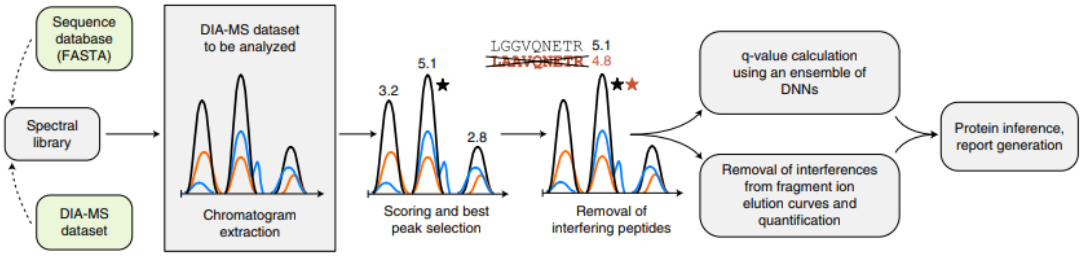

Figure 1.12 *DIA-NN workflow. Adapted from (Demichev et al., 2020)*

Section 1- Chapter 3

Aim of the PhD project

The demand for NPs, especially phytochemicals, in cosmetics is growing. This is leading to an increased pressure on the production of these molecules and particularly of plant extracts, that often are more effective than isolated compounds, due to the synergic effects between the different constituents (Caesar and Cech, 2019). In particular, plant cell culture extracts have been proposed to substitute plant extracts as they are bio-sustainable, contaminant-free and standardized secondary metabolites mixtures (Barbulova et al., 2014).

This PhD project has met the interest of the Arterra Bioscience S.p.A in performing a broad chemical and biological characterization of cell plant extracts in the prospective to exploit them as cosmetic ingredients. Indeed, Arterra is a biotech company involved in the research of various bioactive natural ingredients: it develops technological platforms, extraction processes and raw materials for use in cosmetics, agriculture and nutraceutics sectors.

The determination of the chemical composition of natural extracts is crucial to explore the full spectrum of their biological activities. In particular, we proposed to define the metabolic profile of Arterra's extracts by mass spectrometry, analysing data through the innovative Global Natural Products Social Networking (GNPS) platform (M. Wang et al., 2016).

The evaluation of their biological activities of cosmetic interest was carried out by a panel of *in vitro* and *ex vivo* experiments. Moreover, during my internship as visiting PhD at Necker Proteomics Platform, under the supervision of Dr. Ida Chiara Guerrera, a data-independent mass spectrometry-based label-free global proteomics approach has been employed to elucidate the mechanism of action of one of the investigated Arterra's extracts.

SECTION 2

Oenothera biennis cell extract as skin anti-aging natural weapon

Adapted from

Ceccacci, S., De Lucia, A., Tito, A., Tortora, A., Falanga, D., Arciello, S., Ausanio, G., Di Cicco, C., Monti, M.C., Apone, F., 2021. An *Oenothera biennis* Cell Cultures Extract Endowed with Skin Anti-Ageing Activity Improves Cell Mechanical Properties. Metabolites 11, 527.

Section 2- Chapter 1

Introduction

2.1.1 *Oenothera biennis* L.

The biennial herbaceous plant *Oenothera biennis* L., also known as evening primrose, belongs to the Onagraceae family (Figure 2.1). Originating in America (temperate and tropical climate zones), *Oenothera biennis* L. is currently also distributed throughout Asia and Europe. Its extracts are traditionally used for cosmetic applications due to their anti-inflammatory and antioxidant activities (Granica et al., 2013; Munir et al., 2017; Timoszuk et al., 2018).

Figure 2.1 *Oenothera biennis L.*

Methanolic extracts prepared from aerial parts and aqueous leaf extracts mainly contain phenolic acids and flavonoids, whereas methanolic extracts obtained from roots mostly contain sterols and triterpenes (Timoszuk et al., 2018). Alcoholic extracts from the aerial parts of *O. biennis* can protect HaCaT cells from H_2O_2-induced DNA damage via a mechanism that affects ROS elimination and by activating the Nrf2/HO-

1 signalling pathway (Lee et al., 2020). Hydroalcoholic aerial part extracts also showed anti-inflammatory activity by the inhibition of hyaluronidase and lipoxygenase in a concentration-dependent manner (Fecker et al., 2020; Granica et al., 2013).

Although the biological activities of alcoholic and hydroalcoholic aerial part extracts have been demonstrated, the most frequently used extracts of *O. biennis* are the oils obtained from seeds, which are extremely rich in fatty acids. Indeed, since their high content of linoleic acid (LA) and γ-linolenic acid (GLA), *O. biennis* seed oils improve the proper functioning of the skin and, in particular, they have showed beneficial effects in patients with chronic dermatitis (Schäfer and Kragballe, 1991; Timoszuk et al., 2018).

2.1.2 MYosin Light chain Kinase (MYLK) and skin aging

Skin aging is a process determined by both intrinsic (e.g., time, genetic factors) and extrinsic (e.g., UV exposure, pollution) factors (Wang and Dreesen, 2018). There is increasing evidence that it is enforced by the accumulation of senescent fibroblasts (Wlaschek et al., 2021). This causes a drop of skin mechanical features, mainly due to a decline in the amount of the extra-cellular matrix (ECM) proteins and to a lower fibroblast contraction ability, resulting in dermal thinning, loss of elasticity and increased wrinkling.

Indeed, senescent fibroblasts negatively influence their environment by acquiring a senescence-associated secretory phenotype (SASP). It includes matrix metalloproteinases (MMPs), responsible for the breakdown of the extra-cellular matrix. The most important dermis extra-cellular matrix components are proteins such as collagen I and III, laminin, periostin, tenascin, elastin, fibronectin and

proteoglycans. An alteration of their amount affects the interaction between matrix and cells and thus the proper texture of the dermis (Halper and Kjaer, 2014).

Skin mechanical properties are also based on the action of fibroblasts, the most abundant cells in the dermal matrix: they set up the proper tension of the skin, promoting the contacts between the matrix components. During aging, fibroblast ability to contract and stretch is partially lost. Indeed, senescent fibroblasts are no longer able to act correctly and consequently display a rounded morphology in contrast to the elongated one in young skin (Quan et al., 2013).

At the basis of their cellular cytoskeleton organization, there is the actin-myosin machinery which determines potential changes in their shape and structure. Indeed, the binding of actin and myosin induces a more compact cellular conformation, bringing ECM fibres closer together, guaranteeing the development of a healthy and compact tissue and preventing wrinkles (Mogilner and Keren, 2009).

Current evidence indicates that, during aging, the synthesis of MYosin Light chain Kinase (MYLK) decreases significantly. MYLK is a protein kinase able to phosphorylate a specific myosin domain, named myosin regulatory light chain, promoting actin binding and therefore cell contractility (Fujimura et al., 2011). When a low activity of this protein was detected, due for instance to a lesser protein expression, a corresponding reduction of matrix collagen contraction (Ehrlich et al., 1991) and actin polymerization (Konstantinidis et al., 2011) were measured. Actin cytoskeleton assembly is linked not only to the cell movement and ability to contract, but also to the production of ECM protein through the activation of TGF-β II receptor (TGFBRII) (Qin et al., 2018). TGFBRII belongs to TGF-β cell surface receptor complex that through activation of Smad transcription factors, regulates the expression

of many genes encoding component of ECM, including collagen, laminins, fibronectin and proteoglycan (Verrecchia and Mauviel, 2002). Actin cytoskeleton disassembly downregulates TGF-β II receptor. This down-regulation in turn decreases the production of collagen and other ECM proteins, resulting in loss of dermal mass and skin fragility.

2.1.3 Hydrophilic extract of *Oenothera biennis* cells (ObHEx) as object of study

Based on the biological activities of *Oenothera biennis* plant extracts, Arterra has developed a hydrophilic extract of *Oenothera biennis* cells (ObHEx). As described in detail later, we performed a broad chemical characterization of ObHEx and we tested its skin anti-aging activity, in particular its effects on MYLK and related pathways.

Section 2 – Chapter 2

Results

2.2.1 ObHEx chemical characterization

2.2.1.1 ObHEx qualitative analysis

UHPLC-MS/MS analysis of ObHEx was performed and high-resolution spectrometric data were exploited for the chemical characterization using the web-based mass spectrometry ecosystem Global Natural Products Social Molecular Networking (GNPS), that aids in the annotation of natural products (NPs) (see subparagraph 1.2.3.1) (M. Wang et al., 2016). Firsly, a GNPS spectral library search analysis was performed to identify natural compounds comparing their MS/MS spectra with those of structurally characterized metabolites. Chemical species not identified by GNPS were assigned accordingly to literature. As shown in Figure 2.2 and Table 2.1, the main secondary metabolites identified belong to lignans (salvadoraside, liriodendrin and syringaresinol glucoside) and triterpenes (myrianthic acid, arjunolic acid, asiatic acid and hederagenin). Among them, salvadoraside, liriodendrin and hederagenin have never been found before in *Oenothera* extracts.

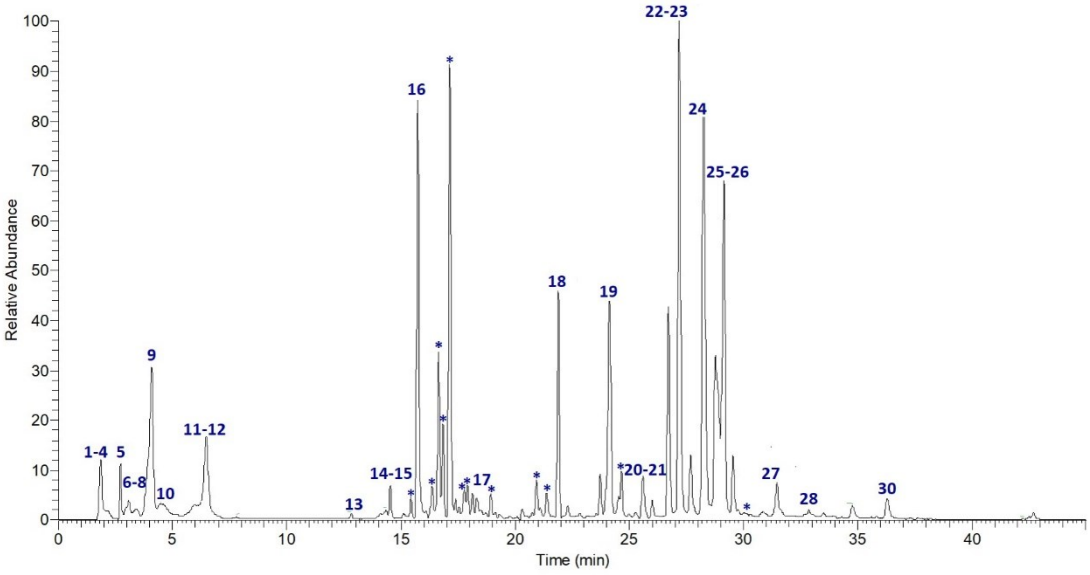

Figure 2.2 *Extracted-ion chromatogram of the main metabolites identified in ObHEx. Those indicated by * were included in molecular networks (MNs).*

Table 2.1 *Molecular formula (MF), Retention time (RT), MS data of compounds identified in ObHEx by GNPS search library and literature study.*

	Compound	MF (Mass error ppm)	RT min	Precursor ions m/z	MS^2 ions m/z (Relative intensity %)
1	Allantoin	$C_4H_6N_4O_3$ (2.5 ppm)	1.79	157.0360	114.0297 (87.36); 97.0031(100)
2	Pyridoxine	$C_8H_{11}NO_3$ (2.4 ppm)	1.79	168.0660	150.0550 (100); 122.0599 (45.03)
3	Cyclic Adenosine Monophosphate	$C_{10}H_{12}N_5O_6P$ (5.8 ppm)	1.88	328.0460	134.0461 (100)
4	Citric acid	$C_6H_8O_7$ (4.2 ppm)	1.88	191.0194	111.0076 (52.28); 87.0075 (24.13)
5	L-tyrosine	$C_9H_{11}NO_3$ (2.8 ppm)	2.73	180.0661	163.0392 (100); 119.0491 (68.65)
6	Arbutin	$C_{12}H_{16}O_7$ (6.6 ppm)	2.95	271.0830	108.0205 (100); 71.0126 (5.30)
7	Adenosine	$C_{10}H_{13}N_5O_4$ (6.4 ppm)	3.08	266.0901	134.0461 (100)
8	Xanthosine	$C_{10}H_{12}N_4O_6$ (6.0 ppm)	3.39	283.0690	151.0252 (100)
9	L-phenylalanine	$C_9H_{11}NO_2$ (3.0 ppm)	4.08	164.0711	147.0441 (100); 72.0078 (31.97)
10	Hydroxybenzoic acid glucoside	$C_{13}H_{16}O_8$ (6.4 ppm)	4.43; 5.92	299.0780	179.0341 (2.00/23.36);

					137.0233 (100/65.11)
11	Beta-D-fructofuranosyl 6-O-(4-hydroxybenzoyl)-alpha-D-glucopyranoside	$C_{19}H_{26}O_{13}$ (4.8 ppm)	6.46	461.1312	137.0234 (100); 93.0333 (16.37)
12	Panthothenic acid	$C_9H_{17}NO_5$ (4.6 ppm)	6.49	218.1033	146.0812 (75.65); 88.0391 (100)
13	Sinapyl alcohol diglucoside	$C_{23}H_{34}O_{14}$ (3.8 ppm)	12.84	533.1885	209.0814 (98.19); 194.0578 (100)
14	‡ Salvadoraside (Eklund et al., 2008)	$C_{34}H_{48}O_{18}$ (4.4 ppm)	13.89; 14.11	743.2790	389.1612 (100)
15	‡ Liriodendrin	$C_{34}H_{46}O_{18}$ (4.4 ppm)	14.35; 14.53	741.2633	417.1556 (41.89); 181.0498 (100)
16	Syringaresinol glucoside	$C_{28}H_{36}O_{13}$ (3.8 ppm)	15.73	579.2094	417.1560 (11.26); 181.0498 (100)
17	Hydroxydecanoate	$C_{10}H_{20}O_3$ (4.3 ppm)	18.37; 24.43	187.1337	169.1229 (2.26/2.99); 141.1273 (6.73/100)
18	‡ Myrianthic acid (Festa et al., 2015)	$C_{30}H_{48}O_6$ (4.4 ppm)	21.89	503.3389	485.3276 (51.41); 459.3505 (5.76)
19	‡ Arjunolic acid and Asiatic acid	$C_{30}H_{48}O_5$ (3.9 ppm)	24.13	487.3437	421.3104 (1.85); 409.3099 (5.57)
20	Dihydroxyoctadecenoic acid	$C_{18}H_{34}O_4$ (6.1 ppm)	24.98; 25.61	313.2392	183.1383 (100); 129.0910 (67.67/56.97)
21	Glycerophosphocholine (18:3)	$C_{26}H_{48}NO_7P$ (4.3 ppm)	25.27	562.3163 $(M+HCOOH-H)^-$	277.2172 (100); 224.0685 (0.97)
22	Glycerophosphoethanolamine (18:2)	$C_{23}H_{44}NO_7P$ (4.4 ppm)	26.71; 27.17	476.2793	279.2328 (100); 196.0374 (1.27/11.69)
23	Glycerophosphocholine (18:2)	$C_{26}H_{50}NO_7P$ (4.6 ppm)	26.79; 27.26	564.3322 $(M+HCOOH-H)^-$	279.2328 (100); 224.0688 (0.86/10.27)
24	Glycerophosphoethanolamine (16:0)	$C_{21}H_{44}NO_7P$ (5.1 ppm)	27.68; 28.25	452.2795	255.2328 (100); 196.0373 (1.29/10.72)
25	‡ Hederagenin	$C_{30}H_{48}O_4$ (4.4 ppm)	28.77	471.3490	405.3163 (2.40); 393.3136 (6.12)
26	Hydroxyoctadecadienoic acid	$C_{18}H_{32}O_3$ (5.1 ppm)	29.14; 29.53	295.2283	277.2172 (100); 171.1018 (64.06/58.66)
27	Glycerophosphoethanolamine (18:0)	$C_{23}H_{48}NO_7P$ (5.0 ppm)	30.87; 31.47	480.3109	283.2643(100); 196.0373 (1.53/11.63)
28	Coumaroyl triterpene	$C_{39}H_{54}O_6$ (4.0 ppm)	32.85	617.3862	453.3399 (0.69); 145.0284 (54.98)

29	Gamma-Linolenic acid	$C_{18}H_{30}O_2$ (5.4 ppm)	34.11	277.2177	233.2277 (0.71); 163.9689 (0.36)
30	Hydroxypalmitic acid	$C_{16}H_{32}O_3$ (6.3 ppm)	36.28	271.2285	253.2173 (2.75); 225.2220 (100)

‡ Identification and quantification have been performed through the comparison with the related analytical standard.

Secondly, for a deeper investigation, a Feature-Based Molecular Networking (FBMN) analysis was also carried out. It is able to group related NPs within a network since structurally similar molecules share similar MS/MS fragmentation patterns (Nothias et al., 2020). The molecular network, reported in Figure 2.3, shows that ObHEx contains many other uncharacterized triterpenes related to myrianthic acid (**18**, m/z 503.3389, RT 21.89 min: myrianthic acid identification has been confirmed by the comparison with its analytical standard). For instance, species at m/z 701 and 665 (red circles) were identified as glycosylated forms related to myrianthic acid or to its isomers. Indeed, in their MS2 spectrum, they show the common fragmentation pattern of glucose (m/z 59, 71, 89, 101, 113) in addition to the peak at m/z 503.

Similarly, reported ions at m/z 729, 703, 687, 685, 683 (blue circles) were assigned to glycosylated forms related to species at m/z 531, 505, 489, 487 and 485: their univocal identification has not been achieved, but they all are supposed to be triterpenes, related to myrianthic acid or to its isomers, due to their MS/MS fragmentation pattern. Recently, myrianthic acid and one triterpene showing $[M–H]^-$ at m/z 485 were isolated from another species of *Oenothera*, *Oenothera maritima*, thus well correlating with our results (Festa et al., 2015).

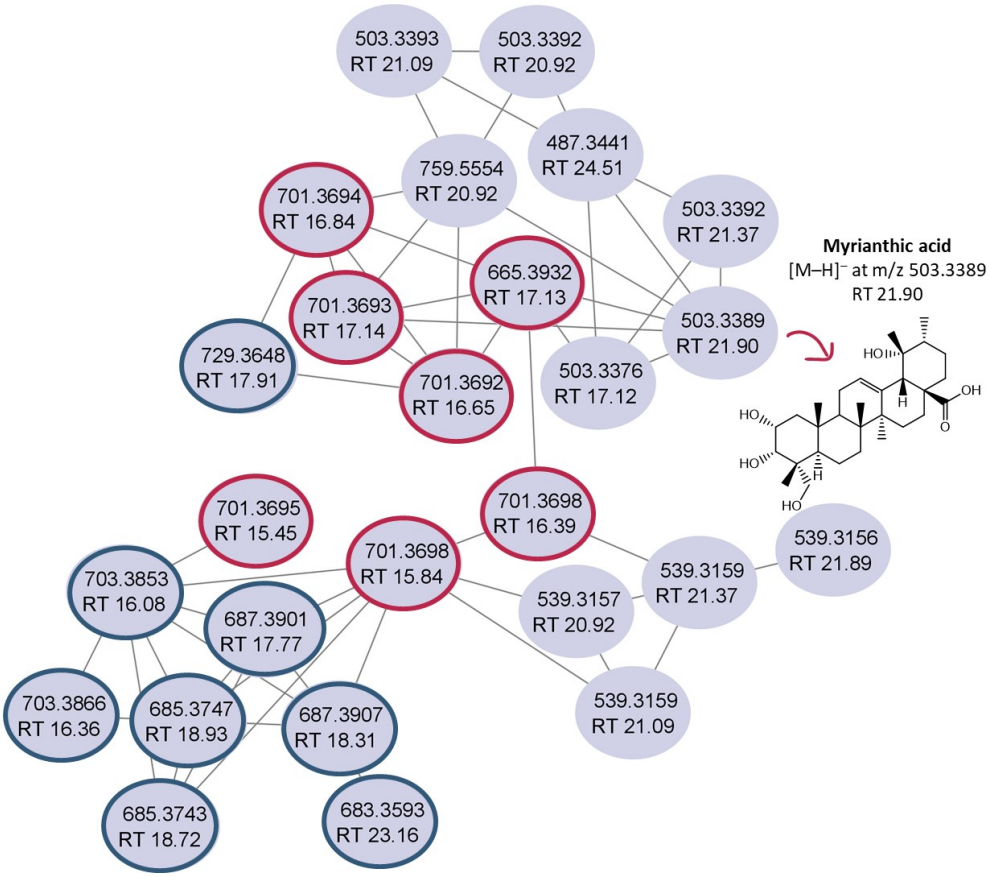

Figure 2.3 *Molecular network showing the presence of glycosylated forms related to myrianthic acid or its isomers (circled in red) or to other uncharacterized triterpenes (circled in blue) in ObHEx.*

FBMN analysis also provided information on the metabolites at m/z 617.3862 (MS2 ions at m/z 453, 145 and 119), present in molecular network shown in Figure 2.4 and not reported in literature for *Oenothera* species. This m/z value and its fragmentation match with 2-O-E-p-coumaroyl alphitolic acid or its isomers proving, at least, the presence of triterpene coumaroyl (green circles) and also caffeoyl (orange circles) esters in the extract. Indeed, MS2 spectra of the species at m/z 649 (RT 25.72 and 27.19) show the presence of ions at m/z 179, 161 and 135 due to the presence of caffeic acid moiety, whereas MS2 spectra of the other species reported in Figure 2.4

at m/z 633 (RT 26.88, 27.20, 28.12 and 28.43), 649 (RT 24.18, 24.65, 24.83) and 661 (RT 30.28) show ions at m/z 145 and 119, which are characteristic for coumaroyl moiety.

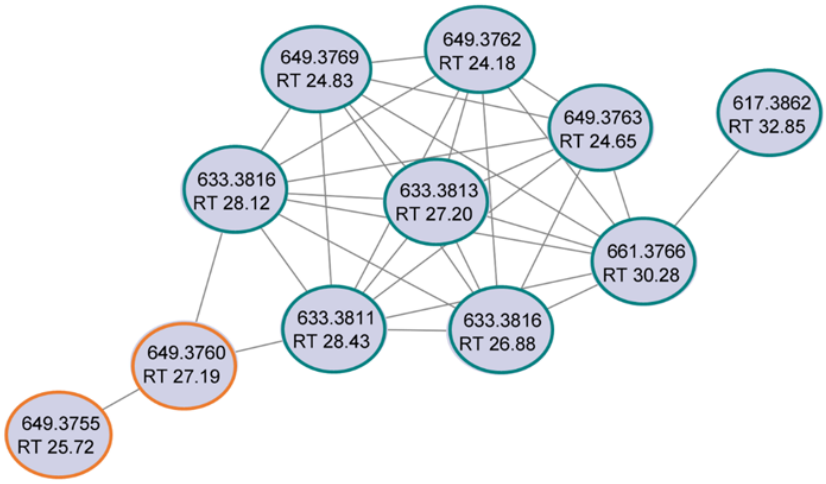

Figure 2.4 *Molecular network showing the presence of triterpene coumaroyl (circled in green) and caffeoyl (circled in orange) esters in ObHEx.*

2.2.1.2 ObHEx quantitative analysis

The content of some identified lignans and triterpenes was determined. Quantification methods were validated as reported in Table 2.2. All calibration curves showed good linearity ($R^2 \geq 0.9911$) within the tested ranges. Moreover, the limit of detection (LOD) and the limit of quantification (LOQ) indicated that the used methods were distinguished by high sensitivity. The obtained results from the quantitative analysis (Table 2.3) showed that liriodendrin and hederagenin were the main represented lignan and triterpene, respectively.

Table 2.2 *Characteristics of the quantitative evaluation of lignanic and triterpenic compounds.*

Compound	Range (nM)	Calibration curve	R^2	LOD (nM)	LOQ (nM)
Salvadoraside	250-25000	y = 1E+07x	R^2 =1.000	76	250
Liriodendrin	250-25000	y = 2E+07x	R^2 =0.9995	76	250
Myrianthic acid	100-25000	y = 2E+07x	R^2 = 0.9999	8	25
Arjunolic acid	100-25000	y = 2E+07x	R^2 = 0.9971	3	10
Asiatic acid	100-25000	y = 3E+07x	R^2 = 0.9911	3	10
Hederagenin	100-25000	y = 4E+07x	R^2 = 0.9967	3	10

Table 2.3 *Lignanic and triterpenic content.*

Compound	Amount (µg/g of extract)	% RSD
Salvadoraside	7.93	3.69
Liriodendrin	51.11	7.21
Myrianthic acid	22.09	3.85
Arjunolic acid	28.58	1.95
Asiatic acid	30.73	3.09
Hederagenin	78.21	0.61

2.2.2 Evaluation of ObHEx biological activity by *in vitro* and *ex vivo* assays

2.2.2.1 Cytotoxicity tests (MTT assay)

Cytotoxicity tests were performed on HDF (Human Dermal Fibroblasts) to determine the range of concentrations in which ObHEx was not dangerous for the human cells in the growth phase. The treatment was carried out with increasing concentrations of the extract between 0.05% and 0.0004% (500 µg/mL and 4 µg/mL) for approximately 48 h, and, after a period of 16 h incubation, the colorimetric reaction was measured at 595 nm. The results of the MTT indicated that the hydro-extract

concentrations equal to or less than 0.01% did not cause any toxicity on the cells. The CC_{50} was 0.026% as calculated using the software provided on the website https://www.aatbio.com/tools/ic50-calculator. For convenience, we decided to use the concentration of 0.006% as the maximum dose in the cell assays.

2.2.2.2 Analysis of MYLK gene expression in HDF

The activity of ObHEx was tested in HDF on the expression of the MYLK gene, which encodes for the kinase responsible for the phosphorylation of myosin light chain. The results, reported in Figure 2.5, showed that the treatment with the extract at both concentrations increased MYLK gene expression by about 50%, similarly to the positive control TGF-β.

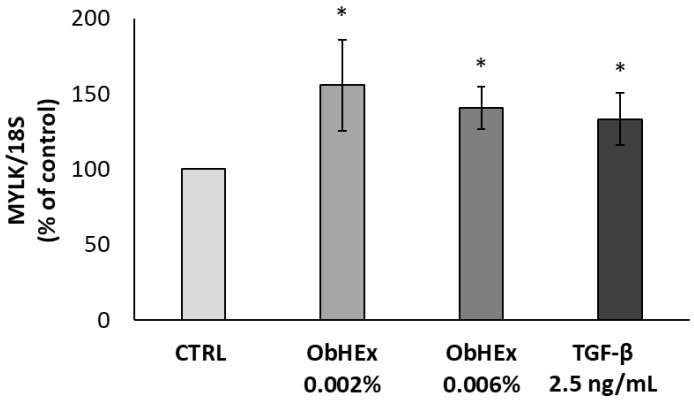

Figure 2.5 *Bar graphs showing the ability of ObHEx to increase the expression of the MYLK gene. The error bars represent the standard deviations while asterisks indicate significant variations (*p<0.05; **p<0.01; ***p<0.001), according to Student's t-test.*

2.2.2.3 Analysis of the contraction capacity of a collagen matrix

To evaluate the activity of ObHEx on the contractile capacity of collagen fibers, we used HDF dispersed in collagen gel discs (Jin et al., 2015). As shown in Figure 2.6, the extract, at the lower concentration, induced a significant increase in the contraction of the collagen disc, suggesting a potential effect on collagen firmness. The treatment with ML7 (1-(5-iodonaphthalene-1-sulfonyl)-1H-hexahydro-1,4-diazepine), a MYLK inhibitor, abolished this increase indicating that both the extract and TGF-β act through MYLK for collagen disc contraction.

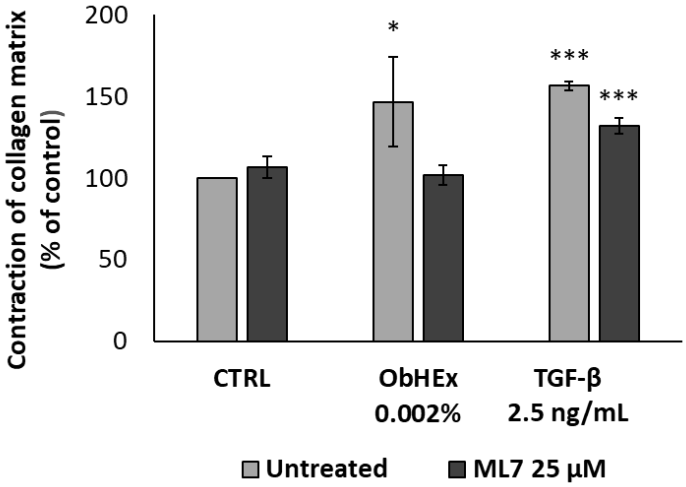

Figure 2.6 *Bar graphs showing the ability of ObHEx to improve contractile capacity of collagen fibers. The error bars represent the standard deviations while asterisks indicate significant variations (*p<0.05; **p<0.01; ***p<0.001), according to Student's t-test.*

2.2.2.4 Measure of actin polymerization level in HDF

The capacity of ObHEx to stimulate actin polymerization was investigated by measuring the level of polymerized actin in the cells treated with the extract or the positive control TGF-β, alone and in the presence of ML7. As shown in Figure 2.7, the

treatment with both the concentrations of the extracts yielded an increase in the amount of polymer actin by about 50%, compared to 33% of TGF-β. Again, the treatment with ML7 completely abolished this effect, suggesting an involvement of MYLK in the polymerization of actin filaments.

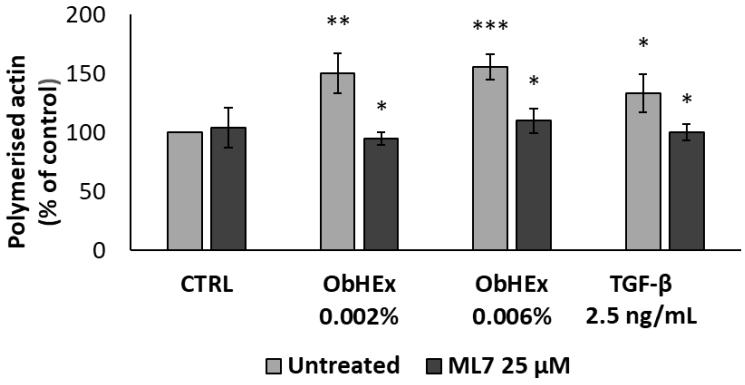

Figure 2.7 *Bar graphs showing the ability of ObHEx to stimulate actin polymerization. The error bars represent the standard deviations while asterisks indicate significant variations (*p<0.05; **p<0.01; ***p<0.001), according to Student's t-test.*

2.2.2.5 Analysis of TGFβRII/SMAD pathway in HDF

To verify whether the increase in actin polymerization and collagen contraction of cells treated with ObHEx was also associated with an activation of signal transduction pathway mediated by TGFβRII, we firstly observed the expression of TGFβRII gene and, then, we transfected HDF with the SMAD2-luciferase reporter plasmid and evaluated the increase in luciferase activity in response to ObHEx treatment. The results, reported in Figure 2.8 (A and B), indicated that the treatment with ObHEx at 0.002% and 0.006% increased the expression of TGFβRII in a way similar to the TGF-β used as positive control and parallelly the increase in luciferase activity linked to SMAD2 was by 80 and 40%, respectively. A significant signal reduction was obtained

when the cells were treated with ML7, showing that also this activity was linked to MYLK.

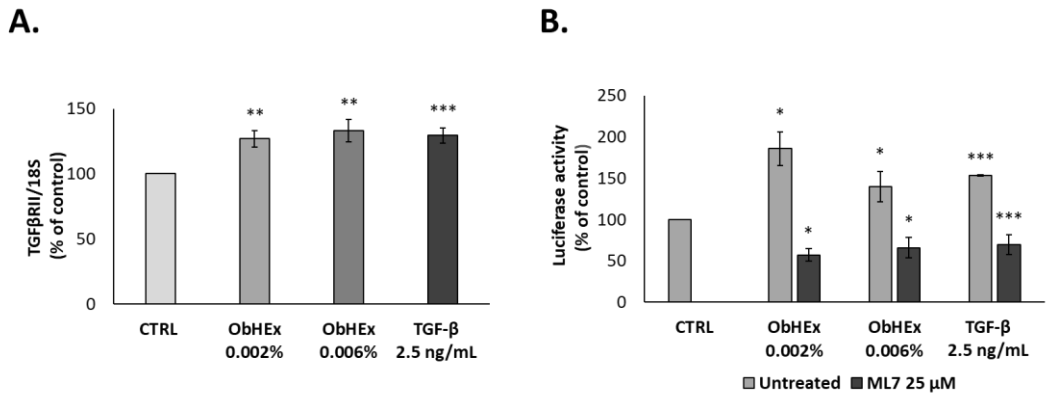

Figure 2.8 (A, B) *Bar graphs showing the ability of ObHEx to increase* TGFβRII *expression (A) and luciferase activity linked to SMAD2 (B). The error bars represent the standard deviations while asterisks indicate significant variations (*p<0.05; **p<0.01; ***p<0.001), according to Student's t-test.*

2.2.2.6 Analysis of pro-collagen I, tropoelastin and periostin synthesis

As consequence of TGFβRII signal transduction activation, we analysed the synthesis of the main extra-cellular matrix proteins such as procollagen type I, tropoelastin and periostin in HDF treated with ObHEx at 0.002%. As shown in Figure 2.9, ObHEx increased the production of the indicated proteins by about 98%, 75% and 51%, respectively, similarly to the positive control TGF-β. The measures were performed by ELISA assay, using specific antibodies against pro-collagen I, tropoelastin and periostin.

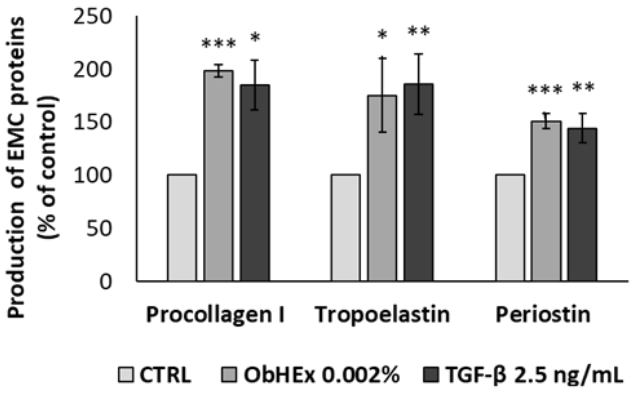

Figure 2.9 *Bar graphs showing the ability of ObHEx to boost the production of pro-collagen I, tropoelastin and periostin in HDF. The error bars represent the standard deviations while asterisks indicate significant variations (*p<0.05; **p<0.01; ***p<0.001), according to Student's t-test.*

2.2.2.7 Analysis of MYLK, phospho-myosin, collagen I and tropoelastin levels in skin explants

As shown in Figure 2.10 (A-C), ObHEx produced a significant increase of the production of MYLK and phosphorylated myosin in human skin explants, too.

Collagen I and tropoelastin induction was also analyzed in skin explants pretreated with ObHEx and then treated with hydrocortisone for 8 days to simulate chronological ageing (Garre et al., 2018). The treatment with hydrocortisone reduced the amount of collagen I and tropoleastin by more than 100% and the presence of 0.002% ObHEx restored the amount of tropoelastin by almost 91% and of collagen I by 120%, comparable to ascorbate used as positive control (Figure 2.11 A-C). This suggests a potential anti-aging effect of ObHEx, particularly effective in increasing the firmness of the skin by acting on the dermal matrix components.

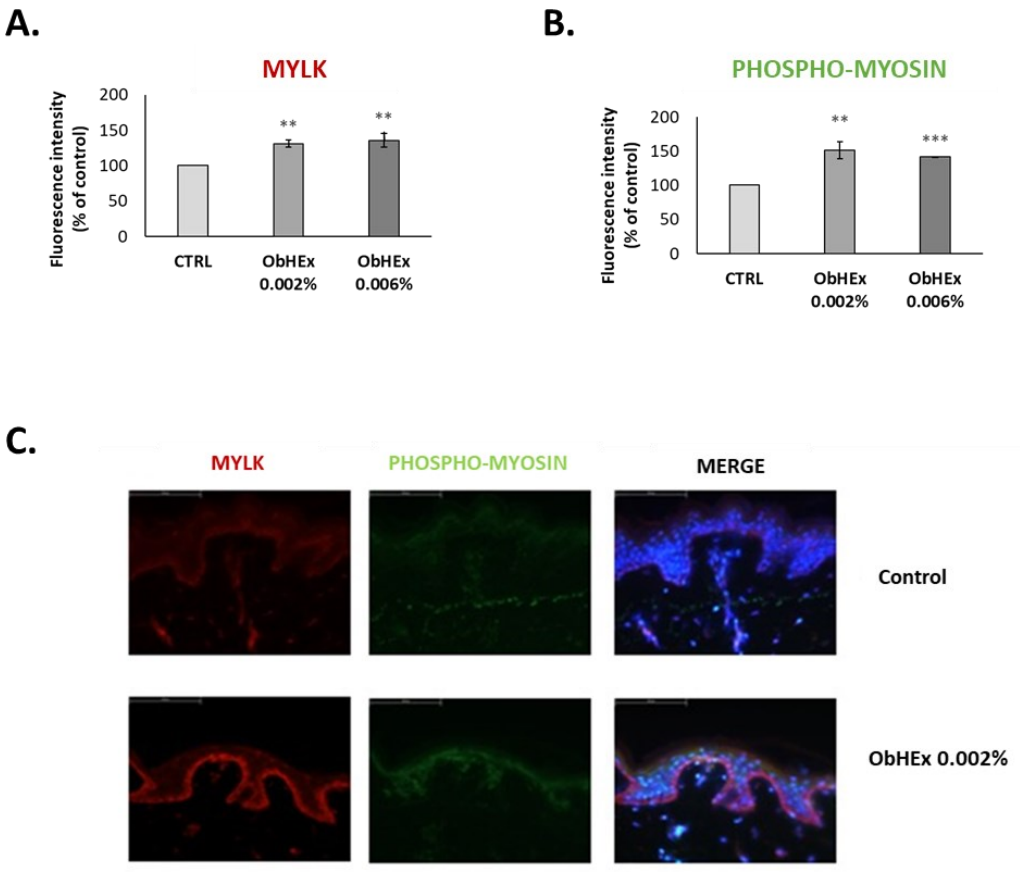

Figure 2.10 *(A,B) Bar graphs showing the effect of ObHEx to increase the production of MYLK (A) and phospho-myosin (B) in skin explants. The quantization was performed by detection with antibody labeled with fluorophore. The error bars represent the standard deviations while asterisks indicate significant variations (*p<0.05; **p<0.01; ***p<0.001) according to Student's t-test. (C) Photographs of skin sections in which the indicated proteins have been labeled with specific antibody. The abbreviation "merge" indicates the overlapping of the photographs where the fluorescence of the specific protein is highlighted with those in which the nuclei have been stained with 4',6-diamidine-2-phenylindole (DAPI).*

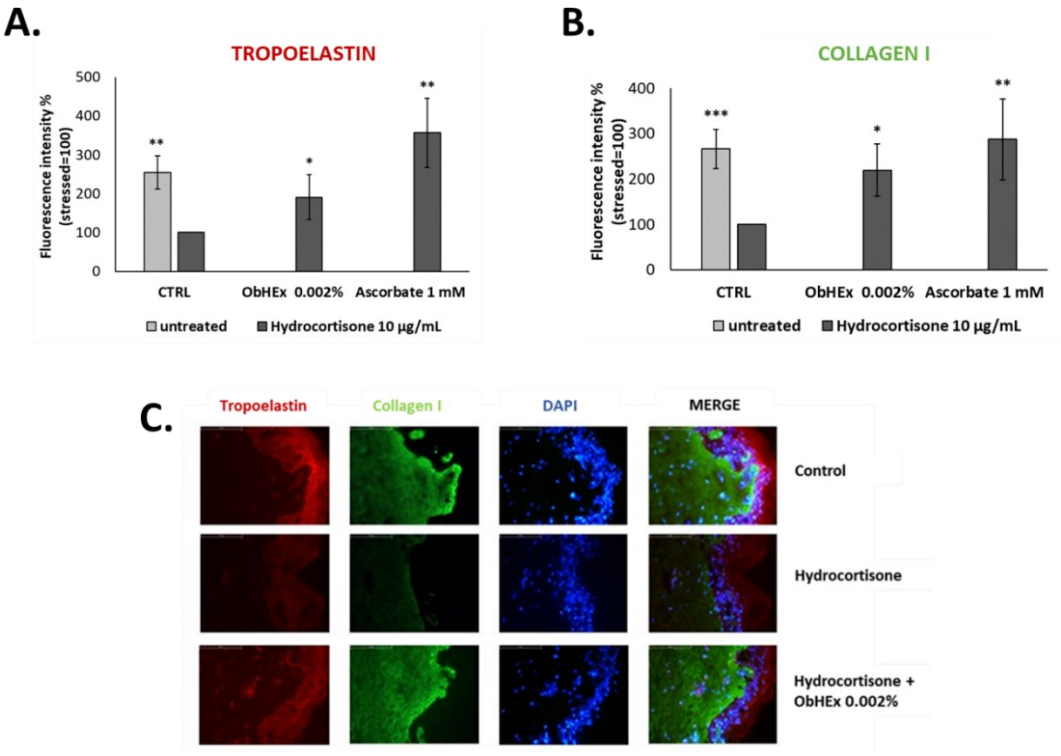

Figure 2.11 *(A,B) Bar graphs showing ObHEx ability to restore the amount of tropoelastin (A) and collagen I (B) in skin explants after treatment with hydrocortisone; the quantization was performed by detection with antibody labeled with fluorophore. The error bars represent the standard deviations while asterisks indicate significant variations (*p<0.05; **p<0.01; ***p<0.001) according to Student's t-test. (C) Photographs of skin sections in which the indicated proteins have been labeled with specific antibody. The abbreviation "merge" indicates the overlapping of the photographs where the fluorescence of the specific protein is highlighted with those in which the nuclei have been stained with 4',6-diamidine-2-phenylindole (DAPI).*

2.2.2.8 Atomic Force Microscopy (AFM) on skin explants

In order to collect more information about skin biomechanical properties promoted by the treatment with ObHEx, in collaboration with Prof. Giovanni Ausanio of the University of Naples "Federico II, we evaluated elasticity, an intrinsic mechanical property of skin samples in terms of their Young's moduli (Iravanimanesh et al., 2017).

To calculate the elastic modulus, both on treated and untreated skin samples, we collected Force curves by an Atomic Force Microscope (AFM) and fit them with Hertz model (Hoffman et al., 2011; Thomas et al., 2013) As shown in Figure 2.12, skin samples treated with the extract had a lower Young's module values compared to untreated samples, suggesting an improvement of skin elastic properties. In particular, untreated skin samples disclosed a mean Young's modulus value of 0.37 ± 0.15 GPa while skin samples treated with ObHEx showed a lower mean value of 0.07 ± 0.02 GPa. Skins Young's modulus values were in accordance with literature (Chen and Bhushan, 2013; Tang et al., 2010; Yuan and Verma, 2006).

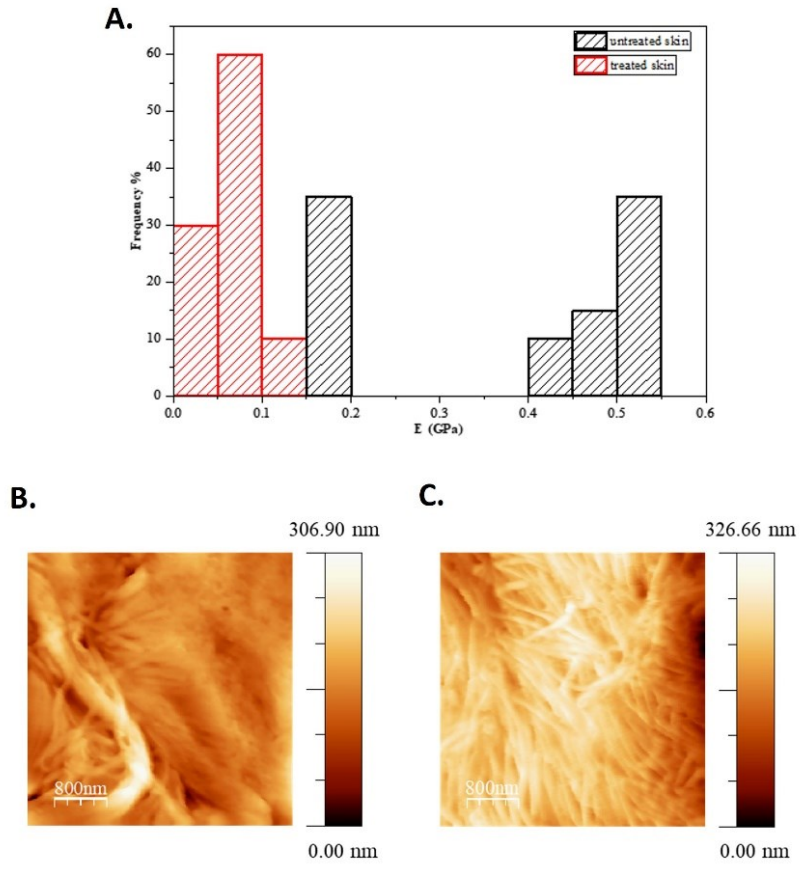

Figure 2.12 *(A) The histogram shows the distribution of Young's modulus values calculated applying Hertz's model on Force curves in ten different points of the same untreated (black bars) and treated (red bars) skin sample surfaces. (B, C) Images of*

fibrils in the case of untreated (B) and treated (C), which were acquired in contact mode.

Section 2 – Chapter 3

Discussion

An *Oenothera biennis* cell culture aqueous extract (ObHEx) was examined as a promising source of bioactive molecules endowed with skin anti-aging activity. Indeed, ObHEx has been investigated by high resolution UHPLC-MSMS analyses coupled to bioinformatics approaches to achieve a wide chemical characterization. It has been realized mainly using GNPS to speed up the identification process, comparing the MS/MS spectra with those of structurally characterized metabolites, and, furthermore, to disclose new unexpected species, grouping similar NPs within a network. Bioactive lignans and triterpenes such as salvadoraside, liriodendrin, myrianthic acid, arjunolic acid, asiatic acid and hederagenin were identified. Liriodendrin (Li et al., 2015) and myrianthic acid (Hu et al., 2013) exhibited strong antioxidant activity, while hederagenin showed skin anti-aging properties due to a reduction of cellular oxidation and activation of proteasome function (Gonos et al., 2010). However, arjunolic and asiatic acids were considered the main responsible for some of the following tested activities since they stimulate collagen I synthesis. Indeed, it has been demonstrated that ObHEx improved the skin biomechanical properties, which mostly depend on the relative amount of the different components of the ECM and on how the fibroblasts are capable of contracting and providing the right tension to the dermal fibers. In fact, ObHEx promotes collagen matrix contraction and actin polymerization by increasing the expression of MYLK gene, thus enhancing the contraction force of dermal fibroblasts. Assembly of actin cytoskeletron

upregulates TGF-β type II receptor and increases the levels of TGF-β regulated ECM proteins, consistent with the stimulation of TGF-β/Smad signaling. Indeed, ObHEx induces the production of type I collagen, periostin and tropoelastin. Therefore, all these properties make it a good promising candidate ingredient to be used in cosmetic formulations to fight the age-associated loss of skin firmness and elasticity. This assumption was supported by the results obtained in the AFM analysis, which showed that the treatment of skin slices with ObHEx produced an improvement of the skin mechanical properties, detected as a decrease of the Young's modulus, indicating a significant reduction of skin stiffness and rigidity.

Section 2 – Chapter 4

Materials and Methods

2.4.1 Plant tissue cultures and extract preparation

Oenothera biennis plants were provided by GEEL Floricultura s.s and they are of Italian origin (avoiding the application of Nagoya protocol). Cell cultures were obtained from leaves of *Oenothera biennis* plants. Once the callus was obtained, the cells were transferred to the liquid growth medium (Gamborg B5, supplemented with 2,4 dichlorophenoxyacetic acid (1 mg/L), adenine (1 mg/L) and kinetine (0.01 mg/L)). Then, they were grown as suspension cultures under orbital shaking. When the cultures of about 150 g/L were obtained, the cells were collected and lysed in a phosphate buffer (PBS) at pH 7.4 to prepare a water-soluble extract, which was lyophilized. The powder was dissolved in water or cell culture media at the appropriate concentrations for testing.

2.4.2 UHPLC-MS/MS analysis for chemical characterization

ObHEx (50 mg/mL) was prepared and submitted to a biphasic butanol/water extraction. The butanolic fraction was dried and dissolved in methanol (10 mg/mL) before the UHPLC-MS/MS analysis. It was carried out on a Q-Exactive Classic Mass Spectrometer from Thermo-Scientific equipped with a Thermo Scientific™ UltiMate™ 3000 UPLC system. All the chromatographic runs were performed using a Phenomenex Luna® C18 100 Å (150 x 2.0 mm, particle size 3 µm) column at 40°C and flow rate of 0.200 mL/min. The injection volume was 5 µL. The mobile phase

consisted of A (water from Romil at 0.1% acetic acid) and B (100% acetonitrile from Romil), using a gradient elution of 5% B at 0-5 min, 5-14% B at 5-8 min, 14-32% B at 8-11 min, 32-95% B at 11-32 min, 95-98% B at 32-33 min, 98% B at 33-38 min, 98-5% B at 38-39 min and 5% B at 39-45 min. All the MS and MSMS analysis were carried out in ESI negative mode with the sheat gas flow rate at 30 (arbitrary units), the auxiliary gas flow rate at 5 (arbitrary units), the spray voltage at 3.2 kV, the capillary temperature and the auxiliary gas heater temperature at 300 °C. Data were acquired with a Full MS/dd-MS2 (Top5) mode. Full MS setting were: resolution of 70.000, AGC target of 1e6, maximum IT of 200 ms and scan range from 100 to 800 m/z. dd-MS2 settings were: resolution of 17.500, AGC target of 2e5, maximum IT of 65 ms, isolation window of 1.5 m/z and NCE of 35.

2.4.3 Global Natural Products Social Molecular Networking analysis

For metabolite identification it has been used Global Natural Products Social Molecular Networking (GNPS at https://gnps.ucsd.edu). All those MS and MSMS signals not assigned by GNPS were carefully inspected and assigned accordingly to literature. Raw files were converted to mzXML format by MS Converter General User Interface software (ProteoWizard; http://proteowizard.sourceforge.net/project.shtml), before the GNPS spectral library search analysis. It was achieved using precursor ion mass tolerance of 0.025 Da, fragment ion mass tolerance of 0.02 Da, minimum matched peaks of 2 and score threshold of 0.7. The results obtained were manually verified. mzXML data were processed using MZmine 2.53 before the Feature-Based Molecular Networking (FBMN) job on GNPS. The mass detection step was performed using the Centroid mass detector and keeping the noise level at $5e^3$. The ADAP

(Automated Data Analysis Pipeline) chromatogram building was realized with the following settings: min group size in number of scans of 5, group intensity threshold of $5e^3$, min highest intensity of $5e^4$, m/z tolerance of 0.01 m/z or 10 ppm. The chromatogram deconvolution was achieved using Wavelets (ADAP) as algorithm, S/N threshold of 3, min feature height of $10e^5$, coefficient/area threshold of 5, peak duration range of 0.10-3.00 min and RT wavelet range 0.00-0.05. Chromatograms were deisotoped using the isotopic peaks grouper algorithm with a m/z tolerance of 0.001 m/z or 5.0 ppm and a RT tolerance of 0.10 min. FBMN job was performed using parent mass tolerance of 0.02 Da and a MS2 fragment ion tolerance of 0.02 Da. Edges were filtered to have a score threshold of 0.7 and minimum 2 matched peaks. Moreover, the maximum number of neighbour nodes for each node was set to 10. The obtained network file was imported into Cytoscape 3.9.1 (Shannon et al., 2003).

2.4.4 Quantitative analysis of lignans and triterpenes

The same UHPLC conditions reported for the qualitative analysis were used for the quantitative analysis of lignans, while for that of triterpenes they were optimized in order to separate two pairs of isomers, arjunolic and asiatic acid. The analysis was performed on a Q-Exactive Classic Mass Spectrometer, as previously described. The separation was carried out by a Phenomenex Kinetex® EVO C18 300 Å (150 x 2.1 mm, particle size 5 μm). The mobile phase consisted of A (5 mM ammonium acetate aqueous solution, pH 9.00 adjusted by ammonium hydroxide) and B (100% acetonitrile) using a gradient elution of 17–28% B at 0–18 min, 28–65% B at 18–22 min, 65–75% B at 22–26min, 75-95% at 26-26,5 min, 95% at 26,5-30 min, 95-17% at 30-30,1 min, 17% at 30,1-42 min. The flow rate was 0.450 mL/min and the injection

volume was 5 µL. For both lignans and triterpenes, data were acquired with a Full MS-SIM and PRM mode. Full MS-SIM settings were: resolution of 70.000, AGC target of $3e^6$, maximum IT of 200 ms and scan range from 200 to 800 m/z for lignans and from 400 to 850 m/z for triterpenes. PRM settings were: resolution of 70.000, AGC target of $2e^5$, maximum IT of 100 ms, isolation window of 1.0 m/z and NCE of 35 in the case of lignans and 50 in that of triterpenes. We purchased salvadoraside (#598- XS172930) from Biosynth Carbosynth, liriodendrin (#SMB00181) and arjunolic acid (#SMB00119) from Sigma-Aldrich, asiatic acid (#0027) from Extrasynthèse and hederagenin (#89706) from PhytoLab GmbH & Co.KG. Myrianthic acid was a gift of Prof. Maria Valeria D'Auria, University of Naples. The calibration curves were obtained by injecting standards solutions in the concentration range of 0.25-25 µM for lignans and 0.1-25 µM for triterpenes. The limit of detection (LOD) and limit of quantification (LOQ) for standards were determined on the basis of the signal to noise (S/N) ratio.

2.4.5 Skin cell cultures and explants

Human Dermal fibroblasts (HDF) were maintained in Dulbecco's Modified Eagle Medium (DMEM; Sigma Aldrich, St. Louis, MO, USA) supplemented with 10% of fetal bovine serum (FBS; Sigma Aldrich, St. Louis, MO, USA) in 95% air, 5% CO_2, and humidified atmosphere at 37°C. Skin explants, obtained from the skin of healthy female donors (aged 44-47) at the surgery center Villa Cinzia (Naples, IT), were cultured in 24-transwell plates in DMEM/FBS plus antibiotics in air-liquid conditions at 37°C in 5% CO_2 humidified air. All donors had given their written informed consent for the use of the skin tissues, according to the Declaration of Helsinki.

2.4.6 Cytotoxicity tests

Cytotoxicity tests were based on the use of the MTT compound [3-(4,5-dimethylthiazolyl)-2,5-diphenyltetrazolium-bromide] (Mosmann, 1983). The cells were grown in 96-well plates in the DMEM (Dulbecco's Modified Eagle Medium) culture medium, supplemented with 10% fetal bovine serum, for approximately 8 hours. After treatment with ObHEx between 0.05% and 0.0004% (500 μg/mL and 4 μg/mL) for 48 hours, the cells were washed in PBS and incubated with 100 μl/well of "reaction buffer" containing: 10 mM of Hepes, 1.3 mM $CaCl_2$, 1 mM $MgSO_4$, 5 mM of glucose and 0.5 mg/mL of MTT colorimetric substrate in buffer PBS at pH 7.4. After 3 hours of incubation at 37 °C in 5% CO_2, 100 μl of solubilizing solution containing 10% of Triton-X100, 0.1 N of HCl in absolute isopropanol were added to each well. After 16 h incubation, the colorimetric reaction was measured at 595 nm with the Victor3 plate reader (PerkinElmer).

2.4.7 Analysis of MYLK and TGFβRII gene expression in HDF

1 x 10^5 of HDF per well were grown in 6-well plates in DMEM at 2% FBS. After 24 h FBS was further diluted to 0.5% and the cells were treated with 0.002% and 0.006% concentrations of ObHEx or TGF-β 2.5 ng/mL, followed by an incubation of 2 h for MYLK and 48 for TGFβRII. For RNA extraction, the "GenElute ™ Total RNA Purification" kit purchased by the company Merck was used. After the indicated treatments, the cells were washed with PBS, collected in lysis buffer and subjected to the extraction procedure as reported. The samples were treated with DNase I (Ambion) at 37 °C for 30 minutes, to remove genomic DNA contaminant. 2 μl of each sample

were loaded onto gel 1% agarose in the presence of denaturing loading dye for the purpose of quantize the amount of RNA in reference to a specific marker for RNA (ThermoScientific). 300 ng of total RNA was retro-transcribed using the enzyme Reverse transcriptase (ThermoScientific). Semi-quantitative RT-PCR were conducted using as internal standards the pair of universal primers 18S primer/competimer (Ambion). The PCR products were separated on 1.5% agarose gel, viewed employing the Geliance tool (PerkinElmer) and analyzed by densitometry using the Genetools software. The sequences of the primers used for amplification were the following: MYLK FW: ATCAAACTGTCAAGTTCAG, MYLK Rv: AGGCACTGCGTGCAGTCCA, TGFBR2 FW: GTCACTGACAACAACGGT, TGFBR2 RV: ATGTCAGAGCGGTCATCT.

2.4.8 Analysis of the contraction capacity of a collagen matrix

2.0 x10^5 HDF cells were resuspended in 5x DMEM growth medium (Gibco) in a 24-well plate, and a 2 mg/mL solution of collagen from bovine skin (Sigma-Aldrich) was added to each well. The pH of the solution was adjusted to 7.2. The plate was incubated at 37 °C for 45 minutes, to allow solidification of the collagen gel. DMEM supplemented with 10% FBS and/or ML7 25 μM, as MYLK protein inhibitor, was added later. After 16h, ML7 was cleared and ObHEx at the concentration of 0.002% in DMEM with 2% FBS was added. TGF-β 2.5 ng/mL was used as a positive control. The disc of collagen formed was immediately detached from the well by using a sterile microspatula in order to promote its contraction. The areas of the disc of each condition were measured at time 0 and at 5 hours and analyzed using ImageJ software.

2.4.9 Analysis of the degree of actin polymerization in HDF

1.5 x 10^5 of HDF cells per well were grown in 24-well plate and the next day the medium was added with 2% FBS and the Cytochalasin B, which is an inhibitor of actin polymerization, at 2 μM for 30 minutes. After 30 minutes, the cells were treated with ObHEx (0.002% and 0.006%) or TGF-β (2.5 ng/mL), used as a positive control, alone or in presence of ML7 (25 μM). After 30 minutes of treatment, the cells were fixed with 4% paraformaldehyde (PFA) in buffer phosphate for 30 minutes on ice. Then, they were washed with PBS and permeabilized with a solution of phosphate buffer and Triton-X100 at 0.2% for 30 minutes. Subsequently, the cells were incubated with a solution of 0.4 μM of phalloidin conjugated with rhodamine (Santa-Cruz Biotechnology) for 1 hour in the dark. At time 0 and after 18h, the fluorescence was measured at 540/570 nm using the Victor3 plate reader (PerkinElmer).

2.4.10 Analysis of SMAD2 pathway in HDF

HDF cells were seeded at a density of 3 × 10^3 in 96-well plates and after 16 h were transfected using X-tremeGene™ HP DNA transfection Reagent (Roche Diagnostics) with SMAD2 reporter vector according to manufacturer's instructions. After 24 h, the cells were treated with ObHEx, or TGF-β 2.5 ng/mL, alone or in combination with ML7 25 μM for 24h. At the end of the incubation, the cells were washed with PBS and the activity of luciferase was determined by using the SteadyGlo Luciferase assay system (Promega Corporation) in the Multiwell Plate Reader Victor Nivo (Perkin Elmer).

2.4.11 Analysis of pro-collagen I, tropoelastin and periostin synthesis

8 x 10^3 HDF per well were grown in 96-well plates and treated with the 0.002% of ObHEx or TGFβ 2.5 ng/mL. After 24 h, the cells were processed for ELISA using monoclonal primary antibody anti-procollagen type I (sc-166572, Santa-Cruz Biotechnology) followed by incubation with the secondary anti-mouse antibody labeled with peroxidase (170-6516, Biorad). The supernatants of the cells were coated on another plate for the detection of tropoelastin and periostin using the anti-tropoelastin rabbit antibody (ab21600, Abcam) or anti-periostin mouse antibody (sc-398631, Santa-Cruz Biotechnology) followed by incubation with secondary antibody anti-rabbit labeled with peroxidase (170-6515, Biorad). The colorimetric reaction was developed by adding 100 µl of an aqueous solution of OPD (O-phenylenediamine) 0.35 mg/mL in 50 mM citrate buffer and 0.012% hydrogen peroxide (H_2O_2). After 30 minutes, the absorbance was measured at 490 nm using the multiplate reader Victor Nivo (Perkin Elmer).

2.4.12 *Ex vivo* tests

ImmunoHistoFluorescence (IHF) of MYLK and phosphorylated myosin was evaluated in skin explants of 44–47-year-old donors. Human skin explants were cut with punch biopsy curettes of 8 mm and cultured in 24-well plates in DMEM with 10% FBS and antibiotics. The obtained punches were treated with 0.002% and 0.006% of ObHEx for 24 hours. They have been incubated in 15% sucrose, then in 30% sucrose and finally frozen. 10 µm sections were obtained using the CM1520 cryostat (Leica Microsystems). Slides with cryosections were hydrated for 30 minutes in PBS and placed in a "blocking" solution (6% BSA, 5% serum, 20 mM $MgCl_2$, 0.2% Tween) for

1 hour. Cryosections were incubated with the primary anti-MYLK rabbit antibody (1: 100, GeneTex) and the antibody primary anti-phospho-myosin (1:100 LifeTechnologies) for 16 hours at 4 °C. The slides were washed with PBS for 30 minutes and then incubated with the secondary anti-rabbit Alexa-Fluor 546 antibody (1: 1000; A11035 ThermoFisher) for 1 hour. The nuclei were stained with DAPI (4 ', 6-5 diamidino-2-phenylindole) 1µg/mL in PBS for 10min. The images were acquired with a fluorescence microscope and analyzed with the ImageJ software.

For IHF of tropoelastin and collagen I, skin explants of 36y old female donors were used. Skin biopsies were obtained as described above and pre-treated with 0.002% and 0.006% of ObHEx for 24 hours. Stress with hydrocortisone 10 µg/mL for 8 days was added in presence of ObHEx. Afterwards, biopsies were frozen as described above and the sections were incubated with the primary antibody anti-tropoelastin rabbit (1: 1000 ab21600, Abcam) and anti-collagen I (1:100 C2456 Merck) for 16 hours at 4 °C. The slides were analyzed as described above and the images were acquired and analyzed with the ImageJ software.

2.4.13 Atomic Force Microscopy (AFM) on skin explants

Elasticity of skin samples untreated and treated with ObHEx was evaluated measuring their Young's moduli by a method in nanometric scale based on Atomic Force Microscopy (AFM), developed not only for biological samples but also inorganic ones. These approaches are based on the Hertz's models assumptions and considered sample and cantilever as two springs in a series in AFM experiment setting. Briefly, skin explant treated with 0.006% of ObHEx and untreated skin samples were cut by cryostat in slices of 10 µm in thickness. Samples were storage at -12 °C, then

washed with PBS and examined at fixed temperature and relative humidity, 22 °C and 55% respectively. Each sample was investigated by a NanoScope IIIA AFM in Force Spectroscopy Single Mode using a pyramidal tip (RESP-20) with a spring constant of 0.9 N/m. To calculate Young's modulus, ten *Force curves* in ten different points of the same sample superficies were acquired. Each *Force curve* is a curve of deflection (Volt) *versus* displacement (nm) and can be converted in curves of Force (nN) *versus* separation (nm). In fact, each *Force curve* reports a loading and an unloading curve. They represent the tip's trend respect to the sample: when the tip is far from the sample, when they come into contact and the tip begins to deflect, and when it moves away again. Only the first part of these curves can be investigated. Each of these parts of curves was fit with a standard Hertzian model, in particular the typical Hertz equation for a pyramid tip, to extract the elastic modulus, known as Young's modulus in GPa.

2.4.14 Statistical analysis

All the biological experiments were performed in triplicate. The asterisks indicate statistical significance calculated in agreement with Student's t-test: * means p-value ≤ 0,05; ** p-value ≤ 0,01; *** p-value ≤ 0,001.

SECTION 3

Promitotic action of ObHEx on senescent human dermal fibroblasts

Adapted from

Ceccacci, S., Roger, K., Metatla, I., Chhuon, C., Tighanimine, K., Fumagalli, S., De Lucia, A., Pranke, I., Cordier, C., Monti, M.C., Guerrera, I.C., 2022. Promitotic Action of *Oenothera biennis* on Senescent Human Dermal Fibroblasts. International Journal of Molecular Sciences 23, 15153.

Section 3 – Chapter 1

Introduction

Senescence is the main cause of ageing and age-related diseases. Senescent cells undergo proliferation arrest as a response to physiological telomere erosion (replicative senescence) or to stress triggers including DNA damage, oxidative stress, organelle strain and oncogene activation (stress induced premature senescence, SIPS) (Di Micco et al., 2021). Senescent cells show several hallmarks (Figure 3.1) including enlarged but dysfunctional mitochondria that produce high levels of reactive oxygen species (ROS), compromised nuclear integrity due to the loss of lamin B1 and, last but not least, increased levels and activity of lysosomal senescence-associated-ß-galactosidase (SA-ß-gal, GAL1). Indeed, despite DNA Damage Response (DDR) induced growth arrest, senescent cells display a high metabolic state and lysosomal activity, crucial for their increased secretory activity, known as senescence-associated secretory phenotype (SASP) (González-Gualda et al., 2021; Sikora et al., 2018). SASP factors include several families of soluble (interleukins, chemokines, growth factors, secreted proteases) and insoluble (secreted insoluble proteins and extracellular matrix components) proteins that negatively affect the surrounding tissue, generating a chronic low-grade inflammatory state.

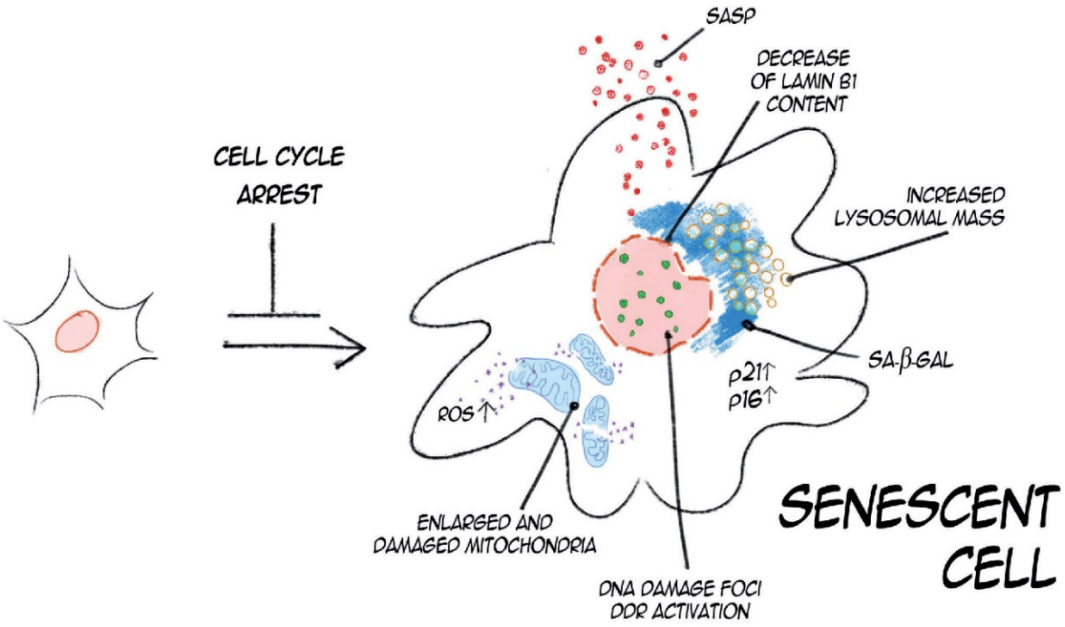

Figure 3.1 *Main hallmarks of senescent cells (Adapted from Sikora et al., 2018)*

The accumulation of senescent fibroblasts in derma drives skin aging, impairing the integrity of the extracellular matrix (ECM) and the function of neighbouring microvascular endothelial cells, epidermal melanocytes and keratinocytes (Choi et al., 2020; Krtolica et al., 2001; Wlaschek et al., 2021). The three main strategies to counteract senescence include: (i) the clearance of senescent cells by the induction of apoptosis or immune activation; (ii) the modulation of the SASP and (iii) the reactivation of cell proliferation. Indeed, although senescence has been originally described as an irreversible cell cycle arrest, current evidence suggests that proliferation can be restored (Latorre et al., 2017; Paez-Ribes et al., 2019; Soto-Gamez and Demaria, 2017).

In this scenario, those ingredients able to prevent and/or modulate cellular senescence are of great interest in the cosmetic field as valuable weapons to counteract skin aging. Therefore, based on the anti-aging properties of ObHEx, proved by *in vitro*

and *ex vivo* assays, we explored its activity on senescent human dermal fibroblasts. We used a data-independent mass spectrometry ultra-deep proteomic approach to obtain hints of the mechanism of action and bio-orthogonal methods to validate and investigate it (Figure 3.2).

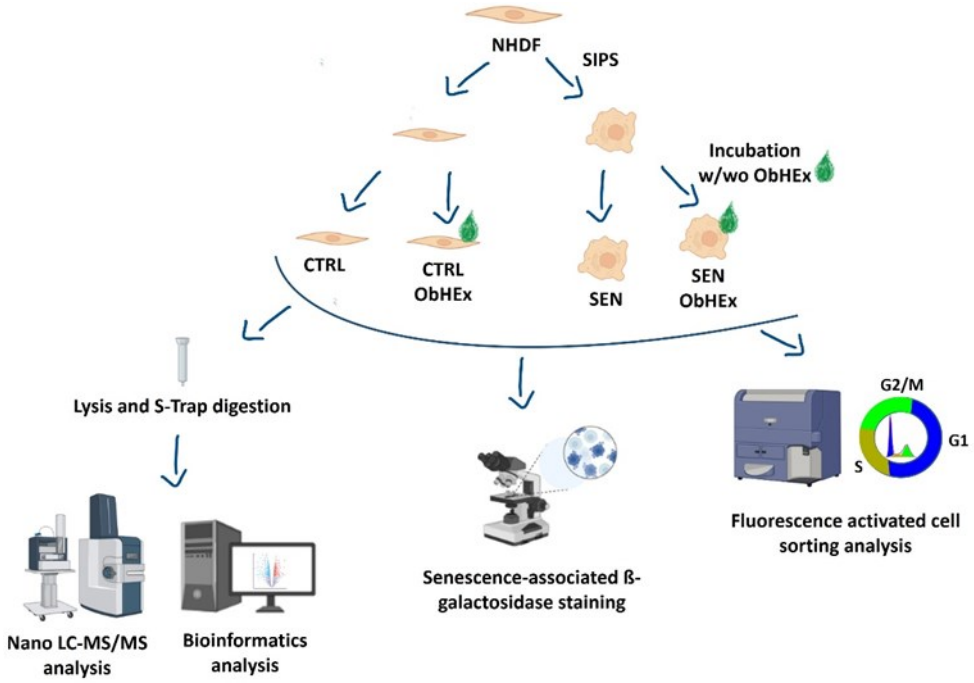

Figure 3.2 *Summary scheme (created with BioRender.com) of the adopted methodology.*

Section 3 – Chapter 2

Results

3.2.1 Global proteomics analysis

Stress-induced premature senescence (SIPS) was performed in normal human dermal fibroblasts (NHDF) by treatment with hydrogen peroxide (H_2O_2). Oxidative stress-induced senescent cells are an excellent *in vitro* model for aging research and H_2O_2 is widely used to achieve it (Chowdhary, 2018; Wang et al., 2013).

To understand the biological pathways altered by ObHEx on senescent NHDF cells, we used an ultra-deep proteomic approach. SIPS and control cells were treated or not for 48 h with the extract at 0.01% (p/v), since, from the MTT assay reported in (Ceccacci et al., 2021), this is the highest concentration that does not cause any cell toxicity after 48 h incubation.

Cell lysates were then subjected to tryptic digestion and nano-UHPLC MS/MS analysis. Mass data were acquired in DDA and DIA mode. DDA data were analysed by MaxQuant, whereas DIA data by DIA-NN software. In particular, we performed both a DIA-NN library free and library-based analysis. In this last case, the spectral library was created from four samples, one for each experimental condition.

We focused on DIANN library-free analysis that allowed the quantification of over 9500 proteins: 50% more than DDA analysis and 9% more than DIANN spectral library-based analysis that turned out to be faster, but less sensitive (Figure 3.3). DIANN library-based search took three hours, in addition to the fourteen hours

necessary for the creation of the spectral library, whereas the library-free analysis took fifty hours and required no previous MS acquisitions for library building.

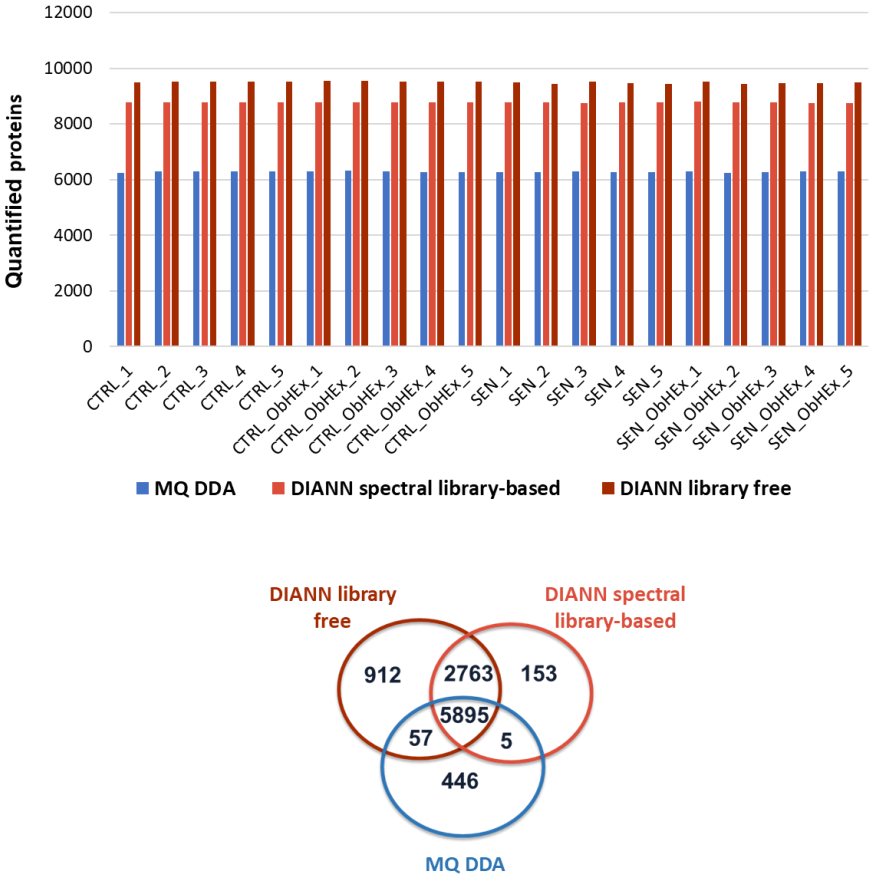

Figure 3.3 *Comparison between DDA and DIA data analysis, performed by MaxQuant and DIA-NN software, respectively.*

3.2.1.1 Stress-induced premature senescence (SIPS) evaluation

First of all, we verified if the senescence induction in NHDF was successful, analysing the global proteome of H_2O_2 treated NHDF versus untreated ones. Among the 3256 proteins that were deregulated, several biomarkers of senescence were found to be significantly altered (Figure 3.4 A and B). Firstly, we observed the upregulation

of the most widely used biomarker of senescent cells, the 'senescence-associated-ß-galactosidase' (SA-β-gal, GLB1). The increased levels of the lysosomal enzymes GLB1 and Tissue alpha-L-fucosidase (FUCA1), which has also been found upregulated by MS, reflect the characteristic increment in lysosomal content of senescent cells (Hildebrand et al., 2013; Lee et al., 2006). Indeed, lysosomes favour catabolic processes, which provide energy and raw materials required by senescence associated secretion (Gorgoulis et al., 2019).

Secondly, the protein level of serine/threonine-protein kinase ATR and serine-protein kinase ATM, both involved in DDR signalling, was also found to be increased (Matsuoka et al., 2007). DDR is activated by nuclear DNA damage, generally associated with the establishment of cellular senescence, and it converges into the activation of tumour suppressor p53. In addition to this, the upregulation of the histone 2A variants MACROH2A1 and MACRO2A2 has also been observed. These proteins participate in the ATR dependent formation of Senescence Associated Heterochromatin Foci (SAHFs), dense and repressive chromatin structures characteristic of senescent cells (Di Micco et al., 2021; González-Gualda et al., 2021; Zhang et al., 2007).

Lastly, the deregulated levels of Cyclin Dependent Kinase Inhibitor 1A or p21 (CDK1NA) and proliferation marker protein Ki-67 (MKI67) reflect senescent cell cycle arrest at the G2 phase (LaBaer et al., 1997; Scholzen and Gerdes, 2000). Indeed, p21 increases levels, promoted by a DNA damage-induced p53 pathway, and inhibits the CDK2-cyclin E complex. This causes the dephosphorylation of retinoblastoma protein (RB), which in its hypo-phosphorylated state sequesters E2F, a transcriptional factor that favours the progression of the cell cycle (González-Gualda et al., 2021).

A.

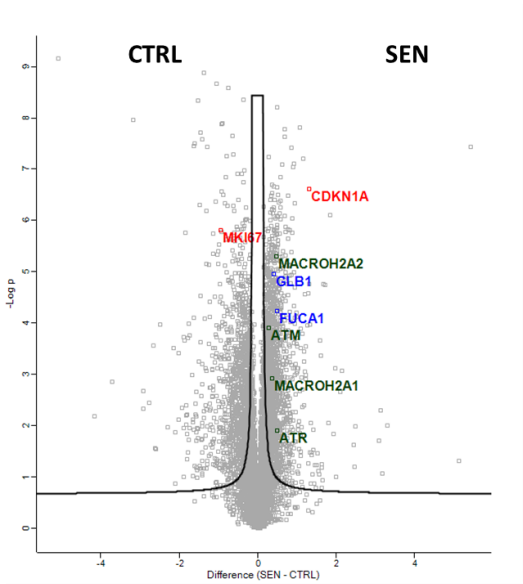

B.

Genes	First Protein Description	Senescent cell hallmark or trait	Reference
FUCA1	Tissue alpha-L-fucosidase	Increased lysosomal compartment and activity	Hildebrand et al.,2013
GLB1	Beta-galactosidase		Lee et al., 2006
ATM	Serine-protein kinase ATM	DNA damage	Matsuoka et al., 2007
ATR	Serine/threonine-protein kinase ATR		
MACROH2A1	Core histone macro-H2A.1	SAHFs formation	Zhang et al., 2007
MACROH2A2	Core histone macro-H2A.2		
CDKN1A	Cyclin-dependent kinase inhibitor 1	Cell cycle arrest	Labaer et al., 1997
MKI67	Proliferation marker protein Ki-67		Scholzen & Gerdes, 2000

Figure 3.4 *(A) Volcano plot representing the statistical comparison of the protein LFQ intensities of H_2O_2 treated cells versus untreated controls. The abscissa reports the fold change in logarithmic scale (difference), and the ordinate −log(p) of t-tests (FDR = 0.05, s0 = 0.1). Deregulated senescent protein markers have been highlighted in different colours in the volcano plot and described in detail in the related table (B).*

Beyond these already known markers of senescence, a broader pathway enrichment analysis of the most upregulated proteins in H_2O_2 treated versus control cells points to p53/p21 pathway activation induced by DNA damage (Figure 3.5 A). Instead, proteins associated with proliferation and mitosis are downregulated, pointing to the consequent proliferation arrest (Figure 3.5 B).

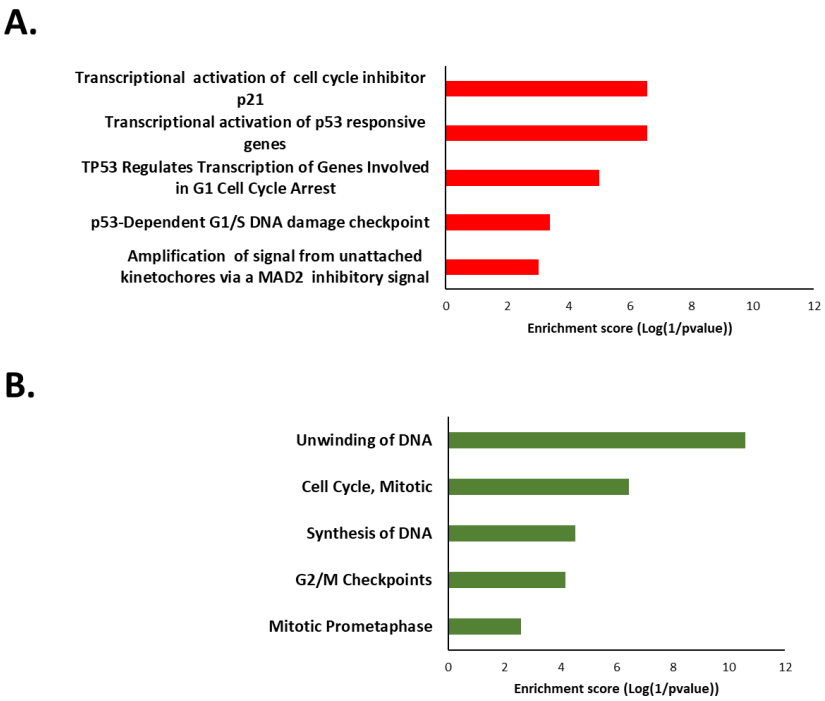

Figure 3.5. *(A, B) Reactome enrichment analysis of the most upregulated (A) and downregulated (B) proteins (FDR = 0.05, s0 = 1) in H_2O_2 treated cells. In both cases, only the main five pathways have been reported ($p < 0.01$).*

Moreover, SIPS has also been confirmed by flow cytometry analysis. We observed an increase in cytoplasmic granularity of H_2O_2 treated cells (Figure 3.6 A, and B), due to the augmentation in number and size of the lysosomes in senescent cells. This is the result of the balance between the gradual accumulation of dysfunctional lysosomes and the production of new ones (Gorgoulis et al., 2019). Moreover, we also detected an intra-lysosomal accumulation of lipofuscin aggresomes: this growth, associated with an increment of autofluorescence in the 525/50 nm bandpass channel of the flow cytometer, is another marker of senescence related to lysosomal malfunction (Figure 3.6 C, and D) (Passos and von Zglinicki, 2007).

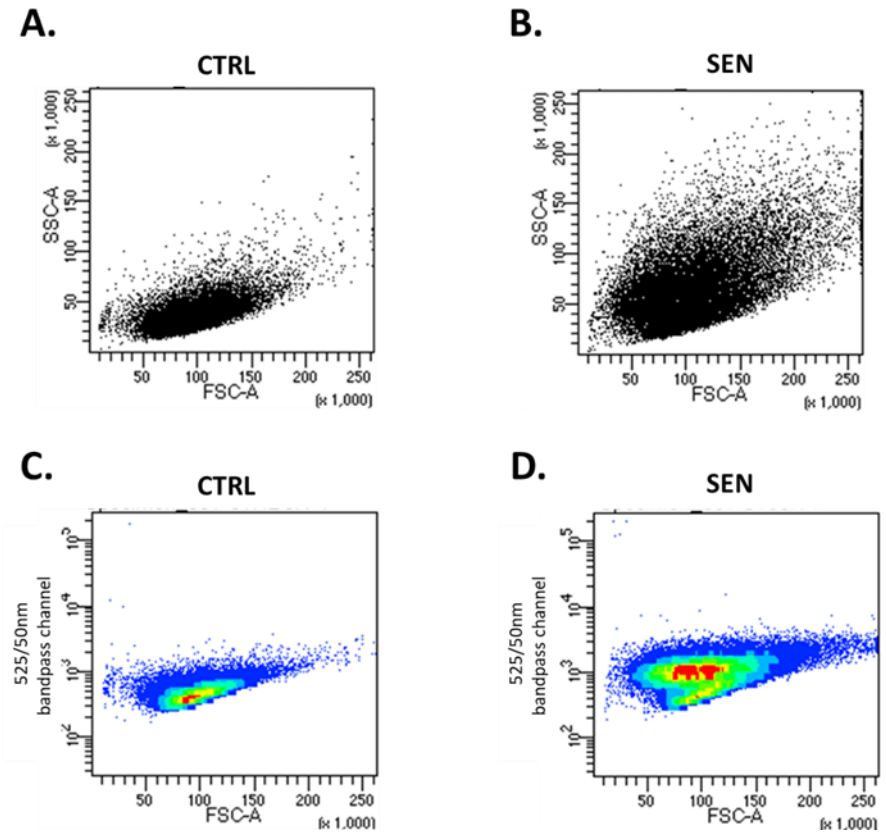

Figure 3.6 *Increase of cytoplasmic granularity and lipofuscin aggresomes in H_2O_2 treated cells. H_2O_2 treated cells (B) in comparison with control ones (A) showed in flow cytometry analysis an increase of SSC intensity (Side SCatter) that is a measure of cytoplasmatic granularity. It reflects the characteristic increment in lysosomal content of senescent cells. FSC (Forward Scatter) intensity represents the measure of the relative size of the cells. Moreover, in H_2O_2 treated cells a population with high autofluorescence in 525/50nm bandpass channel from the 488nm excitation wavelengh has been detected (D) in comparison with the control (C). This is a marker of senescent intra-lysosomal accumulation of lipofuscin aggresomes.*

3.2.1.2 Effects of ObHEx treatment on senescent NHDF

ObHEx treatment was able to partially restore the levels of 71 proteins deregulated in the senescent condition (Two-way ANOVA test q-value < 0.05). More precisely, 46 proteins were downregulated by the extract and 25 were upregulated (Figure 3.7).

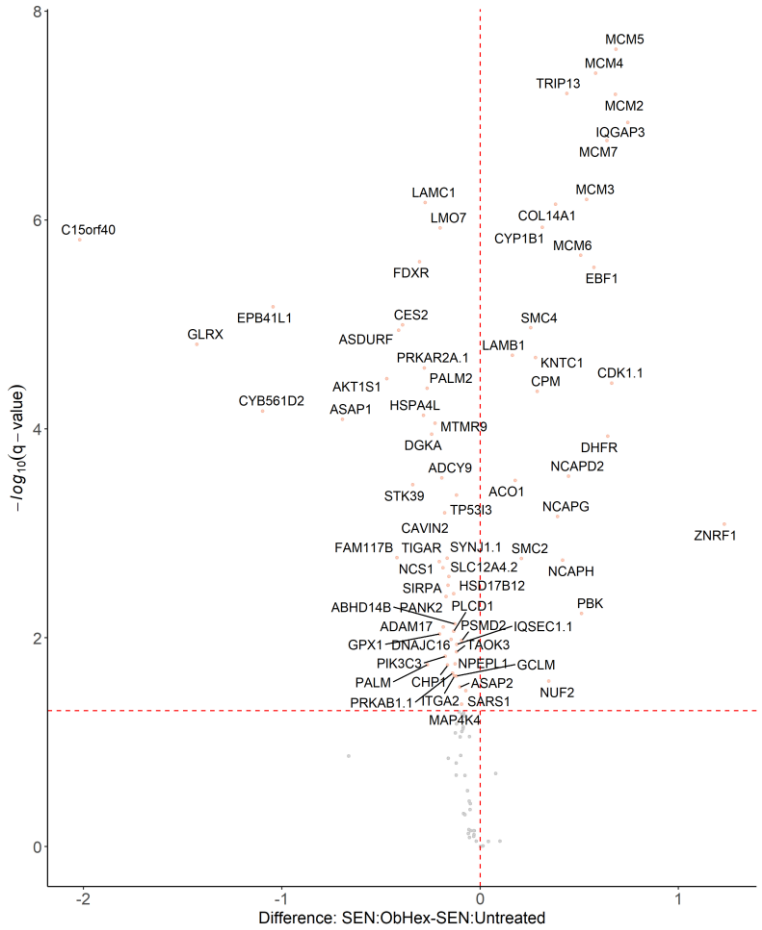

Figure 3.7 *Plot representing the statistical difference between senescent cells with the presence or absence of ObHEx extract resulting from Tukey HSD post-hoc test of Two-way ANOVA interaction factors (i.e., Induction and Treatment). The abscissa reports the fold change in logarithmic scale (difference), and the ordinate −log (q-value) of the Tukey HSD tests for the specific SEN:ObHex/SEN:Untreated pairwise comparison while keeping the family-wise error rate low (family-wise confidence level of 0.95).*

Reactome enrichment analysis of the 46 proteins whose levels were decreased by ObHEx suggests that the extract can reduce p53 pathway activation and affect phosphatidylinositol metabolism and Hedgehog signalling, whose alterations were found in aging (Dai et al., 2021; Dashty, 2014) (Figure 3.8A).

Regarding the 25 upregulated proteins, the enrichment analysis clearly points to mitotic cell cycle pathway reactivation and, in particular, to DNA unwinding and replication, chromosome condensation, and the resolution of sister chromatids (Figure 3.8B).

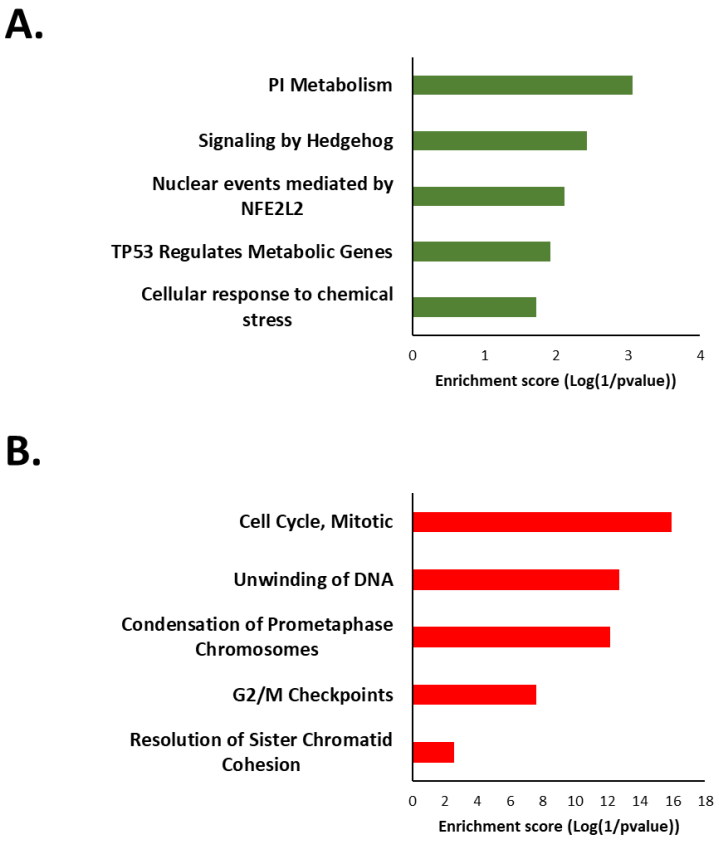

Figure 3.8 *(A, B) Reactome enrichment analysis of downregulated (A) and upregulated (A) proteins in senescent NHDF cells after ObHEx treatment. Only the main five pathways have been reported ($p < 0.05$).*

In depth analysis shows that 18 of the 25 restored proteins strongly cluster together (Figure 3.9). In this cluster, it is possible to discern CDK1, all the subunits of the condensin I complex (SMC2, SMC4, NCAPD2, NCAPH and NCAPG), three kinetochore related proteins (KNTC1, NUF2 and TRIP13), all the six subunits of the

replicative minichromosome maintenance (MCM) complex (MCM2-7) together with IQGAP3, PBK and DHFR.

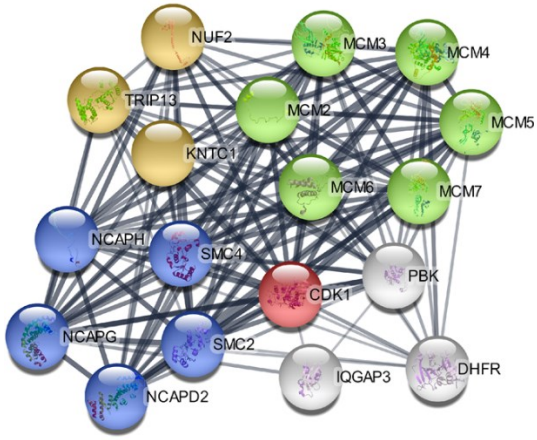

Figure 3.9 *Cluster analysis of upregulated proteins in senescent NHDF cells after ObHEx treatment. It was performed using the Cytoscape StringApp; setting 0.9 as the threshold (highest confidence).*

The ability of ObHEx to partially restore the levels of these proteins is shown well in the profile plots reported in Figure 3.10: protein expression levels were mostly unaltered in the proliferating cells treated or not with the extract, dropped in the senescent cells, and partially increased after ObHEx treatment.

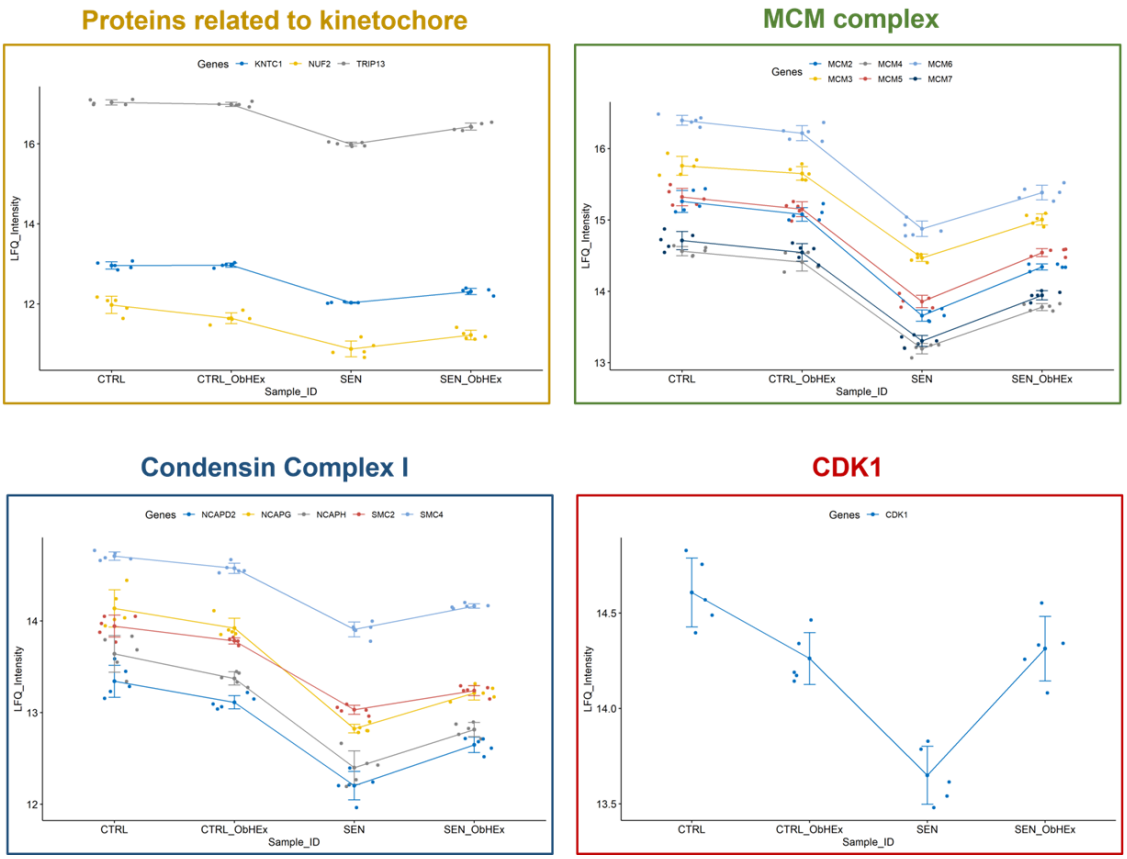

Figure 3.10 *Profile plots of the proteins included in the cluster reported in Figure 3.9. Each plot shows the mean LFQ intensity with error bars representing the error limits defined by the standard deviation.*

3.2.2 Biological assays confirmed ObHEx promitotic mechanism of action

3.2.2.1 Senescence-Associated ß-Galactosidase Staining

The most common hallmark of senescent cells is the increased SA-β-gal activity that can be evaluated by a staining assay. Our results show that H_2O_2 treatment induced a significant increase in the number of SA-β-gal positive cells (blue), from 4.7% to 22.9% (Figure 3.11). ObHEx incubation significantly reduced SA-β-gal activity with a decrease of 38.4% ($p < 0.01$).

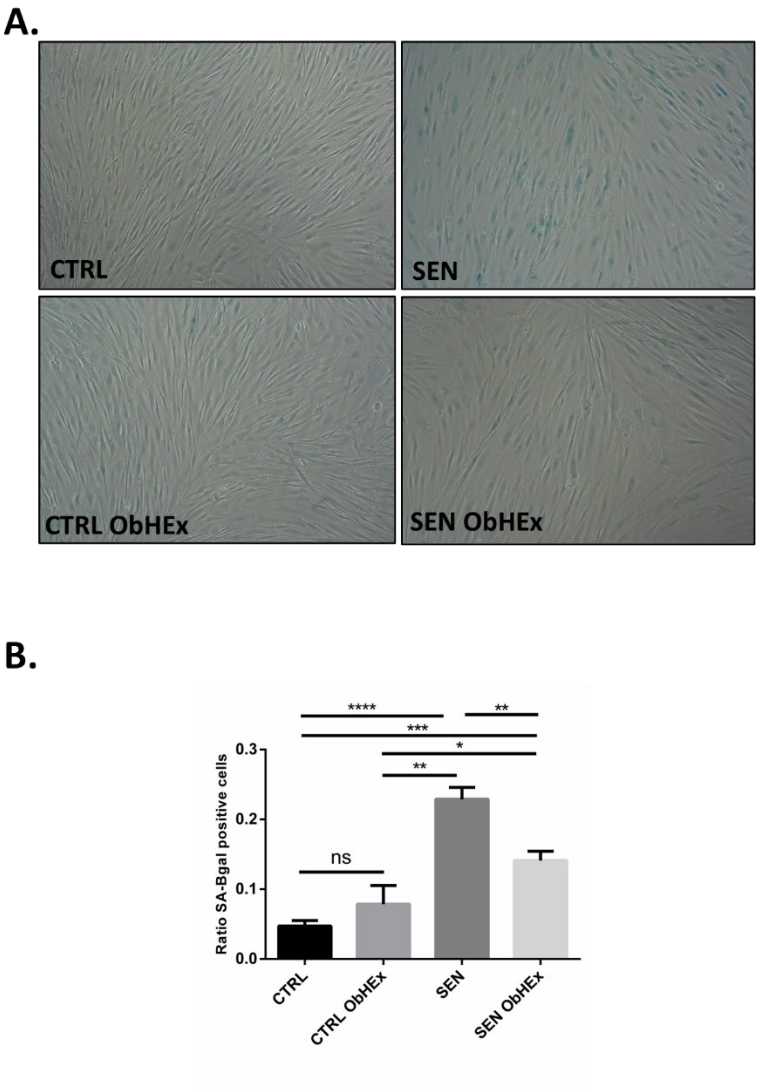

Figure 3.11 *(A) Images (40x magnification) of the control and senescent NHDF cells treated or not with ObHEx after the senescence-associated ß-galactosidase (SA-ß-gal) assay. Positive cells are blue. (B) Bar graph showing the ability of ObHEx to reduce SA-ß-gal activity. The error bars represent the standard deviations while asterisks indicate significant variations (* $p < 0.05$; ** $p < 0.01$; *** $p < 0.001$, **** $p < 0.0001$) according to Student's t-test. ns = not statically significant.*

3.2.2.2 Fluorescence Activated Cell Sorting (FACS) analysis

To assess if the restoration of mitotic protein expression by ObHEx translates to the reactivation of the cell cycle, the control and senescent cells were treated or not with the extract for 72 h and Fluorescence Activated Cell Sorting (FACS) experiments were performed. The senescent cell results showed a block in the G2/M phases of the cell cycle (36.8%), while only a much lower fraction of the control cells (7.2%) were in these phases since they reached confluence, accordingly to the literature (D. Wang et al., 2016) (Figure 3.12 A and B). The treatment of senescent cells with ObHEx was able to reduce the G2/M population by 4.3% ($p < 0.05$). Of notice, when related to the senescence cell portion after SIPS (22.9%), the G2/M escape could be estimated to be 18.9%. The same ObHEx treatment for 48 h has been carried out, but the results were not statistically significant.

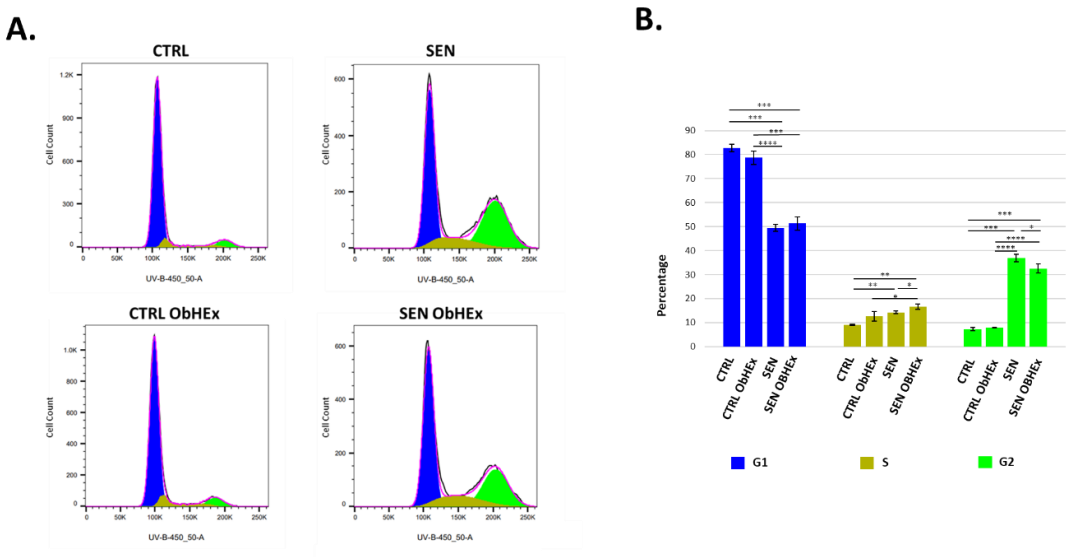

Figure 3.12 *(A) DNA profiles of proliferating and senescent fibroblasts after treatment with ObHEx or not, and (B) related bar graph. The fluorescence intensity of Hoechst 33342 was measured by flow cytometry with a BD LSRFortessa Cell Analyzer using UV laser (355 nm) associated to a 450/50 filter set. G1, S and G2/M phases are reported in blue, brown and green, respectively. The error bars represent*

the standard deviations while asterisks indicate significant variations ($p < 0.05$; ** $p < 0.01$; *** $p < 0.001$, **** $p < 0.0001$) according to Student's t-test. ns = not statically significant.*

Section 3 – Chapter 3

Discussion

In this study, we investigated the effect of a hydrophilic extract of *Oenothera biennis* cells (ObHEx) on cellular senescence, since it showed skin anti-aging properties when tested in *in vitro* and *ex vivo* models (Ceccacci et al., 2021). We used a similar senescent model of NHDF subjected to SIPS for treatment with H_2O_2 (Chowdhary, 2018; Wang et al., 2013).

To understand the mechanism of action of ObHEx on senescent human dermal fibroblasts, by the disclosure of the biological pathways altered by the extract, we performed a data-independent mass spectrometry ultra-deep proteomic approach. It allowed us to obtain the most complete proteome analysis of senescent cells to date and, for the first time, the simultaneous quantification of numerous senescence markers.

First of all, to assess the senescence induction by H_2O_2 treatment on NHFD cells, we quantified the known senescence markers. Our proteomics data confirmed senescence induction by oxidative stress: indeed, we observed altered levels of already known senescence markers related to the increased lysosomal content (GLB1 and FUCA1), DNA damage (ATR, ATM, MACROH2A1 and MACRO2A2) and G2 phase cell cycle arrest (CDK1NA and MKI67). Moreover, the pathway enrichment analysis of the most downregulated proteins in H_2O_2 treated versus control cells points to mitosis, reflecting the senescent proliferation arrest.

Comparing the proteome of SIPS NHDF cells treated with ObHEx versus untreated ones, we found that the treatment with the extract was able to partially restore the levels of proteins and complexes, playing crucial roles in several stages of mitosis. In fact, ObHEx incubation increased the levels of CDK1, a key mitotic protein that triggers the entry into mitosis by forming a complex with cyclin B (Qian et al., 2015). Moreover, all the five subunits of the condensin I complex were upregulated. This complex is composed of two structural maintenance of chromosomes (SMC) subunits, SMC2 and SMC4, and three non-SMC subunits, NCAPD2, NCAPH and NCAPG. In the prometaphase, the function of the condensin I complex is to promote the hypercondensation of chromosomes by the introduction of positive supercoils into the DNA in an ATP-dependent manner (Kong et al., 2020). In addition to this, the extract upregulated KNTC1, NUF2 and TRIP13, which are three proteins associated with the kinetochore, a large complex that, during the prometaphase, connects centromeric chromatin to microtubules from opposite spindle poles to favour the segregation of sister chromatids (Kops and Gassmann, 2020; Ma and Poon, 2018, p. 13). A partial restoration of the levels of MCM proteins has also been detected. These proteins are at the core of the replication helicase complex that unwinds double stranded DNA to provide single strands as templates for DNA polymerase. The MCM complex is converted into an active helicase during the S phase but is already loaded onto chromatin during the telophase (Kuipers et al., 2011; Meng et al., 2018). The extract incremented the levels of IQGAP3, PBK and DHFR, too. The first, IQGAP3, is an important regulator of mitotic progression because it promotes Cdk7 activity, essential for Cdc2 activation (Larochelle et al., 1998; Leone et al., 2021); PBK is a kinase active only in mitosis; when phosphorylated, it interacts with p53, destabilizing it and attenuating the DNA damage pathway (Nandi et al., 2007); and DHFR is a key enzyme

in DNA bio-synthesis whose levels are markedly attenuated in senescent human fibroblasts (Good et al., 1996).

Bio-orthogonal assays also showed the ability of ObHEx to partially revert senescence hallmarks, namely lysosomal activity and cell cycle arrest. Indeed, to verify if the restoration of mitotic protein expression by ObHEx translates to the reactivation of the cell cycle, we performed Fluorescence Activated Cell Sorting (FACS) experiments on SIPS NHDF cells treated or not with the extract. They showed that ObHEx was able to reduce the fraction of cells blocked in the G2 phase and to promote their re-entry into the cell cycle of senescent cells.

Thus, our work proves a promitotic mechanism of action of ObHEx on senescent human dermal fibroblasts: via an increase in mitotic protein expression, it promotes the restoration of the proliferation of senescent cells. Thus, on the basis of these results, we propose ObHEx as a powerful adjuvant against senescence associated with skin aging.

Section 3 – Chapter 4

Materials and Methods

3.4.1 Cell cultures

Normal Human Dermal Fibroblasts (NHDF; Promocell) were cultured in Dulbecco's Modified Eagle Medium (DMEM; Gibco) supplemented with 10% of foetal bovine serum (FBS; Gibco) and 500 U/mL of penicillin-streptomycin (Gibco) in 95% air, 5% CO_2 and a humidified atmosphere at 37 °C.

3.4.2 Induction of Stress Induced Premature Senescence (SIPS)

A total of 1′120′000 NHDF cells were seeded into each of 60 mm cell culture dishes, one day prior to their incubation with 100 µM H_2O_2 at 37 °C for 2 h (Chowdhary, n.d.; Wang et al., 2013). Subsequently, the H_2O_2 was washed with Phosphate Buffered Saline (PBS; Gibco) to terminate the treatment and the cells were grown in a normal medium for 4 days. For the non-senescent cells, used as a control, 224′000 NHDF cells were seeded into each of 60 mm cell culture dishes. The experiment was performed in 5 biological replicates.

3.4.3 ObHEx treatment

NHDF cells were incubated for 24 h with 0.01% (*p*/*v*) ObHEx in complete medium. Subsequently, the cells were washed three times with PBS and treated for an additional 24 h with 0.01% (*p*/*v*) ObHEx in a serum-free medium. They were, then, detached by

trypsinization, centrifuged at 500 g for 10 min at 4 °C and washed twice with PBS. Non-treated control cells underwent the same incubations without ObHEx.

3.4.4 Sample preparation for proteomic analysis

Pellets were resuspended in 60µL of Radioimmunoprecipitation assay (RIPA) buffer and lysated by sonication. The cellular lysates protein concentration was quantified using a DC™ Protein Assay Kit (Biorad; #5000112). S-TrapTM micro spin column (Protifi, Hutington, CA, USA) digestion was performed on 50 µg of cell lysates according to the manufacturer's instructions. Briefly, the samples were reduced with 20 mM tris(2-carboxyethyl)phosphine (TCEP) and alkylated with 50 mM chloracetamide (CAA) for 15 min at room temperature. Aqueous phosphoric acid was then added to a final concentration of 2.5% followed by the addition of an S-Trap binding buffer (90% aqueous methanol, 100 mM TEAB, pH 7.1). The mixtures were then loaded onto S-Trap columns. Five extra washing steps were performed for thorough SDS elimination. Then, the cellular lysates were digested with 2.5 µg of trypsin (Promega) at 47 °C for 1 h. After elution, the peptides were vacuum dried, resuspended in 2% ACN, 0.1% FA and quantified by Nanodrop.

3.4.5 nanoLC-MS/MS protein identification and quantification

A total of 400 ng of each sample was injected on a nanoElute (Bruker Daltonics, Germany) high-performance liquid chromatography (HPLC) system coupled to a timsTOF Pro (Bruker Daltonics, Bremen, Germany) mass spectrometer. HPLC separation (Solvent A: 0.1% formic acid in water; Solvent B: 0.1% formic acid in acetonitrile) was carried out at 250 nL/min using a packed emitter column (C18, 25

cm × 75µm 1.6µm) (Ion Optics, Fitzroy, Australia) using a gradient elution (2 to 13% solvent B during 41 min; 13 to 20% during 23 min; 20% to 30% during 5 min; 30% to 85% for 5 min, and, finally, 85% for 5 min to wash the column).

Parallel accumulation serial fragmentation (PASEF) acquisition method settings were: mass range from 100 to 1700 m/z, ion mobility range from 0.8 to 1.3 V s/cm^2(1/k0), total cycle time of 1.17s and number of PASEF MS/MS ramps of 10.

diaPASEF settings were: mass range from 400 to 1200 m/z, mobility ranges from 0.60 to 1.43 V s/cm^2 1/k0, cycle time estimate of 1.79 s, 16 PASEF scans x 2 steps per PASEF scans (32 windows).

3.4.6 MS data processing and bioinformatics analysis

3.4.6.1 DDA data analysis by using MaxQuant

DDA data were analyzed using MaxQuant version 2.0.1.0 and searched with Andromeda search engine against the UniProtKB/Swiss-Prot *Homo sapiens* database (release 02-2021, 20408 entries). To search parent mass and fragment ions, we set a mass deviation of 10 ppm and 20 ppm, respectively. The minimum peptide length was set to 7 amino acids and strict specificity for trypsin cleavage was required, allowing up to two missed cleavage sites. Carbamidomethylation (Cys) was set as fixed modification, whereas oxidation (Met) and N-term acetylation were set as variable modifications. The false discovery rates (FDRs) at the protein and peptide level were set to 1%. The reverse and common contaminants hits were removed from MaxQuant output. Proteins were quantified according to the MaxQuant label-free algorithm using

LFQ intensities; protein quantification was obtained using at least 1 peptide per protein. Match between runs was allowed.

3.4.6.2 DIA-NN library-free analysis

DIA data were analysed by using DIA-NN software (version 1.8) (Demichev et al., 2020). A search against the human UniProtKB/Swiss-Prot Homo sapiens database (release February 2021, 20408 entries) was performed using library free workflow. For this purpose, "FASTA digest for library free search/library generation" and "Deep learning spectra, RTs and IMs prediction" options were checked for precursor ion generation. A maximum of 2 trypsin missed cleavages was allowed and the maximum variable modification was set to 5. Carbamidomethylation (Cys) was set as the fixed modification, whereas protein N-terminal methionine excision, methionine oxidation and N-terminal acetylation were set as variable modifications. The peptide length range was set to 7–30 amino acids, precursor charge range 2–4, precursor m/z range 300–1800, and fragment ion m/z range 200–1800. To search the parent mass and fragment ions, accuracy was inferred automatically by DIA-NN and was set around 13 ppm for each analysis. The false discovery rates (FDRs) at the protein and peptide level were set to 1%. Match between runs was allowed. For the quantification strategy, Robust LC (high precision) was used as advised in the software documentation, whereas default settings were kept for the other algorithm parameters.

3.4.6.3 DIA-NN library-based analysis

A spectral library was created subjecting four samples, one for each experimental condition, to a DIA-NN library-free analysis, as described in the previous

subparagraph 3.4.6.2. After that, the obtained spectral library was used to analyse all twenty samples, setting the same parameters reported above.

3.4.6.4 Statistical analysis

Statistical analysis of data obtained from DIA-NN library-free analysis was performed with Perseus software (version 1.6.15) freely available at www.perseus-framework.org (Tyanova et al., 2016b) and R/R Studio and RStudio version 2021.09.1 30. All R statistical analysis was performed using the R stats package. The pg report matrix output by DIA-NN was used and intensities were log2 transformed for statistical analysis. For the statistical comparison, we set four groups, each containing 5 biological replicates. We then filtered the data to keep only proteins with at least 3 valid values in at least one group. Next, the data were imputed to fill missing data points by creating a Gaussian distribution of random numbers with a standard deviation of 33% relative to the standard deviation of the measured values and a 1.8 standard deviation downshift of the mean to simulate the distribution of low signal values. Student's *t*-test was performed between SEN and CTRL FDR < 0.05, S0 = 0.1 to confirm the presence of markers specific to senescence. Then, in order to investigate if the difference of the effect size between the absence or presence of the treatment is the same for cells where senescence was induced or not, the interaction between both factors (i.e., Induction and Treatment) was investigated using Two-way ANOVA in R. Then, *p*-values obtained for the interaction of both factors were adjusted for multiple testing using the Benjamini–Hochberg (Benjamini and Hochberg, 1995) method in order to control the False Discovery Rate (FDR). Finally, Tukey HSD post hoc analysis was performed on proteins showing a *q*-value < 0.05. The mass

spectrometry proteomics data have been deposited to the ProteomeXchange Consortium via the PRIDE (Perez-Riverol et al., 2021) partner repository with the dataset identifier PXD034222.

3.4.7 Senescence-Associated ß-Galactosidase staining

Senescence-associated ß-galactosidase (SA-ß-gal) activity was evaluated using a Cell Signalling Technology staining kit (#9860). A total of 125′000 NHDF cells/well were seeded into a 6-well plate one day prior to SIPS; whereas, as a control, 25′000 cells/well. After 4 days in normal medium, the cells were incubated or not with 0.01% (*p*/*v*) ObHEx for 48 h. Subsequently, they were washed with PBS and treated with the fixing solution for 15 min. After two washes with PBS, the cells were incubated with the ß-gal staining solution (final pH of 6.0) containing 5-bromo-4-chloro-3-indolyl-β-D-galacto-pyranoside (X-Gal) at 37 °C in a dry incubator for 20 h. Positive cells are blue. The color is due to the cleavage of X-Gal in galactose and 5-Bromo-4-chloro-3-indoxyl (X) by SA-ß-gal. The indoxyl is oxidized to 5,5′-dibromo-4,4′-dichloro-indigo that forms an intense blue precipitate. The percentage of positive cells in the total cells was assessed by counting 100–150 cells in 5 randomly selected images captured by the microscope, for each condition. Cells were counted using ImageJ software. The experiment was performed in triplicate.

3.4.8 Fluorescence Activated Cell Sorting analysis

A total of 100′000 NHDF cells/well were seeded into a 6-well plate one day prior to SIPS; whereas, as a control, 5′000 cells/well. After 4 days in normal medium, the control and senescent cells were treated or not with 0.01% (*p*/*v*) ObHEx for 72 h. Then,

the cells were incubated in the presence of 5 μg/mL of Hoechst 33342 for 30 min at 37 °C. After trypsinization and centrifugation at 500 g for 2 min, they were resuspended in 200 μL of PBS. Finally, cell fluorescence was measured by a BD LSRFortessa Cell Analyzer. Data were analysed using FlowJo software v10.8.1. The experiment was performed in triplicate.

SECTION 4

Jasminum sambac cell extract as antioxidant booster against skin aging

Adapted from

Ceccacci, S., Lucia, A.D., Tortora, A., Colantuono, A., Carotenuto, G., Tito, A., Monti, M.C., 2022. *Jasminum sambac* Cell Extract as Antioxidant Booster against Skin Aging. Antioxidants 11, 2409.

Section 4 – Chapter 1

Introduction

4.1.1 *Jasminum sambac* L.

Jasminum sambac L. (Arabian or Tuscan jasmine), belonging to *Oleaceae* family, is distributed throughout tropical and sub-tropical regions, mainly in India, China and Malaysia (Toppo, 2017) (Figure 4.1). Its extracts, traditionally used in Asia to treat dermatitis and to heal wounds, are commonly employed in cosmetics field. Indeed, alcoholic extracts derived from *J. sambac* flowers, leaves and roots showed a significant anti-inflammatory activity (Al-Snafi, 2018). Moreover, alcoholic extracts from flowers, hydroalcoholic extracts from leaves and the essential oil also exhibited antioxidant properties. In addition to this, *Jasminum sambac* oil is largely used in cosmetics industry due to its sweet and elegant fragrance. The main chemical components of jasmine oil are benzyl acetate, linalool, benzyl alcohol, indole, benzyl benzoate, cis-jasmone. Other *J. sambac* phytochemicals are iridodial glycosides (flowers), triterpenoids and flavonoids (roots).

Figure 4.1 *Jasminum sambac L.*

4.1.2 Advanced glycation end products (AGEs), oxidative stress and skin aging

Genetic intrinsic factors and extrinsic agents such as ultraviolet irradiation, infrared irradiation, xenobiotics and environmental pollutants cause the production of reactive oxygen species (ROS). They are generated by the activation of the mitochondrial respiratory chain, cytochrome p450 and NADPH oxidases (Bae et al., 2011). ROS include free radicals (superoxide anion, hydroperoxyl radical, alkoxy radical and hydroxyl radical) and nonradical molecules (hydrogen peroxide, and singlet oxygen) (Hasanuzzaman et al., 2020). When antioxidant systems are overwhelmed, ROS accumulate within cells and generate the so-called oxidative stress, that is a main contributor to skin aging (Rinnerthaler et al., 2015).

Indeed, oxidative stress causes both DNA damage and lipid and protein oxidation together with the triggering of the mitogen-activated protein kinases (MAPK) pathway (AKT, JNK, ERK, and p38) (Sárdy, 2009). This, in turn, promotes the expression of pro-inflammatory cytokines, growth factors and adhesive molecules through the stimulation of the transcription factors AP-1 and NF-κB. Moreover, MAPK pathway activation causes dermal matrix alterations by reducing collagen levels. In fact, it accelerates collagen breakdown by modulating the expression of matrix metalloproteinases (MMPs) and their tissue inhibitors TIMPs and it reduces the synthesis of new collagen, by blocking the TGF-β type II receptor/Smad signaling. In addition to this, oxidative stress alters skin conditions disrupting the epidermal calcium gradient, essential for the integrity and the function of the cornified envelope, stimulating sebaceous glands function and inducing melanocyte de-generation (Masaki, 2010).

In parallel, the formation of modified biomolecules known as advanced glycation end products (AGEs) promotes oxidative stress in cells and tissues (Perrone et al., 2020). The development of these aging biomarkers is induced by various environmental factors such as cigarette smoke, high levels of refined and simple carbohydrate diets, high temperature-cooked foods and sedentary lifestyle; AGEs are stable and irreversible products derived from the non-enzymatic reaction between reducing sugars and proteins, nucleic acids or lipids, followed by further rearrangements (Singh et al., 2014). Indeed, the starting point of the AGE formation is the Maillard reaction in which carbonyl groups of reducing sugars react reversibly with free amino groups of proteins, nucleic acids or aminophospholipids to form Schiff bases (Figure 4.2). These imines spontaneously rearrange into more stable ketoamines, called Amadori products. Some Amadori products are converted to AGEs by the Hodge pathway (oxidative degradation or oxidative rearrangement), and others are oxidized and cleaved to active dicarbonyl compounds (as glyoxal or methylglyoxal). These active dicarbonyl intermediates, that can be also generated by Wolff pathway, Namiki pathway, and Polyol pathway, react with lysine and arginine functional groups of proteins, yielding a great variety of AGEs (Cepas et al., 2020; Chen et al., 2022; Twarda-Clapa et al., 2022). They are classified in different groups based on their ability to emit fluorescence and to form crosslinks.

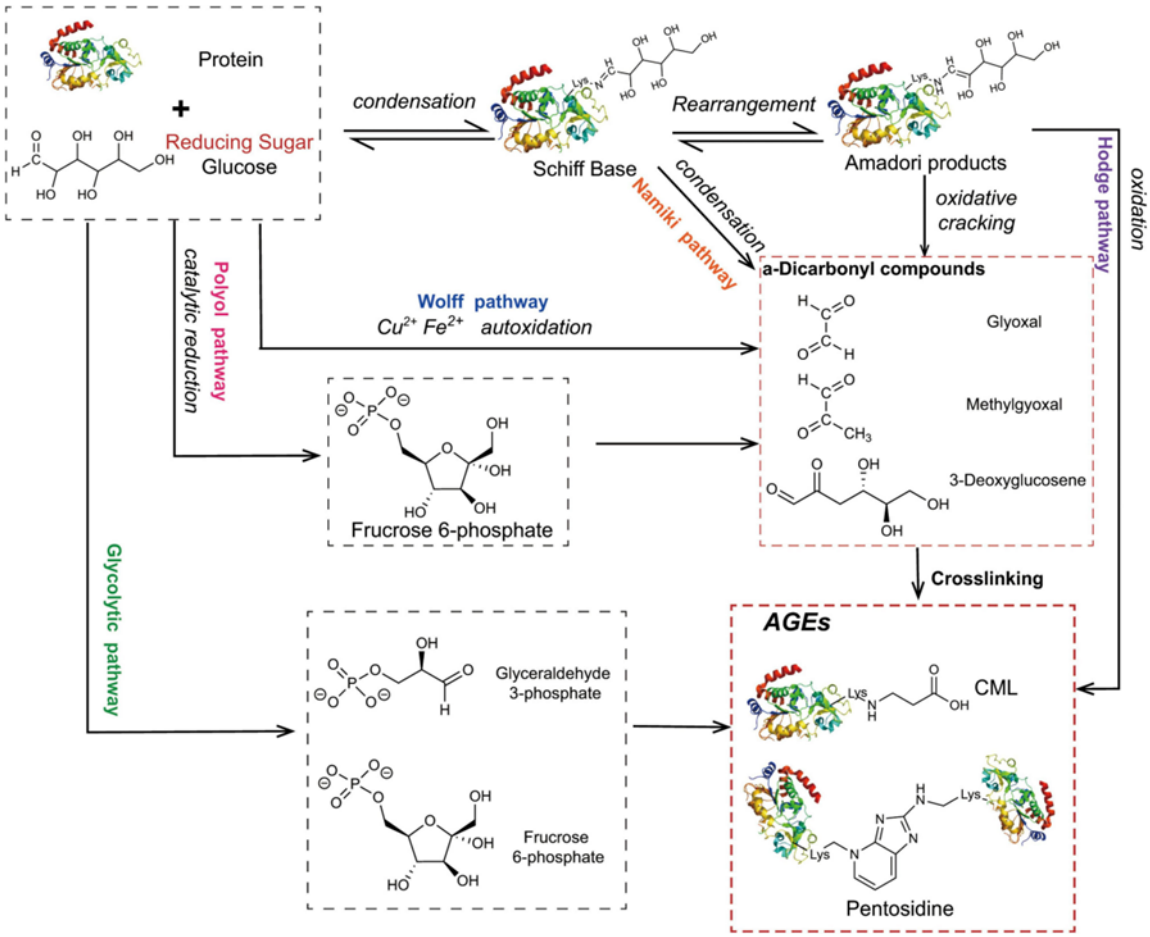

Figure 4.2 *The main pathways for the formation of AGEs. Adapted from (Chen et al., 2022)*

AGE action is mediated by the receptors for AGEs (RAGEs) which are transmembrane proteins belonging to the immunoglobulin superfamily of type I cell surface molecules, expressed in different cell types included keratinocytes, fibroblasts and macrophages. The binding AGEs/RAGEs increases ROS production mainly by the activation of NADPH oxidases (NOXes) and the mitochondrial respiratory chain, leading to oxidative stress and all the above-described consequent effects (Cepas et al., 2020; Perrone et al., 2020)

Moreover, extracellular matrix (ECM) proteins, especially collagen, resulted highly sensitive to glycation. Indeed, the levels of the AGE structure pentosidine, derived from collagen, are significantly higher in old than in young subjects (Dyer et al., 1993). Collagen glycation changes not only the mechanical properties of the collagen itself, which becomes stiffer and more brittle (Verzijl et al., 2000), but also those of the extracellular matrix, affecting the behaviour of the resident cells (growth, differentiation, motility, gene expression and response to cytokines) and matrix-cell interactions (Reiser, 1998).

In this scenario, antioxidant ingredients are in great demand in cosmetic field with the aim of reducing AGE formation and their related oxidative cascade.

4.1.3 Hydroethanolic extract of *Jasminum sambac* cells (JasHEx) as object of study

Here, a hydroethanolic extract derived from *Jasminum sambac* cells (JasHEx) was studied. The aim of our study was a broad chemical and biological characterization of JasHEx, particularly exploring its anti-glycation and anti-aging properties. First, advanced mass spectrometry-based approaches were used to obtain a detailed chemical characterization of the extract. Then, *in vitro* and *ex vivo* experiments were performed to prove JasHEx biological activity as antioxidant.

Section 4 – Chapter 2

Results

4.2.1 JasHEx chemical characterization

4.2.1.1 JasHEx qualitative analysis

UHPLC-MS/MS analysis of JasHEx was performed and high-resolution spectrometric data were analyzed using the web-based mass spectrometry ecosystem Global Natural Products Social Molecular Networking (GNPS) (M. Wang et al., 2016). Firstly, a GNPS spectral library search was performed to achieve online dereplication. Chemical species not identified by GNPS were assigned accordingly to literature. As shown in Figure 4.3 and Table 4.1, more than 50 compounds belonging to several classes of secondary metabolites, mainly polyphenols and terpenes, were identified. Indeed, JasHEx extract contains phenolic acid derivatives, lignans (secoisolariciresinol, nortrachelogenin and matairesinol) and triterpenoids (arjunolic acid, asiatic acid, maslinic acid, oleanolic acid and ursolic acid).

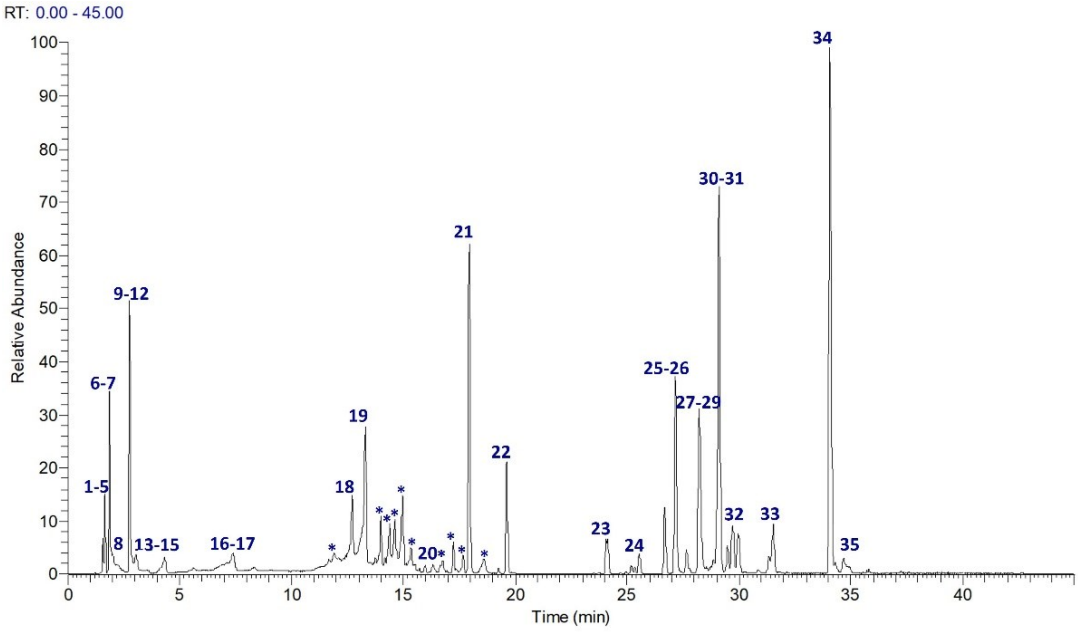

Figure 4.3 *Extracted-ion chromatogram of the main metabolites identified in JasHEx. Those indicated by * were included in Molecular Networks (MNs).*

Table 4.1 *Molecular formula (MF), Retention time (RT), MS data of compounds identified in JasHEx by GNPS search library and literature study.*

	Compound	MF (Mass error ppm)	RT min	Precursor ions m/z	MS^2 ions m/z (Relative intensity %)
1	L-Histidine	$C_6H_9N_3O_2$ (2.60 ppm)	1.49	154.0615	137.0346 (37.67); 110.0712 (16.55); 93.0446 (40.25)
2	Pyridoxine	$C_8H_{11}NO_3$ (2.98 ppm)	1.56	168.0660	150.0551 (100); 122.0600 (46.71)
3	Pyridoxal	$C_8H_9NO_3$ (3.01 ppm)	1.56	166.0504	138.0551 (100); 108.0443 (56.53)
4	L-Asparagine	$C_4H_8N_2O_3$ (1.53 ppm)	1.64	131.0453	114.0185 (100); 95.0239 (21.51); 70.0286 (38.76)
5	L-Glutamine	$C_5H_{10}N_2O_3$ (2.07 ppm)	1.65	145.0611	127.0502 (93.52); 109.0396 (31.30); 84.0442 (21.65)
6	L-glutamic acid	$C_5H_9NO_4$ (1.37 ppm)	1.81	146.0450	128.0342 (52.95); 102.0548 (100)
7	Uridine	$C_9H_{12}N_2O_6$ (5.35 ppm)	1.85	243.0625	200.0558 (9.58); 110.0236 (100)
8	Quinic acid	$C_7H_{12}O_6$ (4.19 ppm)	1.97	191.0558	173.0445 (2.07); 127.0389 (3.40)
9	Niacin	$C_6H_5NO_2$ (0.82 ppm)	2.73	122.0238	94.0286 (5.06); 78.0336 (3.99)

10	L-Tyrosine	$C_9H_{11}NO_3$ (3.89 ppm)	2.73	180.0662	163.0392 (100); 119.0491 (67.29); 93.0334 (24.76)
11	Malic acid	$C_4H_6O_5$ (2.26 ppm)	2.75	133.0134	115.0025 (100); 71.0126 (45.50)
12	Citric acid	$C_6H_8O_7$ (4.19 ppm)	2.82	191.0194	111.0076 (11.67); 85.0282 (100)
13	Guanosine	$C_{10}H_{13}N_5O_5$ (6.38 ppm)	3.01	282.0851	150.0411 (100); 133.0145 (7.54)
14	Adenosine	$C_{10}H_{13}N_5O_4$ (6.39 ppm)	3.23	266.0901	134.0461 (100)
15	L-Phenylalanine	$C_9H_{11}NO_2$ (3.05 ppm)	4.34	164.0711	147.0442 (100); 72.0079 (34.30)
16	Pantothenic Acid	$C_9H_{17}NO_5$ (5.04 ppm)	7.10	218.1034	146.0813 (73.48); 88.0392 (100)
17	L-Tryptophan	$C_{11}H_{12}N_2O_2$ (4.43 ppm)	7.37	203.0824	142.0652 (27.99); 116.0494 (100); 74.0235 (43.29)
18	Caffeoylated monosaccharides (Peng et al., 2021)	$C_{15}H_{18}O_9$ (5.28 ppm)	11.67; 11.91; 12.70; 13.29	341.0885	179.0342; 161.0235; 135.0441
19	Coumaroylated disaccharides	$C_{21}H_{28}O_{13}$ (4.52 ppm)	13.11; 13.54; 13.74; 14.00	487.1468	307.0828; 163.0392; 145.0285
20	‡ Secoisolariciresinol	$C_{20}H_{26}O_6$ (6.09 ppm)	16.76	361.1668	346.1422 (37.86); 179.0706 (26.43); 165.0548 (100)
21	‡ Nortrachelogenin	$C_{20}H_{22}O_7$ (4.82 ppm)	17.94	373.1300	327.1242 (6.65); 312.1009 (3.98); 147.0442 (10.56)
22	‡ Matairesinol	$C_{20}H_{22}O_6$ (5.04 ppm)	19.62	357.1351	342.1109 (8.61); 209.0816 (4.25); 122.0362 (14.23)
23	‡ Arjunolic acid/Asiatic acid	$C_{30}H_{48}O_5$ (4.72 ppm)	24.09	487.3441	421.3155 (0.11); 409.3109 (0.44)
24	Glycerophosphocoline (18:3)	$C_{26}H_{48}NO_7P$ (4.98 ppm)	25.69	562.3167 $(M+HCOOH-H)^-$	277.2173 (100); 224.0690 (13.23)
25	Glycerophosphoethanolamine (18:2)	$C_{23}H_{44}NO_7P$ (4.20 ppm)	26.69; 27.17	476.2792	279.2328; 196.0375
26	Glycerophosphocoline (18:2)	$C_{26}H_{50}NO_7P$ (4.08 ppm)	26.75; 27.24	564.3319 $(M+HCOOH-H)^-$	279.2330; 224.0691
27	Glycoglycerolipid (18:3)	$C_{27}H_{46}O_9$ (3.90 ppm)	27.78	513.3078	277.2171 (100); 253.0928 (5.07)
28	Glycerophosphoethanolamine (16:0)	$C_{21}H_{44}NO_7P$ (3.76 ppm)	27.66; 28.20	452.2789	255.2328; 196.0374
29	Glycerophosphocoline (16:0)	$C_{24}H_{50}NO_7P$ (3.89 ppm)	27.73; 28.32	540.3317 $(M+HCOOH-H)^-$	255.2328; 224.0689

30	Glycerophosphoethanolamine (18:1)	$C_{23}H_{46}NO_7P$ (4.39 ppm)	28.54; 29.06	478.2949	281.2485; 196.0374
31	Hydroxyoctadecadienoic acid	$C_{18}H_{32}O_3$ (5.08 ppm)	29.12	295.2283	277.2173 (100); 195.1384 (26.92); 171.1019 (45.17)
32	‡ Maslinic acid	$C_{30}H_{48}O_4$ (4.24 ppm)	29.71	471.3489	423.3274 (0.39)
33	Glycerophosphoethanolamine (18:0)	$C_{23}H_{48}NO_7P$ (4.16 ppm)	31.44	480.3105	283.2642 (100); 196.0373 (10.91)
34	Octadecatrienoic acid	$C_{18}H_{30}O_2$ (5.41 ppm)	34.05	277.2177	259.2071 (1.72)
35	‡ Oleanolic acid/ Ursolic acid	$C_{30}H_{48}O_3$ (5.05 ppm)	34.93	455.3543	407.3312 (0.07)

‡ Identification and quantification have been performed through the comparison with the related analytical standard.

Subsequently, for a deeper investigation, a Feature-Based Molecular Networking (FBMN) job was also carried out. It is able to group related NPs within a network since structurally similar molecules share similar MS/MS fragmentation patterns (Nothias et al., 2020). FBMN job allowed us to identify several chlorogenic acids, reported in Figure 4.4 and Table 4.2 and circled in green. Compounds eluted at 13.32, 14.39 and 15.34 min and generating the same deprotonated ion $[M-H]^-$ at m/z 353.09 were recognized as mono caffeoylquinic acids (CQA, $C_{16}H_{18}O_9$, mass error of 5.38 ppm). Indeed, MS2 ions at m/z 191.06 and 173.04 correspond to deprotonated and dehydrated quinic acid, while fragments at m/z 179.03 and 135.04 derive from the deprotonation and decarboxylation of the caffeoyl moiety. MS2 base peak of the species with RT 15.34 min at m/z 173.04 allowed its assignation as 4-CQA. The others two compounds provided the same MS2 base peak ion at m/z 191.06, but the intensity of the fragment ion at m/z 179.03 allowed to identify the first compound (RT 13.32; m/z 179.03 intensity of 40%) as 3-CQA and the second (RT 14.39; m/z 179.03 intensity of 4%) as 5-CQA (Clifford et al., 2003).

The compound with RT 16.34 min and parent ion at m/z 367.10 ($C_{17}H_{20}O_9$, mass error of 5.45 ppm) is a feruloylquinic acid (FQA): MS2 ions at m/z 193.05 and 134.04 derive from the deprotonation and from demethylation plus decarboxylation of the feruloyl moiety, respectively. MS2 base peak at m/z 191.06, corresponding to deprotonated quinic acid, allowed its assignation as 5- FQA (Clifford et al., 2003).

Species eluted at 18.58 and 19.60 min and generating the deprotonated ions $[M-H]^-$ at m/z 515.12 are dicaffeoylquinic acids (di-CQA, $C_{25}H_{24}O_{12}$, mass error of 4.08 ppm). They shared the same MS2 base peak at m/z 173.04 that suggests a substitution at position 4. The second compound (RT 19.60 min) was identified as 3,4-diCQA for the presence of the fragment ion at m/z 335.08 $[CQA- H_2O-H^+]^-$, absent in the MS2 spectrum of the first one (RT 18.58 min), assigned to 4,5-diCQA (Clifford et al., 2003).

The compound with RT 16.74 min and parent ion at m/z 337.09 was identified as 4-coumaroyl-quinic acid (4-pCoQA, C16H18O8, mass error of 6.53 ppm), as suggested by the MS2 base peak at m/z 173.04. Ions at m/z 499.13 and 529.14 eluted at 19.80 and 20.14 min were assigned to 3-coumaroyl-4-caffeoylquinic acid ($C_{25}H_{24}O_{11}$, mass error of 4.81 ppm) and a 4-caffeoyl 3-feruloylquinic acid ($C_{26}H_{26}O_{12}$, mass error of 3.78 ppm). The fragments at m/z 173.04 (base peak) and at m/z 353.09 suggest a caffeoyl moiety at position 4, whereas those at m/z 119.05 and 134.04 indicate the presence of a coumaroyl and a feruloyl moiety, respectively, at position 3 (Clifford et al., 2003).

The ions shown in Figure 4.4 and Table 4.2 and circled in orange were assigned to oxidation products of caffeic acid derivates, since they shared the same MS2 peaks at m/z 177.02 and 133.03. In particular, species with parent ion at m/z 513.11 (RT 18.67 min) and 511.09 (RT 18.66 min), showing the MS2 peak at m/z 351.07, were identified

as mono ($C_{25}H_{22}O_{12,}$ mass error of 5.65 ppm) and di-oxidized forms of di-CGA ($C_{25}H_{20}O_{12,}$ mass error of 4.70 ppm).

The ions at m/z 333.06 (RT 14.84 min) and m/z 495.09 (RT 17.36 min), generating the MS2 fragment at m/z 93.03, were assigned as mono-oxidized forms of caffeoylquinic acid lactone (or caffeoyl skimic acid, $C_{16}H_{14}O_8$, mass error of 6.31 ppm) and dicaffeoylquinic acid lactone (or dicaffeoyl skimic acid, $C_{25}H_{20}O_{11}$, mass error of 4.65 ppm), with which they coelute (Peng et al., 2021).

Moreover, the extract contains feruloyl glycosides, circled in blue in Figure 4.4 and Table 4.2. In the MS2 spectrum they showed fragments at m/z 193.05 and 175.04, characteristic of the feruloyl moiety and/or at m/z 337.09, due to the loss of hexosyl moiety and one molecule of water and/or at m/z 295.08, 265.07 and 235.06, derived from by cross-ring cleavage of the remaining sugar residue (Quéméner and Ralet, 2004). In particular, the species at m/z 517.16 (RT 13.62, 13.93, 14.29 min) were feruloyl disaccharides ($C_{22}H_{30}O_{14}$, mass error of 3.87 ppm) and those at m/z 355.10 (RT 12.15 min) were feruloyl monosaccharides ($C_{16}H_{20}O_9$, mass error of 5.91 ppm). The ions at m/z 489.16 (RT 14.17 and 14.26 min) and m/z 459.15 (RT 14.33 min) could be ferulic acids combined with a hexose and a C5 polyalcohol ($C_{21}H_{30}O_{13}$, mass error of 4.50 ppm) or a C4 polyalcohol ($C_{20}H_{28}O_{12}$, mass error of 4.79 ppm), respectively.

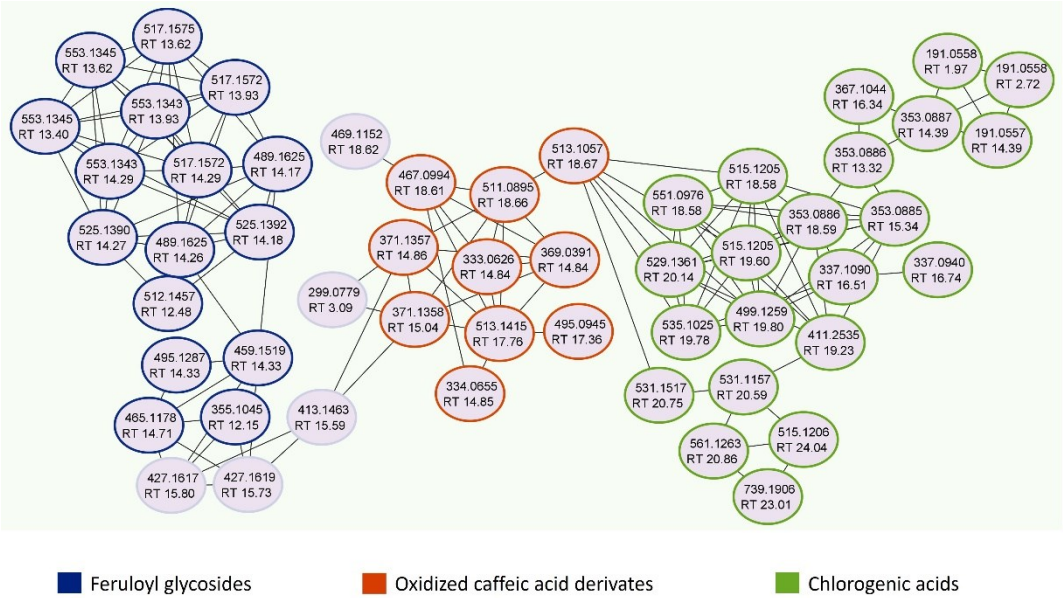

Figure 4.4 *Molecular networks (MNs) showing the presence of chlorogenic acids, oxidized caffeic acid derivates and feruloyl glycosides in JasHEx.*

Table 4.2 *Molecular formula (MF), Retention time (RT), MS data of the identified compounds in the Molecular Networks reported in Figure 4.4.*

Compound	MF (Mass error ppm)	RT min	Precursor ions m/z	MS^2 ions m/z (Relative intensity %)
Quinic acid	$C_7H_{12}O_6$ (4.19 ppm)	1.97; 2.72; 14.39	191.0558	173.0445; 127.0389
3-caffeoylquinic acid	$C_{16}H_{18}O_9$ (5.38 ppm)	13.32	353.0886	191.0555 (100); 179.0343 (39.63); 135.0441 (23.81)
5-caffeoylquinic acid	$C_{16}H_{18}O_9$ (5.66 ppm)	14.39	353.0887	191.0554 (100); 179.0343 (4.18); 135.0441 (3.34)
4-caffeoylquinic acid	$C_{16}H_{18}O_9$ (5.10 ppm)	15.34	353.0885	191.0554 (66.37); 179.0342 (75.16); 173.0447 (100)
5-feruloylquinic acid	$C_{17}H_{20}O_9$ (5.45 ppm)	16.34	367.1044	193. 0500 (13.06); 191.0554 (100); 134.0363 (6.75)
4-coumaroylquinic acid	$C_{16}H_{18}O_8$ (6.53 ppm)	16.74	337.0940	173.0447 (100); 163.0392 (24.31); 93.0333 (14.61)

4,5-dicaffeoylquinic acids	$C_{25}H_{24}O_{12}$ (4.08 ppm)	18.58	515.1205	353.0882 (5.67); 179.0342 (75.69); 173.0447 (100)
3,4-dicaffeoylquinic acids	$C_{25}H_{24}O_{12}$ (4.08 ppm)	19.60	515.1205	353.0883 (4.42); 335.0782 (0.51); 179.0342 (74.88); 173.0447 (100)
3-coumaroyl-4-caffeoylquinic acid	$C_{25}H_{24}O_{11}$ (4.81 ppm)	19.80	499.1259	353.0887 (1.52); 173.0447 (100); 163.0391 (14.24); 119.0491 (1.49)
4-caffeoyl-3-feruloylquinic acid	$C_{26}H_{26}O_{12}$ (3.78 ppm)	20.14	529.1361	353.0882 (2.42); 173.0447 (100); 134.0360 (1.52)
Caffeoyl quinic acid lactone (or caffeoyl skimic acid) mono-oxidized form	$C_{16}H_{14}O_8$ (6.31 ppm)	14.84	333.0626	177.0186 (12.08); 133.0284 (100); 93.0334 (4.39)
Dicaffeoyl quinic acid lactone (or dicaffeoyl skimic acid) mono-oxidized form	$C_{25}H_{20}O_{11}$ (4.65 ppm)	17.36	495.0945	177.0186 (15.72); 133.0285 (100); 93.0334 (25.26)
Dicaffeoylquinic acid mono-oxidized form	$C_{25}H_{22}O_{12}$ (5.65 ppm)	18.67	513.1057	351.0718; 177.0186 (22.11); 173.0447 (100); 133.0285 (42.45)
Dicaffeoylquinic acid di-oxidized form	$C_{25}H_{20}O_{12}$ (4.70 ppm)	18.66	511.0895	351.0727; 177.0186 (7.97); 173.0447 (4.58); 133.0285 (100)
Feruloyl monosaccharide	$C_{16}H_{20}O_9$ (5.91 ppm)	12.15	355.1045	235.0601; 193.0499 (18.43); 175.0393 (100)
Feruloylated disaccharides	$C_{22}H_{30}O_{14}$ (3.87 ppm)	13.62; 13.93; 14.29	517.1572	337.0929; 193.0500; 175.0393

4.2.1.2 JasHEx quantitative analysis

The lignans secoisolariciresinol, nortrachelogenin and matairesinol and the triterpenes arjunolic acid, asiatic acid, maslinic acid were not known to be contained in plants of the genus *Jasminum*, until now. Therefore, we decided to focus on and quantify the metabolites belonging to these two classes. Quantification methods were validated as reported in Table 4.3. Nortrachelogenin and ursolic acid are the most abundant lignan and triterpene, respectively, present in JasHEx (Table 4.4).

Table 4.3 *Characteristics of the quantitative evaluation of lignanic and triterpenic compounds*

Compound	Range (nM)	Calibration curve	R^2	LOD (nM)	LOQ (nM)
Secoisolariciresinol	50-25000	y = 2.00E+08 x	0.9951	3	10
Nortrachelogenin	50-25000	y = 2.00E+08 x	0.9938	15	50
Matairesinol	50-25000	y = 3.00E+08 x	0.9917	3	10
Arjunolic acid	100-25000	y = 2.00E+07 x	0.9929	15	50
Asiatic acid	100-25000	y = 2.00E+07 x	0.9865	8	25
Maslinic acid	100-25000	y = 4.00E+07 x	0.9957	8	25
Oleanolic acid	100-250000	y = 2.00E+07 x	0.9953	0.3	1
Ursolic acid	100-250000	y = 1.00E+07 x	0.9935	0.3	1

Table 4.4 *Lignanic and triterpenic content.*

Compound	Amount (µg/g of extract)	% RSD
Secoisolariciresinol	0.67	0.94
Nortrachelogenin	39.96	2.46
Matairesinol	6.75	0.65
Arjunolic acid	235.80	0.97
Asiatic acid	336.71	2.55
Maslinic acid	144.02	2.82
Oleanolic acid	214.00	3.57
Ursolic acid	542.80	2.17

4.2.2 JasHEx biological activity evaluation

4.2.2.1 Cytosolic ROS detection in H_2O_2 stressed HaCaT cells

Since the large majority of secondary metabolites identified in the extract such as chlorogenic acids, lignans and triterpenes possesses well known antioxidant activity (Agnieszka Loboda and Dulak, n.d.; Touré and Xueming, 2010; Xu et al., 2012), JasHEx effect on cytosolic ROS was evaluated. Therefore, HaCaT cells were treated for 2h with the extract (0.0006%, 0.002% and 0.006% p/v) or with the positive control ascorbic acid (500 μM), incubated with an indicator for ROS and then stressed with H_2O_2 (450 μM). After oxidation, the indicator yields a fluorescent adduct. As shown in Figure 4.5, the H_2O_2 induced stress increased cytosolic ROS formation by 50% and this was reduced by almost 30% both in case of ascorbic acid and JasHEx pretreatment.

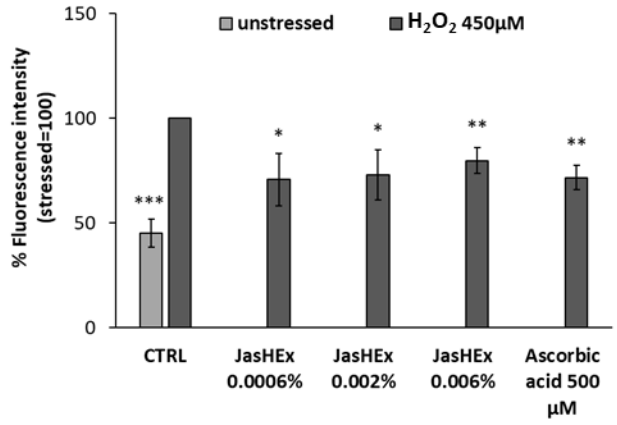

Figure 4.5 *Bar graphs showing JasHEx ability to decrease cytosolic ROS levels in H_2O_2 stressed HaCaT cells. The error bars represent the standard deviations and the asterisks indicate significant variations according to Student's t-test (* $p<0.05$, ** $p<0.01$, *** $p<0.001$).*

4.2.2.2 AGE detection in glyoxal treated HDF

Since AGE formation is dependent on oxidation reactions (Chen et al., 2022), JasHEx anti-glycation activity was evaluated by an enzyme-linked immunosorbent assay (ELISA). It allowed us to detect, by a specific antibody, AGE products in Human Dermal Fibroblasts (HDF), treated or not with the extract (0.0006% and 0.002% p/v), in presence of 0.5% glyoxal at 50°C for one week. Aminoguanidine (AG) 1 µM was used as positive control. The treatment with 0.5% glyoxal stimulated the formation of AGE products by 90%, whereas the incubation with JasHEx at both concentrations was able to reduce it by 20% (Figure 4.6).

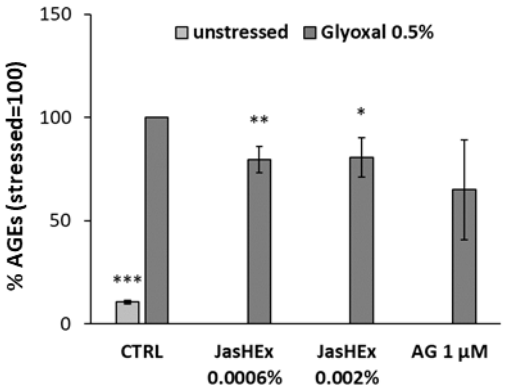

Figure 4.6 *Bar graphs showing JasHEx ability to inhibit AGE formation in glyoxal treated HDF. The error bars represent the standard deviations and the asterisks indicate significant variations according to Student's t-test (* $p<0.05$, ** $p<0.01$, *** $p<0.001$).*

4.2.2.3 Fibrillin-1 detection in methylglyoxal stressed skin explants

On the basis of these results, to confirm antiglycation effect in a physiological context, JasHEx effect was tested on methylglyoxal stressed skin explants. Since fibrillin-1, an ECM protein essential for the dermal elastic network, is highly sensitive

to glycation, we decided to use it as a biomarker. Indeed, the increase of fibrillin-1 glycation induced by methyl-glyoxal significantly alters its conformational structure and the modified protein is not anymore recognized by the used antibody (Gasser et al., 2011). Therefore, skin explants were treated with JasHEx (0.002% and 0.006% p/v) before and after 500 µM methylglyoxal addition and the content of Fibrillin-1 was detected by Immuno-Histo-Fluorescence assay. Aminoguanidine (AG) 1 mM was used as positive control. As shown in Figure 4.7 A and B, the addition of 500 µM methylglyoxal reduced fibrillin-1 levels by 30%. The incubation with the extract was able to protect fibrillin-1 from methylglyoxal-induced glycation. In particular, the treatment with JasHEx at the concentration of 0.002% p/v increased fibrillin-1 content by 35%, similar to the positive control.

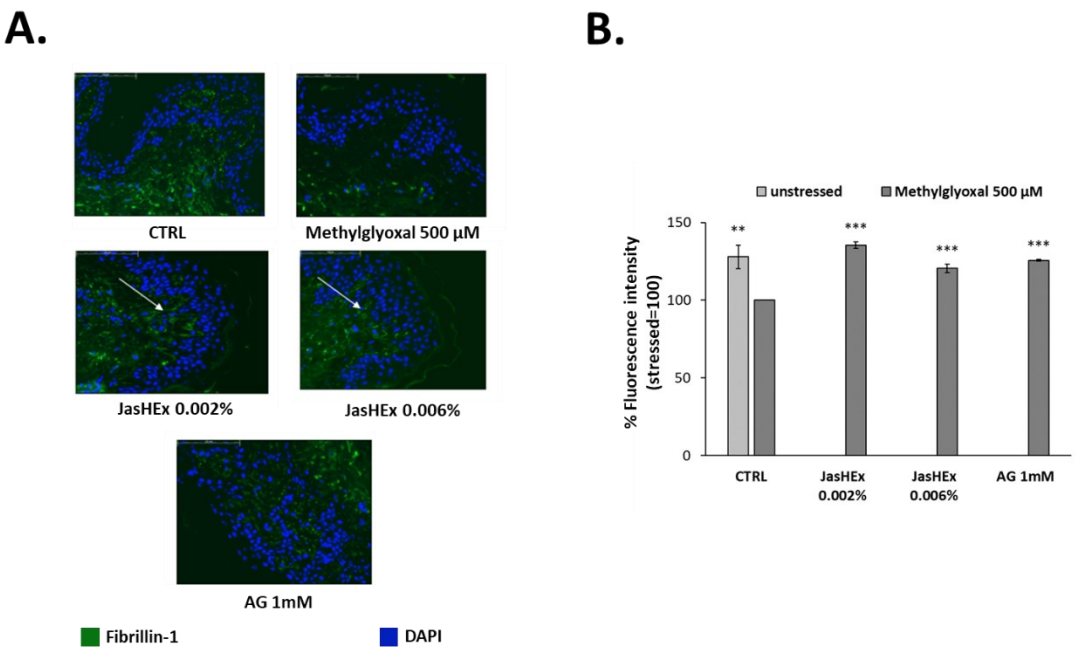

Figure 4.7 (*A) Photographs of skin sections in which fibrillin-1 has been highlighted with a specific antibody labeled with fluorophore (green) and the nuclei (blue) have been stained with 4',6-diamidine-2-phenylindole (DAPI). (B) Bar graphs obtained measuring the fluorescence intensity related to the photographs reported in A. The*

error bars represent the standard deviations and the asterisks indicate significant variations according to Student's t-test (p<0.05, ** p<0.01, *** p<0.001).*

4.2.2.4 Analysis of collagen type I synthesis

To measure JasHEx effect on the synthesis of collagen type I, further than its protective effect from glycation, Procollagen Type I C-peptide (PIP) was used as indicator. Indeed, the collagen type I is synthesized as procollagen that contains peptide sequences (pro-peptides) at both the amino-terminal and carboxy-terminal ends, essential for the winding of procollagen into triple-helix. These pro-peptides are cleaved during secretion and the triple helix collagens polymerize into extracellular fibrils (Prockop, 1985). Therefore, the amount of released PIP reflects the amount of synthesized collagen, stoichiometrically. Thus, HDF were treated for 24 hours with JasHEx (0.0006%, 0.002% and 0.006% p/v) or with TGF-β (2.5 ng/mL), used as positive control, and processed for an AlphaLISA assay to measure PIP levels. As shown in Figure 4.8, the incubation with all extract concentrations significantly increased the content of PIP.

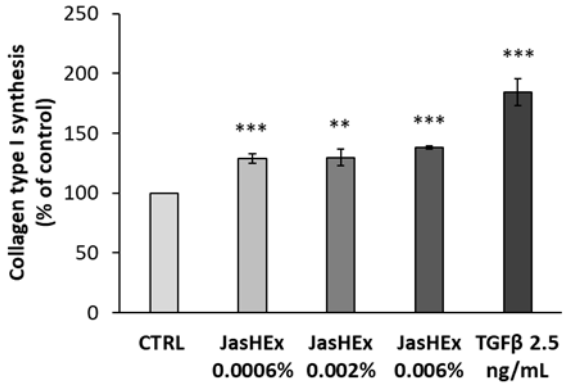

Figure 4.8 *Bar graphs showing JasHEx ability to increase collagen type I synthesis. The error bars represent the standard deviations and the asterisks indicate*

significant variations according to Student's t-test (p<0.05, ** p<0.01, *** p<0.001).*

4.2.2.5 Analysis of Nrf2/ARE pathway in HaCaT cells

Due to the antioxidant and antiglycation activity of JasHEx, the effect of the extract on Nrf2/ARE (Nuclear related factor 2/ Antioxidant Response Element) pathway was investigated, since it is the most pivotal endogenous antioxidative system studied so far (Huang et al., 2013). Therefore, a Nrf2 luciferase-based transcription activation assay on HaCaT cells, incubated for 2 h with the extract (0.0006%, 0.002% and 0.006% p/v) after transduction, was performed. The treatment with 0.006% p/v JasHEx increased luciferase activity linked to Nrf2 by 28% (Figure 4.9), similar to 50 µM resveratrol, used as positive control.

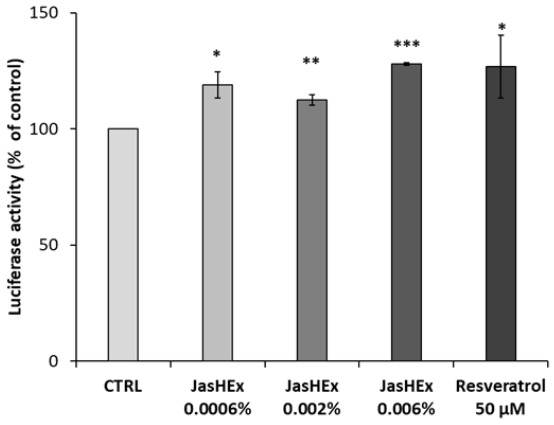

Figure 4.9 *Bar graphs showing JasHEx effect (A) to activate Nrf2/ARE signaling. The error bars represent the standard deviations and the asterisks indicate significant variations according to Student's t-test (* p<0.05, ** p<0.01, *** p<0.001).*

4.2.2.6 Analysis of OH-1 and SOD-1 gene expression in HaCaT cells

The effect of JasHEx in HaCaT cells on the expression of Nrf2 gene targets like Super-oxide dismutase 1 (SOD-1) and Heme oxygenase-1 (HO-1) was also tested. To do this, HaCaT cells were treated with JasHEx (0.002% and 0.006% p/v) for 6 h and then SOD-1 and OH-1 expression was analyzed by RT-PCR. The results, reported in Figure 4.10 A and B, demonstrated that the extract increased the expression of both genes, as the positive control resveratrol (50 μM).

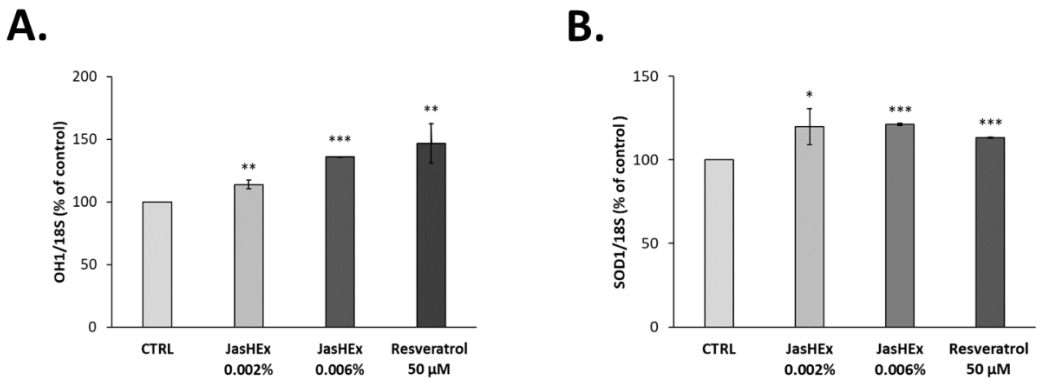

Figure 4. 10 *(A, B) Bar graphs showing JasHEx effect to increase OH-1 (A) and SOD-1 (B) gene expression in HaCaT cells. The error bars represent the standard deviations and the asterisks indicate significant variations according to Student's t-test (* p<0.05, ** p<0.01, *** p<0.001).*

4.2.2.7 NO determination in LPS stimulated RAW 264.7 cells

Since Nrf2 also plays a role in counteracting NF-κB-driven inflammatory response and since inducible Nitric Oxide Synthase (iNOS) is activated through NF-κB pathway (Arias-Salvatierra et al., 2011; Tu et al., 2019), JasHEx anti-inflammatory activity was evaluated performing a nitric oxide assay. RAW 264.7 cells were treated with the extract (0.0006%, 0.002% and 0.006% p/v) or with the positive control TPCK (10 μM)

and, then, were stressed with LPS (2 μg/mL). The amount of NO was revealed by adding Griess reagent and the absorbance was measured at 540 nm. As shown in Figure 4.11, JasHEx reduced the levels of NO approximately by 30% at all tested concentrations.

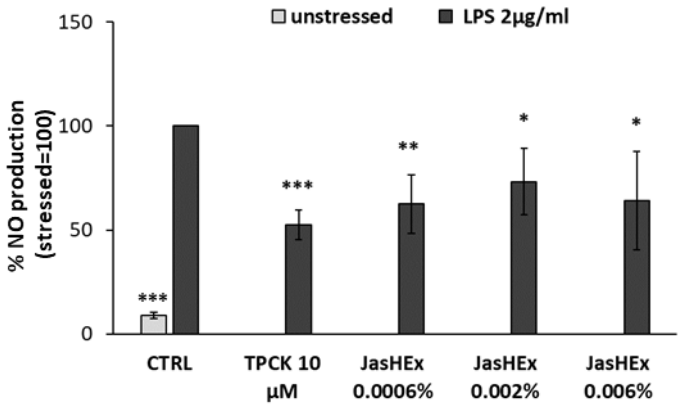

Figure 4.11 *Bar graphs showing JasHEx effect to reduce NO production in LPS stimulated RAW 264.7 cells. The error bars represent the standard deviations and the asterisks indicate significant variations according to Student's t-test (* $p<0.05$, ** $p<0.01$, *** $p<0.001$).*

Section 4 – Chapter 3

Discussion

Here, an hydroethanolic extract derived from *Jasminum sambac* cell cultures (JasHEx) was studied. Its GNPS-aided mass spectrometry based chemical characterization revealed the presence of phenolic acid derivatives (mainly chlorogenic acids), lignans (secoisolariciresinol, nortrachelogenin and matairesinol) and triterpenes (arjunolic acid, asiatic acid, maslinic acid, oleanolic acid and ursolic acid). All of these secondary metabolites possess well known antioxidant properties. Indeed, chlorogenic acids (Xu et al., 2012) and lignans (Pei et al., 2022; Touré and Xueming, 2010), thanks to their phenolic moiety, have free radical scavenging and chain-breaking antioxidant activities: they donate hydrogen atoms to free radicals giving rise to phenoxyl radicals stabilized by resonance and thereby inhibiting the propagation of radical chain reactions and other biological oxidants. Moreover, they act as secondary antioxidants by binding metal ions (Fe(III) and Cu(II)) able to catalyze oxidative processes. Moreover, thanks to an accurate quantitative analysis, it emerged that JasHEx contains relevant amounts of arjunolic acid, asiatic acid, maslinic acid, oleanolic acid and ursolic acid: all these triterpenes can also act as good free radical scavengers, chain-breaking antioxidants or transition metal chelators (Hemalatha et al., 2010; Lozano-Mena et al., 2014; Nagoor Meeran et al., 2018; Samsonowicz et al., 2021; Santiago et al., 2014). On the basis of these results, the antioxidant activity of JasHEx was evaluated. It was able of reducing cytosolic ROS production in H_2O_2 stressed keratinocytes. Furthermore, since AGE formation is

dependent on oxidation reactions (Chen et al., 2022; Twarda-Clapa et al., 2022), the antiglycation potential of the extract was tested. It was confirmed by both *in vitro* and *ex vivo* assays: JasHEx reduced AGE formation in glyoxal treated HDF and methylglyoxal stressed skin explants, an already used model to highlight the anti-glycation activity of natural substances (Gasser et al., 2011).

In addition to this, JasHEx also showed an extracellular matrix booster effect increasing the production of collagen type I, that is highly sensitive to glycation (Dyer et al., 1993; Reiser, 1998; Verzijl et al., 2000) and whose levels are significantly reduced by oxidative stress (Sárdy, 2009).

In vitro assays proved that the antioxidant properties of JasHEx, like those of chlorogenic acids (Wang et al., 2022) and triterpenoids (Agnieszka Loboda and Dulak, 2012), are not only related to free radical scavenging and metal chelating activities, but also to the enhancement of Nrf2/ ARE pathway. This is the most pivotal endogenous antioxidative system studied so far: when cells are exposed to stressing conditions, Nrf2 dissociates from its cytoplasmic repressor kelch like ECH-associated protein 1 (Keap1) and translocates to the nucleus where interacts with ARE, activating the transcription of its target genes; the expression of these genes involved in de-toxification, NADH regeneration, glutathione (GSH) and thioredoxin (TXN) based antioxidant system, lipid, eme and iron metabolism increases cell resistance to oxidative stress (Hayes and Dinkova-Kostova, 2014; Tonelli et al., 2018).

Moreover, the extract also showed an anti-inflammatory activity, decreasing the re-lease of NO in LPS stimulated macrophages. This effect is also related to the triggering of Nrf2/ARE pathway: Nrf2 upregulates the expression of HO-1, that, creating a more

reducing environment, inhibits the activation of the pro-inflammatory transcription factor NF-κB (Tu et al., 2019).

On the basis of the chemical composition and the biological activity proved by *in vitro* and *ex vivo* experiments, JasHEx can be considered as a natural powerful antioxidant booster against oxidative stress induced skin aging.

Section 4 – Chapter 4

Materials and Methods

4.4.1 Plant tissue cultures and extract preparation

A certified Arabian jasmine (*Jasminum sambac*) was obtained from a local nursery ("Ladre di Piante," Pistoia, Toscana Region, Italy). *Jasminum sambac* leaves were soaked in 70% ethanol (Sigma Aldrich, St. Louis, MO, USA) for 1 min and surface-sterilized with 1% (v/v) of commercial bleach supplemented with Tween 20 (Sigma Aldrich, St. Louis, MO, USA) for 8 min, followed by three rinses in sterile distilled water. Then, the leaves were excised into 0.5–1.0 cm pieces and cultured on full-strength MS medium (Murashige and Skoog, 1962) containing 3% (w/v) sucrose, 0.2 mg/l 2,4D, and 8 g/L phytoagar. The explants were monthly subcultured onto a fresh medium for three months. Once a yellow-green, friable and fast-growing callus was obtained, the plant cells were transferred to the liquid MS medium, supplemented with 3% (w/v) sucrose and 0.2 mg/l 2,4D. The suspension was stirred in a gyratory shaker at 110 rpm and 27°C in dark climate room. The dark-grown cells were scaled up every week from small-scale to large-scale flasks, until to reach liquid suspension cultures of about 177 g/l. The preparation of *Jasminum sambac* cell culture hydro-ethanolic extract (JasHEx) was performed by adding 2000 mL of a solution ethanol/water (90/10, v/v) to 500g of fresh cells. The mixture was homogenized 3 min at 1,500 rpm and 6 min at 3,800 rpm using a Grindomix GM300 knifemill (Retsch GmbH, Haan, Germany). The resulting suspension was left under stirring at 400 rpm for 2 h at 25°C,

avoiding light exposure. The suspension was then centrifuged at 6,300 rpm for 10 min at 4°C. The supernatant was re-covered, filtered and then concentrated under vacuum in a rotary evaporator (IKA RV8, IKA-Werke GmbH & Co, Staufen, Germany) set to 25°C. Finally, the pH of the concentrated extract was adjusted to 7.0 with 10 N NaOH and then freeze-dried until obtaining a fine powder.

4.4.2 UHPLC-MS/MS analysis for JasHEx chemical characterization

A biphasic butanol/water extraction was performed. The butanolic fraction was dried and dissolved in methanol (10 mg/mL) before the UHPLC-MS/MS analysis, carried out on a Q-Exactive Classic Mass Spectrometer from Thermo-Scientific equipped with a Thermo Scientific™ UltiMate™ 3000 UPLC system. All the chromatographic runs were performed using a Phenomenex Luna® C18 100 Å (150 x 2.0 mm, particle size 3 µm) column at 40°C and flow rate of 0.200 mL/min. The injection volume was 5 µL. The mobile phase consisted of A (water from Romil at 0.1% acetic acid) and B (100% acetonitrile from Romil), using a gradient elution of 5% B at 0-5 min, 5-14% B at 5-8 min, 14-32% B at 8-11 min, 32-95% B at 11-32 min, 95-98% B at 32-33 min, 98% B at 33-38 min, 98-5% B at 38-39 min and 5% B at 39-45 min. All the MS and MSMS analysis were carried out in ESI negative mode with the sheat gas flow rate at 30 (arbitrary units), the auxiliary gas flow rate at 5 (arbitrary units), the spray voltage at 3.2 kV, the capillary temperature and the auxiliary gas heater temperature at 300 °C. Data were acquired with a Full MS/dd-MS2 (Top5) mode. Full MS setting were: resolution of 70.000, AGC target of 1e6, maximum IT of 200 ms and scan range from 100 to 800 m/z. dd-MS2 settings were: resolution of

17.500, AGC target of 2e5, maximum IT of 65 ms, isolation window of 1.5 m/z and NCE of 35.

4.4.3 Global Natural Products Social Molecular Networking analysis

For metabolite identification, Global Natural Products Social Molecular Networking (GNPS; https://gnps.ucsd.edu) was used (M. Wang et al., 2016). All those MS and MSMS signals not assigned by GNPS were carefully inspected and assigned accordingly to literature. Raw files were converted to mzXML format by MS Converter General User Interface software (ProteoWizard; http://proteowizard.sourceforge.net/project.shtml), before GNPS spectral library search analysis. It was achieved using precursor ion mass tolerance of 0.025 Da, fragment ion mass tolerance of 0.02 Da, minimum matched peaks of 2 and score threshold of 0.7. The results obtained were manually verified.

mzXML data were processed using MZmine 2.53 (Pluskal et al., 2010) before the Feature-Based Molecular Networking (FBMN) job (Nothias et al., 2020). The mass detection step was performed using the Centroid mass detector and keeping the noise level at $5e^3$. The ADAP (Automated Data Analysis Pipeline) chromatogram building was realized with the following settings: min group size in number of scans of 5, group intensity threshold of $5e^3$, min highest intensity of $5e^4$, m/z tolerance of 0.01 m/z or 10 ppm. The chromatogram deconvolution was achieved using Wavelets (ADAP) as algorithm, S/N threshold of 3, min feature height of $10e^5$, coefficient/area threshold of 5, peak duration range of 0.10-3.00 min and RT wavelet range 0.00-0.05. Chromatograms were deisotoped using the isotopic peaks grouper algorithm with a m/z tolerance of 0.001 m/z or 5.0 ppm and a RT tolerance of 0.10 min. FBMN job was

performed using parent mass tolerance of 0.02 Da and a MS2 fragment ion tolerance of 0.02 Da. Edges were filtered to have a score threshold of 0.7 and minimum 2 matched peaks. Moreover, the maximum number of neighbour nodes for each node was set to 10. The obtained network file was imported into Cytoscape 3.9.1 (Shannon et al., 2003).

4.4.4 Quantitative analysis of lignans and triterpenes

The same UHPLC conditions reported for the qualitative analysis were used for the quantitative analysis of lignans, while for that of triterpenes they were optimized in order to separate two pairs of isomers, arjunolic/asiatic acid and oleanolic/ursolic acid. The analysis was performed on a Q-Exactive Classic Mass Spectrometer as previously described. The separation was carried out by a Phenomenex Kinetex® EVO C18 300 Å (150 x 2.1 mm, particle size 5 μm). The mobile phase consisted of A (5 mM ammonium acetate aqueous solution, pH 9.00 adjusted by ammonium hydroxide) and B (100% acetonitrile) using a gradient elution of 13–28% B at 0–20 min, 28–65% B at 20-24 min, 65–75% B at 24-28min, 75-95% at 28-28,5 min, 95% at 28,5-32 min, 95-13% at 32-32,1 min, 13% at 32,1-44 min. The flow rate was 0.450 mL/min and the injection volume was 5 μL. For both lignans and triterpenes, data were acquired with a Full MS-SIM and PRM mode. Full MS-SIM settings were: resolution of 70.000, AGC target of $3e^6$, maximum IT of 200 ms and scan range from 200 to 800 m/z for lignans and from 400 to 850 m/z for triterpenes. PRM settings were: resolution of 70.000, AGC target of $2e^5$, maximum IT of 100 ms, isolation window of 1.0 m/z and NCE of 35 in the case of lignans and 50 in that of triterpenes. We purchased nortachelogenin (#LCA52174) from Biosynth Carbosynth, matairesinol (#80497) and

maslinic acid (#83209) from PhytoLab GmbH & Co.KG, secoisolariciresinol (#60372) and arjunolic acid (#SMB00119) from Sigma-Aldrich, asiatic acid (#0027), oleanolic acid (#0041 S) and ursolic acid (#0037 S) from Extrasynthèse. The calibration curves were obtained by injecting standards solutions in the concentration range of 0.05-25 μM for lignans and 0.1-25/250 μM for triterpenes. The limit of detection (LOD) and limit of quantification (LOQ) for standards were determined on the basis of the signal to noise (S/N) ratio.

4.4.5 Skin cell cultures and explants

Immortalized Human Keratinocytes (HaCaT), purchased from Addexbio Technologies (San Diego, CA, USA), were maintained in Dulbecco's Modified Eagle Medium (DMEM; Sigma Aldrich, St. Louis, MO, USA) that was supplemented with 10% fetal bovine serum (FBS; Sigma Aldrich, St. Louis, MO, USA) in 95% air, 5% CO2, and humidified atmosphere at 37°C. Human dermal fibroblasts (HDF) were maintained in Dulbecco's Modified Eagle Medium (DMEM; Sigma–Aldrich, St. Louis, MO, USA) supplemented with 10% of fetal bovine serum (FBS; Sigma–Aldrich, St. Louis, MO, USA) in 95% air, 5% CO2, and humidified atmosphere at 37°C. Skin explants, obtained from the skin of healthy female donors (aged 31 and 40) at the surgery center Villa Cinzia (Naples, Italy), were cultured in 24-transwell plates in DMEM/FBS plus antibiotics in air–liquid conditions at 37 °C in 5% CO2 humidified air. All donors had given their written informed consent for the use of the skin tissues, according to the Declaration of Helsinki.

4.4.6 Cytosolic ROS assay in H_2O_2 stressed HaCaT cells

1.8 x 10^4 HaCaT were seeded in 96-well plates and grown for 20h. The cells were then treated for 2h with different concentrations of JasHEx (0.0006%, 0.002% and 0.006% p/v) or with 500 µM ascorbic acid, used as positive control. After that, they were washed in PBS (Phosphate-buffered saline) and incubated at 37°C with 100 µl/well of a solution containing: 10 mM of Hepes, 1.3 mM CaCl2, 1 mM MgSO4, 5 mM of glucose and 5 µM CM-H2DCFDA (5-(and-6)-chloromethyl-2',7'-dichlorodihydrofluorescein diacetate, Invitro-gen). After 45 minutes, a PBS wash was performed and the baseline fluorescence intensity of the cells was measured at 535 nm (excitation 485 nm), using the instrument EnVision (PerkinElmer). Then, the oxidative stress was induced by adding 450 µM H_2O_2 and the fluorescence of the samples measured after 30 minutes.

4.4.7 Enzyme-linked immunosorbent assay (ELISA) for AGE detection in glyoxal stressed Human Dermal Fibroblast (HDF) cells

1.5 x 10^4 HDF were seeded in 96-well plates and grown for 2 days. After washing with PBS, cells were fixed for 10 minutes with 100 µl of 4% formaldehyde in PBS. Subsequently, they were treated with JasHEx (0.0006% and 0.002% p/v) or the positive control 1 µM Aminoguanidine in presence of 0.5% glyoxal at 50°C for 1 week. After incubation, they were processed for an enzyme-linked immunosorbent assay (ELISA) using a specific anti-body against AGE (abcam ab23722).

4.4.8 ImmunoHistoFluorescence assay on methyl-glyoxal stressed skin explants for Fibrillin-1 detection

Skin explants were derived from two patients, 31 and 40 years old. From each skin biopsy, three punches were generated for each treatment occurred at air liquid interface. The first day, the punches were treated with JasHEx (0.002% and 0.006% p/v) or the positive control (1 mM Aminoguanidine) and after 24 hours 500 µM methyl-glyoxal was added. The treatments were refreshed up each two days to total of seven days. At the end of the period, the punches were processed for histological analysis, fixed in 4% paraformaldehyde (PFA), incubated in 15% sucrose, then in 30% sucrose and cryostored in OCT compound (Optimal cutting temperature) at -80°C. Cryosection of 5 µm were obtained with the cryostat CM1520 Leica. Slides with cryosections were hydrated for 30 min in PBS and placed in a "blocking" solution (6% BSA, 5% serum, 20 mM MgCl2, 0.2% Tween) for 1 h. Subsequently, they were incubated with the primary anti-Fibrillin 1 antibody (MA5-12770, Thermo Fisher) for 16 h at 4°C. The slides were washed with PBS for 30 min and then incubated with the secondary anti-rabbit Alexa-Fluor 546 antibody (A11035 Thermo Fisher) for 1 h. The nuclei were stained with DAPI (4', 6-5 diamidino-2-phenylindole) 1 g/mL in PBS for 10 min. The images were acquired with a fluorescence microscope and analyzed with the ImageJ software.

4.4.9 AlphaLISA assay to measure Procollagen Type I C-peptide (PIP) content

8 x 10^3 HDF were seeded in 96 well plate and treated for 24 hours with JasHEx (0.0006%, 0.002% and 0.006% p/v) or with TGF-β (2.5 ng/mL). After treatment, the

cells were processed according to the instructions of alpha LISA hPIP collagen kit provider (AL353HV, Perkin Elmer).

4.4.10 Nrf2 luciferase-based transcription activation assay

$6x10^3$ HaCaT cells in 96 well plate were seeded and grown for 16hours. After that, they were subjected to a Nrf2 luciferase-based transcription activation assay, using the ARE reporter kit BPS Bioscience, #60514. A transfection-ready ARE luciferase reporter vector (containing a firefly luciferase gene under the control of ARE responsive elements located upstream of a minimal promoter) together with an internal control (a constitutively expressing Renilla luciferase vector) were transiently co-transfected into HaCaT cells using X-TREME gene HP DNA transfection reagent (Roche, #6366244001). After transduction for 24 h, cells were treated for 2 h with the extract (0.0006%, 0.002% and 0.006% p/v) or the positive control Resveratrol (50 μM). After that, they were subjected to the luciferase assay with the Dual-Glo Luciferase Assay System (Promega, #E2920). Briefly, cells were incubated with firefly luciferase substrate for 10 min prior to measuring luminescence in a 96-well plate reader (Victor Nivo, Perkin Elmer). The ratio of luminescence from firefly and Renilla was calculated to normalize and compare Nrf2 transcriptional activity.

4.4.11 Analysis of SOD-1 and OH-1 gene expression in HaCaT cells

1.5 x 10^5 HaCaT cells per well were grown in 6-well plates for 16 hours and incubated for 6 h with the extract (0.002% and 0.006% p/v) or 50 μM Resveratrol as positive control. At the end of incubation, total RNA was extracted using the "GenElute ™ Total RNA Purification" kit (Merck; Millipore) and treated with DNase

I (Thermo Fisher) at 37 °C for 30 minutes, to remove genomic DNA contaminant. 500 ng of total RNA was retro-transcribed using the enzyme Reverse transcriptase (Thermo Scientific). Semi-quantitative RT-PCR were conducted using as internal standards the pair of universal primers 18S primer / competimer (Invitrogen). The PCR products were separated on 1.5% agarose gel, viewed using the iBright instrument (Invitrogen) and analyzed by densitometry using the iBright analysis software. The sequences of the primers used for amplification were the following: HsSOD1Fw: GAAAGTAATGGACCAGTGAAGG; HsSOD1Rv: ATT-GGGCGATCCCAATTACACC; OH-1Fw GAACTTTCAGAAGGGTCAGG; OH-1Rv GCTCAATGTTGAGCAGGAA.

4.4.12 Nitric oxide assay in LPS stimulated RAW 264.7

NO concentration was determined in RAW 264.7 murine macrophages, seeded at a concentration of 1.5×10^5 cells/well in 96-well plates for 24 h, and pre-treated with the ex-ract (0.0006%, 0.002% and 0.006% p/v) or with 10 μM TPCK (positive control) for 2 h, before the incubation with 2 μg/mL LPS for 18 h. The amount of NO, converted into nitrite, was calculated by adding Griess reagent (solution of N-(1-naphthyl)ethylenediamine and sulfanilic acid, Invitrogen-Life Technologies) and, after 30 min, measuring the absorbance at 540 nm by the multiwell-plate reader (EnVision, PerkinElmer).

SECTION 5

CONCLUSIONS

This PhD project evaluated the potential of some plant cell extracts as cosmetic ingredients in collaboration with Arterra Bioscience S.p.A. In particular, we focused on the hydrophilic extract of *Oenothera biennis* cells (ObHEx) and on the hydroethanolic extract of *Jasminum sambac* cells (JasHEx).

Global Natural Products Social Molecular Networking (GNPS) has proved to be a valuable tool for the annotation of the acquired high-resolution mass spectrometry data (M. Wang et al., 2016). It allowed to identify, in both extracts, several secondary metabolites mainly belonging to polyphenols and triterpenes, some of which were not known to be contained in plant of the genus *Oenothera* and *Jasminum* until now. However, regarding the use of Feature based Molecular Networking analysis (Nothias et al., 2020), in several cases it was not possible to unambiguously identify the interconnected nodes. This is due both to their absence in the spectral libraries and to the difficulty of propagating the annotation by chemical rationale in the case of compounds with complex scaffolds and fragmentation patterns (e.g. triterpenes).

The chemical composition of the extracts, thus determined, is consistent with the biological activity they have shown in *in vitro* and *ex vivo* assays.

ObHEx was able to improve skin mechanical properties via increase of Myosin light chain kinase (MYLK) gene expression, rising matrix collagen contraction, actin polymerization and the synthesis of ECM proteins (Ceccacci et al., 2021). In addition to this, global proteomics experiments, performed during my period as visiting PhD student at the Proteomics Platform of the INSERM US24, proved a pro-mitotic mechanism of action of ObHEx on senescent human dermal fibroblasts. The treatment with the extract was able to partially restore the levels of proteins and complexes, playing crucial roles in several stages of mitosis, promoting the re-entry into cell cycle

of senescent cells. Moreover, the dia-PASEF acquisition allowed us to obtain the most complete proteome analysis of senescent cells to date and, for the first time, the simultaneous quantification of numerous senescence markers. The deep senescence-associated global proteome profiling published by us provides a panel of hundreds of proteins deregulated by SIPS that can be used by the community to further understand senescence and the effect of new potential modulators (Ceccacci et al., 2022b).

In JasHEx several triterpenoids, lignans and chlorogenic acids were identified and it showed strong antioxidant properties which are not only related to free radical scavenging and metal chelating activities, but also to the enhancement of Nrf2/ ARE pathway (Ceccacci et al., 2022a). Such bioassays were performed during my research period at Arterra Bioscience.

Thus, the broad chemical and biological characterization of ObHEx and JasHEx, performed during this PhD project, confirmed the value of plant cells as source of bioactive cosmetic ingredients: both the extracts can be used to prevent and reduce skin aging, for their matrix boosting/anti-senescence and antioxidant/antiglycation activities, respectively.

Bibliography

Abdallah, C., Dumas-Gaudot, E., Renaut, J., Sergeant, K., 2012. Gel-Based and Gel-Free Quantitative Proteomics Approaches at a Glance. International Journal of Plant Genomics 2012, e494572. https://doi.org/10.1155/2012/494572

Aebersold, R., Mann, M., 2003. Mass spectrometry-based proteomics. Nature 422, 198–207. https://doi.org/10.1038/nature01511

Agnieszka Loboda, E.R.-G., Dulak, J., n.d. Targeting Nrf2-Mediated Gene Transcription by Triterpenoids and Their Derivatives. Biomol Ther (Seoul) 20, 499–505. https://doi.org/10.4062/biomolther.2012.20.6.499

Allard, P.-M., Genta-Jouve, G., Wolfender, J.-L., 2017. Deep metabolome annotation in natural products research: towards a virtuous cycle in metabolite identification. Current Opinion in Chemical Biology, Omics 36, 40–49. https://doi.org/10.1016/j.cbpa.2016.12.022

Allen, D.R., McWhinney, B.C., 2019. Quadrupole Time-of-Flight Mass Spectrometry: A Paradigm Shift in Toxicology Screening Applications. Clin Biochem Rev 40, 135–146. https://doi.org/10.33176/AACB-19-00023

Alpert, A.J., 1990. Hydrophilic-interaction chromatography for the separation of peptides, nucleic acids and other polar compounds. J Chromatogr 499, 177–196. https://doi.org/10.1016/s0021-9673(00)96972-3

Al-Snafi, A.E., 2018. PHARMACOLOGICAL AND THERAPEUTIC EFFECTS OF JASMINUM SAMBAC- A REVIEW. INDO AMERICAN JOURNAL OF PHARMACEUTICAL SCIENCES 05, 1766–1778. https://doi.org/10.5281/zenodo.1210527

Amy, J.W., Baitinger, W.E., Cooks, R.G., 1990. Building mass spectrometers and a philosophy of research. J. Am. Soc. Mass Spectrom. 1, 119–128. https://doi.org/10.1016/1044-0305(90)85047-P

Antignac, E., Nohynek, G.J., Re, T., Clouzeau, J., Toutain, H., 2011. Safety of botanical ingredients in personal care products/cosmetics. Food Chem Toxicol 49, 324–341. https://doi.org/10.1016/j.fct.2010.11.022

Arias-Salvatierra, D., Silbergeld, E.K., Acosta-Saavedra, L.C., Calderon-Aranda, E.S., 2011. Role of nitric oxide produced by iNOS through NF-κB pathway in migration of cerebellar granule neurons induced by Lipopolysaccharide. Cell Signal 23, 425–435. https://doi.org/10.1016/j.cellsig.2010.10.017

Aron, A.T., Gentry, E.C., McPhail, K.L., Nothias, L.-F., Nothias-Esposito, M., Bouslimani, A., Petras, D., Gauglitz, J.M., Sikora, N., Vargas, F., van der Hooft, J.J.J., Ernst, M., Kang, K.B., Aceves, C.M., Caraballo-Rodríguez, A.M., Koester, I., Weldon, K.C., Bertrand, S., Roullier, C., Sun, K., Tehan, R.M., Boya P., C.A., Christian, M.H., Gutiérrez, M., Ulloa, A.M., Tejeda Mora, J.A., Mojica-Flores, R., Lakey-Beitia, J., Vásquez-Chaves, V., Zhang, Y., Calderón, A.I., Tayler, N., Keyzers, R.A., Tugizimana, F., Ndlovu, N., Aksenov, A.A., Jarmusch, A.K., Schmid, R., Truman, A.W., Bandeira, N., Wang, M., Dorrestein, P.C., 2020. Reproducible molecular networking of untargeted mass spectrometry data using GNPS. Nat Protoc 15, 1954–1991. https://doi.org/10.1038/s41596-020-0317-5

Bae, Y.S., Oh, H., Rhee, S.G., Yoo, Y.D., 2011. Regulation of reactive oxygen species generation in cell signaling. Mol Cells 32, 491–509. https://doi.org/10.1007/s10059-011-0276-3

Bakalarski, C.E., Kirkpatrick, D.S., 2016. A Biologist's Field Guide to Multiplexed Quantitative Proteomics. Molecular & Cellular Proteomics 15, 1489–1497. https://doi.org/10.1074/mcp.O115.056986

Bantscheff, M., Lemeer, S., Savitski, M.M., Kuster, B., 2012. Quantitative mass spectrometry in proteomics: critical review update from 2007 to the present. Anal Bioanal Chem 404, 939–965. https://doi.org/10.1007/s00216-012-6203-4

Barbulova, A., Apone, F., Colucci, G., 2014. Plant Cell Cultures as Source of Cosmetic Active Ingredients. https://doi.org/10.3390/COSMETICS1020094

Benjamini, Y., Hochberg, Y., 1995. Controlling the False Discovery Rate: A Practical and Powerful Approach to Multiple Testing. Journal of the Royal Statistical Society: Series B (Methodological) 57, 289–300. https://doi.org/10.1111/j.2517-6161.1995.tb02031.x

Bick, D., Dimmock, D., 2011. Whole exome and whole genome sequencing. Curr Opin Pediatr 23, 594–600. https://doi.org/10.1097/MOP.0b013e32834b20ec

Boersema, P.J., Aye, T.T., van Veen, T.A.B., Heck, A.J.R., Mohammed, S., 2008. Triplex protein quantification based on stable isotope labeling by peptide dimethylation applied to cell and tissue lysates. Proteomics 8, 4624–4632. https://doi.org/10.1002/pmic.200800297

Boersema, P.J., Raijmakers, R., Lemeer, S., Mohammed, S., Heck, A.J.R., 2009. Multiplex peptide stable isotope dimethyl labeling for quantitative proteomics. Nat Protoc 4, 484–494. https://doi.org/10.1038/nprot.2009.21

Bonte, F., Dumas, M., Chaudagne, C., Meybeck, A., 1994. Influence of asiatic acid, madecassic acid, and asiaticoside on human collagen I synthesis. Planta Med 60, 133–135. https://doi.org/10.1055/s-2006-959434

Bush, W.S., Moore, J.H., 2012. Chapter 11: Genome-wide association studies. PLoS Comput Biol 8, e1002822. https://doi.org/10.1371/journal.pcbi.1002822

Caesar, L.K., Cech, N.B., 2019. Synergy and antagonism in natural product extracts: when 1 + 1 does not equal 2. Nat Prod Rep 36, 869–888. https://doi.org/10.1039/c9np00011a

Ceccacci, S., De Lucia, A., Tito, A., Tortora, A., Falanga, D., Arciello, S., Ausanio, G., Di Cicco, C., Monti, M.C., Apone, F., 2021. An Oenothera biennis Cell Cultures Extract Endowed with Skin Anti-Ageing Activity Improves Cell Mechanical Properties. Metabolites 11, 527. https://doi.org/10.3390/metabo11080527

Ceccacci, S., Lucia, A.D., Tortora, A., Colantuono, A., Carotenuto, G., Tito, A., Monti, M.C., 2022a. Jasminum sambac Cell Extract as Antioxidant Booster against Skin Aging. Antioxidants 11, 2409. https://doi.org/10.3390/antiox11122409

Ceccacci, S., Roger, K., Metatla, I., Chhuon, C., Tighanimine, K., Fumagalli, S., De Lucia, A., Pranke, I., Cordier, C., Monti, M.C., Guerrera, I.C., 2022b. Promitotic Action of Oenothera biennis on Senescent Human Dermal Fibroblasts. International Journal of Molecular Sciences 23, 15153. https://doi.org/10.3390/ijms232315153

Cepas, V., Collino, M., Mayo, J.C., Sainz, R.M., 2020. Redox Signaling and Advanced Glycation Endproducts (AGEs) in Diet-Related Diseases. Antioxidants (Basel) 9, E142. https://doi.org/10.3390/antiox9020142

Chait, B.T., 2006. Chemistry. Mass spectrometry: bottom-up or top-down? Science 314, 65–66. https://doi.org/10.1126/science.1133987

Chaleckis, R., Meister, I., Zhang, P., Wheelock, C.E., 2019. Challenges, progress and promises of metabolite annotation for LC-MS-based metabolomics. Curr Opin Biotechnol 55, 44–50. https://doi.org/10.1016/j.copbio.2018.07.010

Chen, C., Zhang, J.-Q., Li, L., Guo, M., He, Y., Dong, Y., Meng, H., Yi, F., 2022. Advanced Glycation End Products in the Skin: Molecular Mechanisms, Methods of Measurement, and Inhibitory Pathways. Frontiers in Medicine 9.

Chen, S., Bhushan, B., 2013. Nanomechanical and nanotribological characterization of two synthetic skins with and without skin cream treatment using atomic force microscopy. J Colloid Interface Sci 398, 247–254. https://doi.org/10.1016/j.jcis.2013.02.026

Choi, E.-J., Kil, I.S., Cho, E.-G., 2020. Extracellular Vesicles Derived from Senescent Fibroblasts Attenuate the Dermal Effect on Keratinocyte Differentiation. Int J Mol Sci 21, E1022. https://doi.org/10.3390/ijms21031022

Chowdhary, S., n.d. The Effects of Oxidative Stress on Inducing Senescence in Human Fibroblasts 4.

Clifford, M.N., Johnston, K.L., Knight, S., Kuhnert, N., 2003. Hierarchical Scheme for LC-MSn Identification of Chlorogenic Acids. J. Agric. Food Chem. 51, 2900–2911. https://doi.org/10.1021/jf026187q

Coles, J., Guilhaus, M., 1993. Orthogonal acceleration — a new direction for time-of-flight mass spectrometry: Fast, sensitive mass analysis for continuous ion sources. TrAC Trends in Analytical Chemistry 12, 203–213. https://doi.org/10.1016/0165-9936(93)80021-B

Cotter, R.J., 1992. Time-of-Flight Mass Spectrometry for the Structural Analysis of Biological Molecules. Anal. Chem. 64, 1027A-1039A. https://doi.org/10.1021/ac00045a726

Cox, J., Mann, M., 2008. MaxQuant enables high peptide identification rates, individualized p.p.b.-range mass accuracies and proteome-wide protein quantification. Nat Biotechnol 26, 1367–1372. https://doi.org/10.1038/nbt.1511

Cox, J., Michalski, A., Mann, M., 2011. Software lock mass by two-dimensional minimization of peptide mass errors. J Am Soc Mass Spectrom 22, 1373–1380. https://doi.org/10.1007/s13361-011-0142-8

Dai, J., Wang, L.-S., Wu, Y.-B., Sheng, Q.-H., Wu, J.-R., Shieh, C.-H., Zeng, R., 2009. Fully automatic separation and identification of phosphopeptides by continuous pH-gradient anion exchange online coupled with reversed-phase liquid chromatography mass spectrometry. J Proteome Res 8, 133–141. https://doi.org/10.1021/pr800381w

Dai, Y., Tang, H., Pang, S., 2021. The Crucial Roles of Phospholipids in Aging and Lifespan Regulation. Frontiers in Physiology 12.

Dashty, M., 2014. Hedgehog Signaling Pathway is Linked with Age-Related Diseases. J Diabetes Metab 05. https://doi.org/10.4172/2155-6156.1000350

Dawson, J.H.J., Guilhaus, M., 1989. Orthogonal-acceleration time-of-flight mass spectrometer. Rapid Communications in Mass Spectrometry 3, 155–159. https://doi.org/10.1002/rcm.1290030511

Demichev, V., Messner, C.B., Vernardis, S.I., Lilley, K.S., Ralser, M., 2020. DIA-NN: Neural networks and interference correction enable deep proteome coverage in high throughput. Nat Methods 17, 41–44. https://doi.org/10.1038/s41592-019-0638-x

Di Micco, R., Krizhanovsky, V., Baker, D., d'Adda di Fagagna, F., 2021. Cellular senescence in ageing: from mechanisms to therapeutic opportunities. Nat Rev Mol Cell Biol 22, 75–95. https://doi.org/10.1038/s41580-020-00314-w

Dodds, J.N., Baker, E.S., 2019. Ion Mobility Spectrometry: Fundamental Concepts, Instrumentation, Applications, and the Road Ahead. J Am Soc Mass Spectrom 30, 2185–2195. https://doi.org/10.1007/s13361-019-02288-2

Dole, M., Mack, L.L., Hines, R.L., Mobley, R.C., Ferguson, L.D., Alice, M.B., 1968. Molecular Beams of Macroions. J. Chem. Phys. 49, 2240–2249. https://doi.org/10.1063/1.1670391

Domon, B., Aebersold, R., 2010. Options and considerations when selecting a quantitative proteomics strategy. Nat Biotechnol 28, 710–721. https://doi.org/10.1038/nbt.1661

Domon, B., Aebersold, R., 2006. Mass spectrometry and protein analysis. Science 312, 212–217. https://doi.org/10.1126/science.1124619

Dormeyer, W., Mohammed, S., Breukelen, B. van, Krijgsveld, J., Heck, A.J.R., 2007. Targeted analysis of protein termini. J Proteome Res 6, 4634–4645. https://doi.org/10.1021/pr070375k

Du, X., Smirnov, A., Pluskal, T., Jia, W., Sumner, S., 2020. Metabolomics Data Preprocessing Using ADAP and MZmine 2. Methods Mol Biol 2104, 25–48. https://doi.org/10.1007/978-1-0716-0239-3_3

Dyer, D.G., Dunn, J.A., Thorpe, S.R., Bailie, K.E., Lyons, T.J., McCance, D.R., Baynes, J.W., 1993. Accumulation of Maillard reaction products in skin collagen in diabetes and aging. J Clin Invest 91, 2463–2469.

Ehrlich, H.P., Rockwell, W.B., Cornwell, T.L., Rajaratnam, J.B., 1991. Demonstration of a direct role for myosin light chain kinase in fibroblast-populated collagen

lattice contraction. J Cell Physiol 146, 1–7. https://doi.org/10.1002/jcp.1041460102

Eklund, P.C., Backman, M.J., Kronberg, L.A., Smeds, A.I., Sjöholm, R.E., 2008. Identification of lignans by liquid chromatography-electrospray ionization ion-trap mass spectrometry. J Mass Spectrom 43, 97–107. https://doi.org/10.1002/jms.1276

El-Metwally, S., Hamza, T., Zakaria, M., Helmy, M., 2013. Next-generation sequence assembly: four stages of data processing and computational challenges. PLoS Comput Biol 9, e1003345. https://doi.org/10.1371/journal.pcbi.1003345

Farwick, M., Köhler, T., Schild, J., Mentel, M., Maczkiewitz, U., Pagani, V., Bonfigli, A., Rigano, L., Bureik, D., Gauglitz, G.G., 2014. Pentacyclic triterpenes from Terminalia arjuna show multiple benefits on aged and dry skin. Skin Pharmacol Physiol 27, 71–81. https://doi.org/10.1159/000351387

Fecker, R., Buda, V., Alexa, E., Avram, S., Pavel, I.Z., Muntean, D., Cocan, I., Watz, C., Minda, D., Dehelean, C.A., Soica, C., Danciu, C., 2020. Phytochemical and Biological Screening of Oenothera Biennis L. Hydroalcoholic Extract. Biomolecules 10, E818. https://doi.org/10.3390/biom10060818

Fehér, A., 2019. Callus, Dedifferentiation, Totipotency, Somatic Embryogenesis: What These Terms Mean in the Era of Molecular Plant Biology? Front Plant Sci 10, 536. https://doi.org/10.3389/fpls.2019.00536

Felitsyn, N., Peschke, M., Kebarle, P., 2002. Origin and number of charges observed on multiply-protonated native proteins produced by ESI. International Journal of Mass Spectrometry, Structure of Biological Molecules 219, 39–62. https://doi.org/10.1016/S1387-3806(02)00588-2

Fenn, J.B., 2003. Electrospray Wings for Molecular Elephants (Nobel Lecture). Angewandte Chemie International Edition 42, 3871–3894. https://doi.org/10.1002/anie.200300605

Fenn, J.B., Mann, M., Meng, C.K., Wong, S.F., Whitehouse, C.M., 1990. Electrospray ionization–principles and practice. Mass Spectrometry Reviews 9, 37–70. https://doi.org/10.1002/mas.1280090103

Festa, C., D'Auria, M.V., Sepe, V., Ilaš, J., Leick, A., N'Gom, S., De Marino, S., 2015. Triterpenoid profile and bioactivity study of Oenothera maritima. Phytochemistry Letters 13, 324–329. https://doi.org/10.1016/j.phytol.2015.07.011

Flanagan, J.M., 2015. Epigenome-wide association studies (EWAS): past, present, and future. Methods Mol Biol 1238, 51–63. https://doi.org/10.1007/978-1-4939-1804-1_3

Frese, C.K., Altelaar, A.F.M., Hennrich, M.L., Nolting, D., Zeller, M., Griep-Raming, J., Heck, A.J.R., Mohammed, S., 2011. Improved peptide identification by targeted fragmentation using CID, HCD and ETD on an LTQ-Orbitrap Velos. J Proteome Res 10, 2377–2388. https://doi.org/10.1021/pr1011729

Fujimura, T., Hotta, M., Kitahara, T., Takema, Y., 2011. Loss of contraction force in dermal fibroblasts with aging due to decreases in myosin light chain phosphorylation enzymes. Arch Pharm Res 34, 1015–1022. https://doi.org/10.1007/s12272-011-0619-9

Futrell, J.H., 2000. Development of tandem mass spectrometry: one perspective. International Journal of Mass Spectrometry, Volume 200: The state of the field as we move into a new millenium 200, 495–508. https://doi.org/10.1016/S1387-3806(00)00353-5

Garre, A., Narda, M., Valderas-Martinez, P., Piquero, J., Granger, C., 2018. Antiaging effects of a novel facial serum containing L-Ascorbic acid, proteoglycans, and proteoglycan-stimulating tripeptide: ex vivo skin explant studies and in vivo clinical studies in women. Clin Cosmet Investig Dermatol 11, 253–263. https://doi.org/10.2147/CCID.S161352

Gasser, P., Arnold, F., Peno-Mazzarino, L., Bouzoud, D., Luu, M.T., Lati, E., Mercier, M., 2011. Glycation induction and antiglycation activity of skin care ingredients on living human skin explants. Int J Cosmet Sci 33, 366–370. https://doi.org/10.1111/j.1468-2494.2011.00640.x

Gieger, C., Geistlinger, L., Altmaier, E., Hrabé de Angelis, M., Kronenberg, F., Meitinger, T., Mewes, H.-W., Wichmann, H.-E., Weinberger, K.M., Adamski, J., Illig, T., Suhre, K., 2008. Genetics meets metabolomics: a genome-wide association study of metabolite profiles in human serum. PLoS Genet 4, e1000282. https://doi.org/10.1371/journal.pgen.1000282

Giles, K., Pringle, S.D., Worthington, K.R., Little, D., Wildgoose, J.L., Bateman, R.H., 2004. Applications of a travelling wave-based radio-frequency-only stacked ring ion guide. Rapid Communications in Mass Spectrometry 18, 2401–2414. https://doi.org/10.1002/rcm.1641

Gonos, E., Chinou, I., Chondrogianni, N., 2010. Anti-aging and whitening properties of quercetin, 18a-glycyrrhetinic acid, hederagenin and its derivatives. EP2246037A2.

González-Gualda, E., Baker, A.G., Fruk, L., Muñoz-Espín, D., 2021. A guide to assessing cellular senescence in vitro and in vivo. FEBS J 288, 56–80. https://doi.org/10.1111/febs.15570

Good, L., Dimri, G.P., Campisi, J., Chen, K.Y., 1996. Regulation of dihydrofolate reductase gene expression and E2F components in human diploid fibroblasts during growth and senescence. J Cell Physiol 168, 580–588. https://doi.org/10.1002/(SICI)1097-4652(199609)168:3<580::AID-JCP10>3.0.CO;2-3

Gorgoulis, V., Adams, P.D., Alimonti, A., Bennett, D.C., Bischof, O., Bishop, C., Campisi, J., Collado, M., Evangelou, K., Ferbeyre, G., Gil, J., Hara, E., Krizhanovsky, V., Jurk, D., Maier, A.B., Narita, M., Niedernhofer, L., Passos, J.F., Robbins, P.D., Schmitt, C.A., Sedivy, J., Vougas, K., von Zglinicki, T., Zhou, D., Serrano, M., Demaria, M., 2019. Cellular Senescence: Defining a Path Forward. Cell 179, 813–827. https://doi.org/10.1016/j.cell.2019.10.005

Granica, S., Czerwińska, M.E., Piwowarski, J.P., Ziaja, M., Kiss, A.K., 2013. Chemical Composition, Antioxidative and Anti-Inflammatory Activity of Extracts Prepared from Aerial Parts of Oenothera biennis L. and Oenothera paradoxa Hudziok Obtained after Seeds Cultivation. J. Agric. Food Chem. 61, 801–810. https://doi.org/10.1021/jf304002h

Gross, J.H., 2017a. Introduction, in: Gross, J.H. (Ed.), Mass Spectrometry: A Textbook. Springer International Publishing, Cham, pp. 1–28. https://doi.org/10.1007/978-3-319-54398-7_1

Gross, J.H., 2017b. Electrospray Ionization, in: Gross, J.H. (Ed.), Mass Spectrometry: A Textbook. Springer International Publishing, Cham, pp. 721–778. https://doi.org/10.1007/978-3-319-54398-7_12

Gross, J.H., 2017c. Instrumentation, in: Gross, J.H. (Ed.), Mass Spectrometry: A Textbook. Springer International Publishing, Cham, pp. 151–292. https://doi.org/10.1007/978-3-319-54398-7_4

Guerriero, G., Berni, R., Muñoz-Sanchez, J.A., Apone, F., Abdel-Salam, E.M., Qahtan, A.A., Alatar, A.A., Cantini, C., Cai, G., Hausman, J.-F., Siddiqui, K.S., Hernández-Sotomayor, S.M.T., Faisal, M., 2018. Production of Plant Secondary Metabolites: Examples, Tips and Suggestions for Biotechnologists. Genes (Basel) 9, E309. https://doi.org/10.3390/genes9060309

Guilhaus, M., 1995. Special feature: Tutorial. Principles and instrumentation in time-of-flight mass spectrometry. Physical and instrumental concepts. Journal of Mass Spectrometry 30, 1519–1532. https://doi.org/10.1002/jms.1190301102

Guilhaus, M., Selby, D., Mlynski, V., 2000. Orthogonal acceleration time-of-flight mass spectrometry. Mass Spectrom Rev 19, 65–107. https://doi.org/10.1002/(SICI)1098-2787(2000)19:2<65::AID-MAS1>3.0.CO;2-E

Halper, J., Kjaer, M., 2014. Basic components of connective tissues and extracellular matrix: elastin, fibrillin, fibulins, fibrinogen, fibronectin, laminin, tenascins and thrombospondins. Adv Exp Med Biol 802, 31–47. https://doi.org/10.1007/978-94-007-7893-1_3

Harvey, A.L., Edrada-Ebel, R., Quinn, R.J., 2015. The re-emergence of natural products for drug discovery in the genomics era. Nat Rev Drug Discov 14, 111–129. https://doi.org/10.1038/nrd4510

Hasanuzzaman, M., Bhuyan, M.H.M.B., Zulfiqar, F., Raza, A., Mohsin, S.M., Mahmud, J.A., Fujita, M., Fotopoulos, V., 2020. Reactive Oxygen Species and Antioxidant Defense in Plants under Abiotic Stress: Revisiting the Crucial Role of a Universal Defense Regulator. Antioxidants 9, 681. https://doi.org/10.3390/antiox9080681

Hayes, J.D., Dinkova-Kostova, A.T., 2014. The Nrf2 regulatory network provides an interface between redox and intermediary metabolism. Trends Biochem Sci 39, 199–218. https://doi.org/10.1016/j.tibs.2014.02.002

Heck, A.J.R., van den Heuvel, R.H.H., 2004. Investigation of intact protein complexes by mass spectrometry. Mass Spectrometry Reviews 23, 368–389. https://doi.org/10.1002/mas.10081

Hemalatha, T., Pulavendran, S., Balachandran, C., Manohar, B.M., Puvanakrishnan, R., 2010. Arjunolic acid: a novel phytomedicine with multifunctional therapeutic applications. Indian J Exp Biol 48, 238–247.

Henzel, W.J., Watanabe, C., Stults, J.T., 2003. Protein identification: the origins of peptide mass fingerprinting. J Am Soc Mass Spectrom 14, 931–942. https://doi.org/10.1016/S1044-0305(03)00214-9

Hildebrand, D.G., Lehle, S., Borst, A., Haferkamp, S., Essmann, F., Schulze-Osthoff, K., 2013. α-Fucosidase as a novel convenient biomarker for cellular senescence. Cell Cycle 12, 1922–1927. https://doi.org/10.4161/cc.24944

Hoffman, D., Miskioglu, I., Drelich, J., Aifantis, K., 2011. Measuring the elastic modulus of polymers by nanoindentation with an atomic force microscope. TMS Annual Meeting 1, 243–251. https://doi.org/10.1002/9781118495285.ch30

Hoffmann, E. de, Stroobant, V., 2007. Mass Spectrometry: Principles and Applications. John Wiley & Sons.

Hsu, J.-L., Chen, S.-H., 2016. Stable isotope dimethyl labelling for quantitative proteomics and beyond. Philos Trans A Math Phys Eng Sci 374, 20150364. https://doi.org/10.1098/rsta.2015.0364

Hu, A., Noble, W.S., Wolf-Yadlin, A., 2016. Technical advances in proteomics: new developments in data-independent acquisition. https://doi.org/10.12688/f1000research.7042.1

Hu, J., Zhao, J., Chen, W., Lin, S., Zhang, J., Hong, Z., 2013. Hepatoprotection of 1β-hydroxyeuscaphic acid - the major constituent from Rubus aleaefolius against CCl4-induced injury in hepatocytes cells. Pharm Biol 51, 686–690. https://doi.org/10.3109/13880209.2012.762406

Huang, K., Huang, J., Xie, X., Wang, S., Chen, C., Shen, X., Liu, P., Huang, H., 2013. Sirt1 resists advanced glycation end products-induced expressions of fibronectin and TGF-β1 by activating the Nrf2/ARE pathway in glomerular mesangial cells. Free Radic Biol Med 65, 528–540. https://doi.org/10.1016/j.freeradbiomed.2013.07.029

Ioanoviciu, D., 1995. Ion-Optical solutions in time-of-flight mass spectrometry. Rapid Communications in Mass Spectrometry 9, 985–997. https://doi.org/10.1002/rcm.1290091104

Iravanimanesh, S., Ali Nazari, M., Mahjoob, M.J., Azadi, M., 2017. Human Skin Micro-Mechanics Measured in Vivo Using Atomic Force Microscopy(AFM), in: 2017 24th National and 2nd International Iranian Conference on Biomedical Engineering (ICBME). Presented at the 2017 24th National and 2nd International Iranian Conference on Biomedical Engineering (ICBME), pp. 1–5. https://doi.org/10.1109/ICBME.2017.8430265

Iribarne, J.V., Thomson, B.A., 1976. On the evaporation of small ions from charged droplets. J. Chem. Phys. 64, 2287–2294. https://doi.org/10.1063/1.432536

Issaq, H.J., Chan, K.C., Janini, G.M., Conrads, T.P., Veenstra, T.D., 2005. Multidimensional separation of peptides for effective proteomic analysis. J

Chromatogr B Analyt Technol Biomed Life Sci 817, 35–47. https://doi.org/10.1016/j.jchromb.2004.07.042

Jiang, Z., Zhou, X., Li, R., Michal, J.J., Zhang, S., Dodson, M.V., Zhang, Z., Harland, R.M., 2015. Whole transcriptome analysis with sequencing: methods, challenges and potential solutions. Cell Mol Life Sci 72, 3425–3439. https://doi.org/10.1007/s00018-015-1934-y

Jin, T., Li, L., Siow, R.C.M., Liu, K.-K., 2015. A novel collagen gel-based measurement technique for quantitation of cell contraction force. J. R. Soc. Interface. 12, 20141365. https://doi.org/10.1098/rsif.2014.1365

Johnson, J.V., Yost, R.A., Kelley, P.E., Bradford, D.C., 1990. Tandem-in-space and tandem-in-time mass spectrometry: triple quadrupoles and quadrupole ion traps. Anal. Chem. 62, 2162–2172. https://doi.org/10.1021/ac00219a003

Karp, N.A., Huber, W., Sadowski, P.G., Charles, P.D., Hester, S.V., Lilley, K.S., 2010. Addressing accuracy and precision issues in iTRAQ quantitation. Mol Cell Proteomics 9, 1885–1897. https://doi.org/10.1074/mcp.M900628-MCP200

Kinsel, G.R., 1998. Time-of-Flight Mass Spectrometry: Instrumentation and Applications in Biological Research By Robert J. Cotter (The Johns Hopkins University). ACS: Washington, DC. 1997. xvi + 326 pp. $119.95. ISBN 0-8412-3474-4. J. Am. Chem. Soc. 120, 4256–4257. https://doi.org/10.1021/ja975651i

Klose, J., 1975. Protein mapping by combined isoelectric focusing and electrophoresis of mouse tissues. A novel approach to testing for induced point mutations in mammals. Humangenetik 26, 231–243. https://doi.org/10.1007/BF00281458

Kong, M., Cutts, E.E., Pan, D., Beuron, F., Kaliyappan, T., Xue, C., Morris, E.P., Musacchio, A., Vannini, A., Greene, E.C., 2020. Human Condensin I and II

Drive Extensive ATP-Dependent Compaction of Nucleosome-Bound DNA. Mol Cell 79, 99-114.e9. https://doi.org/10.1016/j.molcel.2020.04.026

Konstantinidis, G., Moustakas, A., Stournaras, C., 2011. Regulation of myosin light chain function by BMP signaling controls actin cytoskeleton remodeling. Cell Physiol Biochem 28, 1031–1044. https://doi.org/10.1159/000335790

Kops, G.J.P.L., Gassmann, R., 2020. Crowning the Kinetochore: The Fibrous Corona in Chromosome Segregation. Trends Cell Biol 30, 653–667. https://doi.org/10.1016/j.tcb.2020.04.006

Krasny, L., Huang, P.H., 2021. Data-independent acquisition mass spectrometry (DIA-MS) for proteomic applications in oncology. Mol Omics 17, 29–42. https://doi.org/10.1039/d0mo00072h

Krtolica, A., Parrinello, S., Lockett, S., Desprez, P.Y., Campisi, J., 2001. Senescent fibroblasts promote epithelial cell growth and tumorigenesis: a link between cancer and aging. Proc Natl Acad Sci U S A 98, 12072–12077. https://doi.org/10.1073/pnas.211053698

Kuipers, M.A., Stasevich, T.J., Sasaki, T., Wilson, K.A., Hazelwood, K.L., McNally, J.G., Davidson, M.W., Gilbert, D.M., 2011. Highly stable loading of Mcm proteins onto chromatin in living cells requires replication to unload. J Cell Biol 192, 29–41. https://doi.org/10.1083/jcb.201007111

Kunej, T., Godnic, I., Horvat, S., Zorc, M., Calin, G.A., 2012. Cross talk between microRNA and coding cancer genes. Cancer J 18, 223–231. https://doi.org/10.1097/PPO.0b013e318258b771

LaBaer, J., Garrett, M.D., Stevenson, L.F., Slingerland, J.M., Sandhu, C., Chou, H.S., Fattaey, A., Harlow, E., 1997. New functional activities for the p21 family of CDK inhibitors. Genes Dev 11, 847–862. https://doi.org/10.1101/gad.11.7.847

Labowsky, M., Fenn, J.B., Fernandez de la Mora, J., 2000. A continuum model for ion evaporation from a drop: effect of curvature and charge on ion solvation energy. Analytica Chimica Acta 406, 105–118. https://doi.org/10.1016/S0003-2670(99)00595-4

Laemmli, U.K., 1970. Cleavage of Structural Proteins during the Assembly of the Head of Bacteriophage T4. Nature 227, 680–685. https://doi.org/10.1038/227680a0

Larbi, N.B., Jefferies, C., 2009. 2D-DIGE: comparative proteomics of cellular signalling pathways. Methods Mol Biol 517, 105–132. https://doi.org/10.1007/978-1-59745-541-1_8

Larochelle, S., Pandur, J., Fisher, R.P., Salz, H.K., Suter, B., 1998. Cdk7 is essential for mitosis and for in vivo Cdk-activating kinase activity. Genes Dev 12, 370–381. https://doi.org/10.1101/gad.12.3.370

Latorre, E., Birar, V.C., Sheerin, A.N., Jeynes, J.C.C., Hooper, A., Dawe, H.R., Melzer, D., Cox, L.S., Faragher, R.G.A., Ostler, E.L., Harries, L.W., 2017. Small molecule modulation of splicing factor expression is associated with rescue from cellular senescence. BMC Cell Biol 18, 31. https://doi.org/10.1186/s12860-017-0147-7

Lau, K.W., Hart, S.R., Lynch, J.A., Wong, S.C.C., Hubbard, S.J., Gaskell, S.J., 2009. Observations on the detection of b- and y-type ions in the collisionally activated decomposition spectra of protonated peptides. Rapid Commun Mass Spectrom 23, 1508–1514. https://doi.org/10.1002/rcm.4032

Lee, A.Y.H., Paweletz, C.P., Pollock, R.M., Settlage, R.E., Cruz, J.C., Secrist, J.P., Miller, T.A., Stanton, M.G., Kral, A.M., Ozerova, N.D.S., Meng, F., Yates, N.A., Richon, V., Hendrickson, R.C., 2008. Quantitative analysis of histone

deacetylase-1 selective histone modifications by differential mass spectrometry. J Proteome Res 7, 5177–5186. https://doi.org/10.1021/pr800510p

Lee, B.Y., Han, J.A., Im, J.S., Morrone, A., Johung, K., Goodwin, E.C., Kleijer, W.J., DiMaio, D., Hwang, E.S., 2006. Senescence-associated beta-galactosidase is lysosomal beta-galactosidase. Aging Cell 5, 187–195. https://doi.org/10.1111/j.1474-9726.2006.00199.x

Lee, S.Y., Kim, C.H., Hwang, B.S., Choi, K.-M., Yang, I.-J., Kim, G.-Y., Choi, Y.H., Park, C., Jeong, J.-W., 2020. Protective Effects of Oenothera biennis against Hydrogen Peroxide-Induced Oxidative Stress and Cell Death in Skin Keratinocytes. Life (Basel) 10, E255. https://doi.org/10.3390/life10110255

Leone, M., Cazorla-Vázquez, S., Ferrazzi, F., Wiederstein, J.L., Gründl, M., Weinstock, G., Vergarajauregui, S., Eckstein, M., Krüger, M., Gaubatz, S., Engel, F.B., 2021. IQGAP3, a YAP Target, Is Required for Proper Cell-Cycle Progression and Genome Stability. Mol Cancer Res 19, 1712–1726. https://doi.org/10.1158/1541-7786.MCR-20-0639

Levsen, K., Schwarz, H., 1976. Collisional Activation Mass Spectrometry—A New Probe for Determining the Structure of Ions in the Gas Phase. Angewandte Chemie International Edition in English 15, 509–519. https://doi.org/10.1002/anie.197605091

Li, D.-H., Wang, Y., Lv, Y.-S., Liu, J.-H., Yang, L., Zhang, S.-K., Zhuo, Y.-Z., 2015. Preparative Purification of Liriodendrin from Sargentodoxa cuneata by Macroporous Resin. Biomed Res Int 2015, 861256. https://doi.org/10.1155/2015/861256

Li, J., Smith, L.S., Zhu, H.-J., 2021. Data-independent acquisition (DIA): An emerging proteomics technology for analysis of drug-metabolizing enzymes and transporters. Drug Discovery Today: Technologies 39, 49–56. https://doi.org/10.1016/j.ddtec.2021.06.006

López, J.L., 2007. Two-dimensional electrophoresis in proteome expression analysis. J Chromatogr B Analyt Technol Biomed Life Sci 849, 190–202. https://doi.org/10.1016/j.jchromb.2006.11.049

Lozano-Mena, G., Sánchez-González, M., Juan, M.E., Planas, J.M., 2014. Maslinic Acid, a Natural Phytoalexin-Type Triterpene from Olives — A Promising Nutraceutical? Molecules 19, 11538–11559. https://doi.org/10.3390/molecules190811538

Lv, Q., Ma, W., Liu, H., Li, J., Wang, H., Lu, F., Zhao, C., Shi, T., 2015. Genome-wide protein-protein interactions and protein function exploration in cyanobacteria. Sci Rep 5, 15519. https://doi.org/10.1038/srep15519

Ma, H.T., Poon, R.Y.C., 2018. TRIP13 Functions in the Establishment of the Spindle Assembly Checkpoint by Replenishing O-MAD2. Cell Rep 22, 1439–1450. https://doi.org/10.1016/j.celrep.2018.01.027

Mack, L.L., Kralik, P., Rheude, A., Dole, M., 1970. Molecular Beams of Macroions. II. J. Chem. Phys. 52, 4977–4986. https://doi.org/10.1063/1.1672733

Mahoney, D.W., Therneau, T.M., Heppelmann, C.J., Higgins, L., Benson, L.M., Zenka, R.M., Jagtap, P., Nelsestuen, G.L., Bergen, H.R., Oberg, A.L., 2011. Relative quantification: characterization of bias, variability and fold changes in mass spectrometry data from iTRAQ-labeled peptides. J Proteome Res 10, 4325–4333. https://doi.org/10.1021/pr2001308

Makarov, A., 2000. Electrostatic Axially Harmonic Orbital Trapping: A High-Performance Technique of Mass Analysis. Anal. Chem. 72, 1156–1162. https://doi.org/10.1021/ac991131p

March, R.E., 2009. Quadrupole ion traps. Mass Spectrometry Reviews 28, 961–989. https://doi.org/10.1002/mas.20250

Masaki, H., 2010. Role of antioxidants in the skin: anti-aging effects. J Dermatol Sci 58, 85–90. https://doi.org/10.1016/j.jdermsci.2010.03.003

Matsuoka, S., Ballif, B.A., Smogorzewska, A., McDonald, E.R., Hurov, K.E., Luo, J., Bakalarski, C.E., Zhao, Z., Solimini, N., Lerenthal, Y., Shiloh, Y., Gygi, S.P., Elledge, S.J., 2007. ATM and ATR substrate analysis reveals extensive protein networks responsive to DNA damage. Science 316, 1160–1166. https://doi.org/10.1126/science.1140321

McLafferty, F.W., 1981. Tandem mass spectrometry. Science 214, 280–287. https://doi.org/10.1126/science.7280693

McLafferty, F.W., Bente, P.F., Kornfeld, Richard., Tsai, S.-Chuan., Howe, Ian., 1973. Metastable ion characteristics. XXII. Collisional activation spectra of organic ions. J. Am. Chem. Soc. 95, 2120–2129. https://doi.org/10.1021/ja00788a007

McLafferty, F.W., Breuker, K., Jin, M., Han, X., Infusini, G., Jiang, H., Kong, X., Begley, T.P., 2007. Top-down MS, a powerful complement to the high capabilities of proteolysis proteomics. FEBS J 274, 6256–6268. https://doi.org/10.1111/j.1742-4658.2007.06147.x

Meier, F., Beck, S., Grassl, N., Lubeck, M., Park, M.A., Raether, O., Mann, M., 2015. Parallel Accumulation–Serial Fragmentation (PASEF): Multiplying Sequencing Speed and Sensitivity by Synchronized Scans in a Trapped Ion

Mobility Device. J. Proteome Res. 14, 5378–5387. https://doi.org/10.1021/acs.jproteome.5b00932

Meier, F., Brunner, A.-D., Frank, M., Ha, A., Bludau, I., Voytik, E., Kaspar-Schoenefeld, S., Lubeck, M., Raether, O., Bache, N., Aebersold, R., Collins, B.C., Röst, H.L., Mann, M., 2020. diaPASEF: parallel accumulation–serial fragmentation combined with data-independent acquisition. Nat Methods 17, 1229–1236. https://doi.org/10.1038/s41592-020-00998-0

Meier, F., Brunner, A.-D., Koch, S., Koch, H., Lubeck, M., Krause, M., Goedecke, N., Decker, J., Kosinski, T., Park, M.A., Bache, N., Hoerning, O., Cox, J., Räther, O., Mann, M., 2018. Online Parallel Accumulation-Serial Fragmentation (PASEF) with a Novel Trapped Ion Mobility Mass Spectrometer. Mol Cell Proteomics 17, 2534–2545. https://doi.org/10.1074/mcp.TIR118.000900

Meier, F., Park, M.A., Mann, M., 2021. Trapped Ion Mobility Spectrometry and Parallel Accumulation–Serial Fragmentation in Proteomics. Molecular & Cellular Proteomics 20. https://doi.org/10.1016/j.mcpro.2021.100138

Meng, Q., Gao, J., Zhu, H., He, H., Lu, Z., Hong, M., Zhou, H., 2018. The proteomic study of serially passaged human skin fibroblast cells uncovers down-regulation of the chromosome condensin complex proteins involved in replicative senescence. Biochem Biophys Res Commun 505, 1112–1120. https://doi.org/10.1016/j.bbrc.2018.10.065

Mirgorodskaya, O.A., Shevchenko, A.A., Chernushevich, I.V., Dodonov, A.F., Miroshnikov, A.I., 1994. Electrospray-ionization time-of-flight mass spectrometry in protein chemistry. Anal. Chem. 66, 99–107. https://doi.org/10.1021/ac00073a018

Mischerikow, N., van Nierop, P., Li, K.W., Bernstein, H.-G., Smit, A.B., Heck, A.J.R., Altelaar, A.F.M., 2010. Gaining efficiency by parallel quantification and identification of iTRAQ-labeled peptides using HCD and decision tree guided CID/ETD on an LTQ Orbitrap. Analyst 135, 2643–2652. https://doi.org/10.1039/c0an00267d

Mogilner, A., Keren, K., 2009. The shape of motile cells. Curr Biol 19, R762-771. https://doi.org/10.1016/j.cub.2009.06.053

Monnerie, S., Comte, B., Ziegler, D., Morais, J.A., Pujos-Guillot, E., Gaudreau, P., 2020. Metabolomic and Lipidomic Signatures of Metabolic Syndrome and its Physiological Components in Adults: A Systematic Review. Sci Rep 10, 669. https://doi.org/10.1038/s41598-019-56909-7

Morrison, N., Wood, A.J., Hancock, D., Shah, S., Hakes, L., Gray, T., Tiwari, B., Kille, P., Cossins, A., Hegarty, M., Allen, M.J., Wilson, W.H., Olive, P., Last, K., Kramer, C., Bailhache, T., Reeves, J., Pallett, D., Warne, J., Nashar, K., Parkinson, H., Sansone, S.-A., Rocca-Serra, P., Stevens, R., Snape, J., Brass, A., Field, D., 2006. Annotation of environmental OMICS data: application to the transcriptomics domain. OMICS 10, 172–178. https://doi.org/10.1089/omi.2006.10.172

Mosmann, T., 1983. Rapid colorimetric assay for cellular growth and survival: application to proliferation and cytotoxicity assays. J Immunol Methods 65, 55–63. https://doi.org/10.1016/0022-1759(83)90303-4

Munir, R., Semmar, N., Farman, M., Ahmad, N.S., 2017. An updated review on pharmacological activities and phytochemical constituents of evening primrose (genus Oenothera). Asian Pacific Journal of Tropical Biomedicine 7, 1046–1054. https://doi.org/10.1016/j.apjtb.2017.10.004

Murashige, T., Skoog, F., 1962. A Revised Medium for Rapid Growth and Bio Assays with Tobacco Tissue Cultures. Physiologia Plantarum 15, 473–497. https://doi.org/10.1111/j.1399-3054.1962.tb08052.x

Murray, K.K., Boyd, R.K., Eberlin, M.N., Langley, G.J., Li, L., Naito, Y., 2013. Definitions of terms relating to mass spectrometry (IUPAC Recommendations 2013). Pure and Applied Chemistry 85, 1515–1609. https://doi.org/10.1351/PAC-REC-06-04-06

Nagoor Meeran, M.F., Goyal, S.N., Suchal, K., Sharma, C., Patil, C.R., Ojha, S.K., 2018. Pharmacological Properties, Molecular Mechanisms, and Pharmaceutical Development of Asiatic Acid: A Pentacyclic Triterpenoid of Therapeutic Promise. Front Pharmacol 9, 892. https://doi.org/10.3389/fphar.2018.00892

Nandi, A.K., Ford, T., Fleksher, D., Neuman, B., Rapoport, A.P., 2007. Attenuation of DNA damage checkpoint by PBK, a novel mitotic kinase, involves protein-protein interaction with tumor suppressor p53. Biochem Biophys Res Commun 358, 181–188. https://doi.org/10.1016/j.bbrc.2007.04.125

Nemes, P., Marginean, I., Vertes, A., 2007. Spraying Mode Effect on Droplet Formation and Ion Chemistry in Electrosprays. Anal. Chem. 79, 3105–3116. https://doi.org/10.1021/ac062382i

Nothias, L.-F., Petras, D., Schmid, R., Dührkop, K., Rainer, J., Sarvepalli, A., Protsyuk, I., Ernst, M., Tsugawa, H., Fleischauer, M., Aicheler, F., Aksenov, A.A., Alka, O., Allard, P.-M., Barsch, A., Cachet, X., Caraballo-Rodriguez, A.M., Da Silva, R.R., Dang, T., Garg, N., Gauglitz, J.M., Gurevich, A., Isaac, G., Jarmusch, A.K., Kameník, Z., Kang, K.B., Kessler, N., Koester, I., Korf, A., Le Gouellec, A., Ludwig, M., Martin H., C., McCall, L.-I., McSayles, J.,

Meyer, S.W., Mohimani, H., Morsy, M., Moyne, O., Neumann, S., Neuweger, H., Nguyen, N.H., Nothias-Esposito, M., Paolini, J., Phelan, V.V., Pluskal, T., Quinn, R.A., Rogers, S., Shrestha, B., Tripathi, A., van der Hooft, J.J.J., Vargas, F., Weldon, K.C., Witting, M., Yang, H., Zhang, Z., Zubeil, F., Kohlbacher, O., Böcker, S., Alexandrov, T., Bandeira, N., Wang, M., Dorrestein, P.C., 2020. Feature-based molecular networking in the GNPS analysis environment. Nat Methods 17, 905–908. https://doi.org/10.1038/s41592-020-0933-6

Ochoa-Villarreal, M., Howat, S., Jang, M.O., Kim, I.S., Jin, Y.-W., Lee, E.-K., Loake, G.J., 2015. Cambial meristematic cells: a platform for the production of plant natural products. N Biotechnol 32, 581–587. https://doi.org/10.1016/j.nbt.2015.02.003

O'Farrell, P.H., 1975. High resolution two-dimensional electrophoresis of proteins. J Biol Chem 250, 4007–4021.

Olivon, F., Grelier, G., Roussi, F., Litaudon, M., Touboul, D., 2017. MZmine 2 Data-Preprocessing To Enhance Molecular Networking Reliability. Anal Chem 89, 7836–7840. https://doi.org/10.1021/acs.analchem.7b01563

Olsen, J.V., Godoy, L.M.F. de, Li, G., Macek, B., Mortensen, P., Pesch, R., Makarov, A., Lange, O., Horning, S., Mann, M., 2005. Parts per Million Mass Accuracy on an Orbitrap Mass Spectrometer via Lock Mass Injection into a C-trap. Molecular & Cellular Proteomics 4, 2010–2021. https://doi.org/10.1074/mcp.T500030-MCP200

Olsen, J.V., Macek, B., Lange, O., Makarov, A., Horning, S., Mann, M., 2007. Higher-energy C-trap dissociation for peptide modification analysis. Nat Methods 4, 709–712. https://doi.org/10.1038/nmeth1060

Olsen, J.V., Mann, M., 2004. Improved peptide identification in proteomics by two consecutive stages of mass spectrometric fragmentation. Proceedings of the National Academy of Sciences 101, 13417–13422. https://doi.org/10.1073/pnas.0405549101

Ong, S.-E., Blagoev, B., Kratchmarova, I., Kristensen, D.B., Steen, H., Pandey, A., Mann, M., 2002. Stable isotope labeling by amino acids in cell culture, SILAC, as a simple and accurate approach to expression proteomics. Mol Cell Proteomics 1, 376–386. https://doi.org/10.1074/mcp.m200025-mcp200

Ong, S.-E., Kratchmarova, I., Mann, M., 2003. Properties of 13C-substituted arginine in stable isotope labeling by amino acids in cell culture (SILAC). J Proteome Res 2, 173–181. https://doi.org/10.1021/pr0255708

Ong, S.-E., Mann, M., 2007. Stable isotope labeling by amino acids in cell culture for quantitative proteomics. Methods Mol Biol 359, 37–52. https://doi.org/10.1007/978-1-59745-255-7_3

Ong, S.-E., Mann, M., 2006. A practical recipe for stable isotope labeling by amino acids in cell culture (SILAC). Nat Protoc 1, 2650–2660. https://doi.org/10.1038/nprot.2006.427

Paez-Ribes, M., González-Gualda, E., Doherty, G.J., Muñoz-Espín, D., 2019. Targeting senescent cells in translational medicine. EMBO Mol Med 11, e10234. https://doi.org/10.15252/emmm.201810234

Pareek, C.S., Smoczynski, R., Tretyn, A., 2011. Sequencing technologies and genome sequencing. J Appl Genet 52, 413–435. https://doi.org/10.1007/s13353-011-0057-x

Partap, M., Warghat, A.R., Kumar, S., 2022. Cambial meristematic cell culture: a sustainable technology toward in vitro specialized metabolites production. Crit Rev Biotechnol 1–19. https://doi.org/10.1080/07388551.2022.2055995

Passos, J.F., von Zglinicki, T., 2007. Methods for cell sorting of young and senescent cells. Methods Mol Biol 371, 33–44. https://doi.org/10.1007/978-1-59745-361-5_4

Pei, W., Deng, J., Wang, P., Wang, X., Zheng, L., Zhang, Y., Huang, C., 2022. Sustainable lignin and lignin-derived compounds as potential therapeutic agents for degenerative orthopaedic diseases: A systemic review. International Journal of Biological Macromolecules 212, 547–560. https://doi.org/10.1016/j.ijbiomac.2022.05.152

Pendergrass, S.A., Dudek, S.M., Crawford, D.C., Ritchie, M.D., 2012. Visually integrating and exploring high throughput Phenome-Wide Association Study (PheWAS) results using PheWAS-View. BioData Min 5, 5. https://doi.org/10.1186/1756-0381-5-5

Peng, J., Xie, J., Shi, S., Luo, L., Li, K., Xiong, P., Cai, W., 2021. Diagnostic Fragment-Ion-Based for Rapid Identification of Chlorogenic Acids Derivatives in Inula cappa Using UHPLC-Q-Exactive Orbitrap Mass Spectrometry. J Anal Methods Chem 2021, 6393246. https://doi.org/10.1155/2021/6393246

Perez-Riverol, Y., Bai, J., Bandla, C., García-Seisdedos, D., Hewapathirana, S., Kamatchinathan, S., Kundu, D.J., Prakash, A., Frericks-Zipper, A., Eisenacher, M., Walzer, M., Wang, S., Brazma, A., Vizcaíno, J.A., 2021. The PRIDE database resources in 2022: a hub for mass spectrometry-based proteomics evidences. Nucleic Acids Res 50, D543–D552. https://doi.org/10.1093/nar/gkab1038

Perrone, A., Giovino, A., Benny, J., Martinelli, F., 2020. Advanced Glycation End Products (AGEs): Biochemistry, Signaling, Analytical Methods, and Epigenetic Effects. Oxid Med Cell Longev 2020, 3818196. https://doi.org/10.1155/2020/3818196

Perry, R.H., Cooks, R.G., Noll, R.J., 2008. Orbitrap mass spectrometry: Instrumentation, ion motion and applications. Mass Spectrometry Reviews 27, 661–699. https://doi.org/10.1002/mas.20186

Pirih, N., Kunej, T., 2018. An Updated Taxonomy and a Graphical Summary Tool for Optimal Classification and Comprehension of Omics Research. OMICS 22, 337–353. https://doi.org/10.1089/omi.2017.0186

Pirih, N., Kunej, T., 2017. Toward a Taxonomy for Multi-Omics Science? Terminology Development for Whole Genome Study Approaches by Omics Technology and Hierarchy. OMICS 21, 1–16. https://doi.org/10.1089/omi.2016.0144

Pluskal, T., Castillo, S., Villar-Briones, A., Orešič, M., 2010. MZmine 2: Modular framework for processing, visualizing, and analyzing mass spectrometry-based molecular profile data. BMC Bioinformatics 11, 395. https://doi.org/10.1186/1471-2105-11-395

Prockop, D.J., 1985. Mutations in collagen genes. Consequences for rare and common diseases. J. Clin. Invest. 75, 783–787. https://doi.org/10.1172/JCI111773

Qian, J., Beullens, M., Huang, J., De Munter, S., Lesage, B., Bollen, M., 2015. Cdk1 orders mitotic events through coordination of a chromosome-associated phosphatase switch. Nat Commun 6, 10215. https://doi.org/10.1038/ncomms10215

Qin, Z., Fisher, G.J., Voorhees, J.J., Quan, T., 2018. Actin cytoskeleton assembly regulates collagen production via TGF-β type II receptor in human skin fibroblasts. J Cell Mol Med 22, 4085–4096. https://doi.org/10.1111/jcmm.13685

Quan, T., Wang, F., Shao, Y., Rittié, L., Xia, W., Orringer, J.S., Voorhees, J.J., Fisher, G.J., 2013. Enhancing structural support of the dermal microenvironment activates fibroblasts, endothelial cells and keratinocytes in aged human skin in vivo. J Invest Dermatol 133, 658–667. https://doi.org/10.1038/jid.2012.364

Quéméner, B., Ralet, M.-C., 2004. Evidence for linkage position determination in known feruloylated mono- and disaccharides using electrospray ion trap mass spectrometry. J Mass Spectrom 39, 1153–1160. https://doi.org/10.1002/jms.698

Ramos, A.E.F., Evanno, L., Poupon, E., Champy, P., Beniddir, M.A., 2019. Natural products targeting strategies involving molecular networking: different manners, one goal. Nat. Prod. Rep. 36, 960–980. https://doi.org/10.1039/C9NP00006B

Rayleigh, Lord, 1882. XX. On the equilibrium of liquid conducting masses charged with electricity. The London, Edinburgh, and Dublin Philosophical Magazine and Journal of Science 14, 184–186. https://doi.org/10.1080/14786448208628425

Reiser, K.M., 1998. Nonenzymatic glycation of collagen in aging and diabetes. Proc Soc Exp Biol Med 218, 23–37. https://doi.org/10.3181/00379727-218-44264

Rinnerthaler, M., Bischof, J., Streubel, M.K., Trost, A., Richter, K., 2015. Oxidative Stress in Aging Human Skin. Biomolecules 5, 545–589. https://doi.org/10.3390/biom5020545

Rix, U., Superti-Furga, G., 2009. Target profiling of small molecules by chemical proteomics. Nat Chem Biol 5, 616–624. https://doi.org/10.1038/nchembio.216

Ross, P.L., Huang, Y.N., Marchese, J.N., Williamson, B., Parker, K., Hattan, S., Khainovski, N., Pillai, S., Dey, S., Daniels, S., Purkayastha, S., Juhasz, P., Martin, S., Bartlet-Jones, M., He, F., Jacobson, A., Pappin, D.J., 2004. Multiplexed protein quantitation in Saccharomyces cerevisiae using amine-reactive isobaric tagging reagents. Mol Cell Proteomics 3, 1154–1169. https://doi.org/10.1074/mcp.M400129-MCP200

Rudd, P., Karlsson, N.G., Khoo, K.-H., Packer, N.H., 2015. Glycomics and Glycoproteomics, in: Varki, A., Cummings, R.D., Esko, J.D., Stanley, P., Hart, G.W., Aebi, M., Darvill, A.G., Kinoshita, T., Packer, N.H., Prestegard, J.H., Schnaar, R.L., Seeberger, P.H. (Eds.), Essentials of Glycobiology. Cold Spring Harbor Laboratory Press, Cold Spring Harbor (NY).

Samsonowicz, M., Kalinowska, M., Gryko, K., 2021. Enhanced Antioxidant Activity of Ursolic Acid by Complexation with Copper (II): Experimental and Theoretical Study. Materials (Basel) 14, E264. https://doi.org/10.3390/ma14020264

Santiago, L., Dayrit, K., Correa, P., Mayor, A.B., 2014. Comparison of antioxidant and free radical scavenging activity of triterpenes α-amyrin, oleanolic acid and ursolic acid. J Nat Prod 7, 29–36.

Sárdy, M., 2009. Role of matrix metalloproteinases in skin ageing. Connect Tissue Res 50, 132–138. https://doi.org/10.1080/03008200802585622

Schäfer, L., Kragballe, K., 1991. Supplementation with evening primrose oil in atopic dermatitis: effect on fatty acids in neutrophils and epidermis. Lipids 26, 557–560. https://doi.org/10.1007/BF02536604

Scholzen, T., Gerdes, J., 2000. The Ki-67 protein: from the known and the unknown. J Cell Physiol 182, 311–322. https://doi.org/10.1002/(SICI)1097-4652(200003)182:3<311::AID-JCP1>3.0.CO;2-9

Scigelova, M., Makarov, A., 2006. Orbitrap Mass Analyzer – Overview and Applications in Proteomics. PROTEOMICS 6, 16–21. https://doi.org/10.1002/pmic.200600528

Selby, D.S., Mlynski, V., Guilhaus, M., 2001. A 20 kV orthogonal acceleration time-of-flight mass spectrometer for matrix-assisted laser desorption/ionization11Dedicated to Professor Nico Nibbering on the occasion of his retirement. International Journal of Mass Spectrometry 210–211, 89–100. https://doi.org/10.1016/S1387-3806(01)00438-9

Shannon, P., Markiel, A., Ozier, O., Baliga, N.S., Wang, J.T., Ramage, D., Amin, N., Schwikowski, B., Ideker, T., 2003. Cytoscape: a software environment for integrated models of biomolecular interaction networks. Genome Res 13, 2498–2504. https://doi.org/10.1101/gr.1239303

Shevchenko, A., Tomas, H., Havli, J., Olsen, J.V., Mann, M., 2006. In-gel digestion for mass spectrometric characterization of proteins and proteomes. Nat Protoc 1, 2856–2860. https://doi.org/10.1038/nprot.2006.468

Shiio, Y., Aebersold, R., 2006. Quantitative proteome analysis using isotope-coded affinity tags and mass spectrometry. Nat Protoc 1, 139–145. https://doi.org/10.1038/nprot.2006.22

Sikora, E., Bielak-Żmijewska, A., Mosieniak, G., 2018. What is and what is not cell senescence. Postepy Biochem 64, 110–118. https://doi.org/10.18388/pb.2018_120

Singh, V.P., Bali, A., Singh, N., Jaggi, A.S., 2014. Advanced Glycation End Products and Diabetic Complications. Korean J Physiol Pharmacol 18, 1–14. https://doi.org/10.4196/kjpp.2014.18.1.1

Smith, R.D., Loo, J.A., Edmonds, C.G., Barinaga, C.J., Udseth, H.R., 1990. New developments in biochemical mass spectrometry: electrospray ionization. Anal. Chem. 62, 882–899. https://doi.org/10.1021/ac00208a002

Soto-Gamez, A., Demaria, M., 2017. Therapeutic interventions for aging: the case of cellular senescence. Drug Discov Today 22, 786–795. https://doi.org/10.1016/j.drudis.2017.01.004

Syka, J.E.P., Coon, J.J., Schroeder, M.J., Shabanowitz, J., Hunt, D.F., 2004. Peptide and protein sequence analysis by electron transfer dissociation mass spectrometry. Proc Natl Acad Sci U S A 101, 9528–9533. https://doi.org/10.1073/pnas.0402700101

Tang, W., Bhushan, B., Ge, S., 2010. Friction, adhesion and durability and influence of humidity on adhesion and surface charging of skin and various skin creams using atomic force microscopy. J Microsc 239, 99–116. https://doi.org/10.1111/j.1365-2818.2009.03362.x

Taouatas, N., Altelaar, A.F.M., Drugan, M.M., Helbig, A.O., Mohammed, S., Heck, A.J.R., 2009. Strong cation exchange-based fractionation of Lys-N-generated peptides facilitates the targeted analysis of post-translational modifications. Mol Cell Proteomics 8, 190–200. https://doi.org/10.1074/mcp.M800285-MCP200

Taylor, G.I., 1964. Disintegration of water drops in an electric field. Proceedings of the Royal Society of London. Series A. Mathematical and Physical Sciences 280, 383–397. https://doi.org/10.1098/rspa.1964.0151

Thomas, G., Burnham, N.A., Camesano, T.A., Wen, Q., 2013. Measuring the mechanical properties of living cells using atomic force microscopy. J Vis Exp 50497. https://doi.org/10.3791/50497

Thomas, S.N., 2019. Chapter 10 - Mass spectrometry, in: Clarke, W., Marzinke, M.A. (Eds.), Contemporary Practice in Clinical Chemistry (Fourth Edition). Academic Press, pp. 171–185. https://doi.org/10.1016/B978-0-12-815499-1.00010-7

Thompson, A., Schäfer, J., Kuhn, K., Kienle, S., Schwarz, J., Schmidt, G., Neumann, T., Hamon, C., 2003. Tandem Mass Tags: A Novel Quantification Strategy for Comparative Analysis of Complex Protein Mixtures by MS/MS. Anal. Chem. 75, 1895–1904. https://doi.org/10.1021/ac0262560

Thomson, B.A., Iribarne, J.V., 1979. Field induced ion evaporation from liquid surfaces at atmospheric pressure. J. Chem. Phys. 71, 4451–4463. https://doi.org/10.1063/1.438198

Timms, J.F., Cramer, R., 2008. Difference gel electrophoresis. Proteomics 8, 4886–4897. https://doi.org/10.1002/pmic.200800298

Timoszuk, M., Bielawska, K., Skrzydlewska, E., 2018. Evening Primrose (Oenothera biennis) Biological Activity Dependent on Chemical Composition. Antioxidants (Basel) 7, E108. https://doi.org/10.3390/antiox7080108

Tonelli, C., Chio, I.I.C., Tuveson, D.A., 2018. Transcriptional Regulation by Nrf2. Antioxid Redox Signal 29, 1727–1745. https://doi.org/10.1089/ars.2017.7342

Toppo, A., n.d. A review on Jasminum sambac: A potential medicinal plant. Int J Ind Herbs Drugs 2017; 2(5): 13-16. A review on Jasminum sambac: A potential medicinal plant.

Touré, A., Xueming, X., 2010. Flaxseed Lignans: Source, Biosynthesis, Metabolism, Antioxidant Activity, Bio-Active Components, and Health Benefits. Compr Rev Food Sci Food Saf 9, 261–269. https://doi.org/10.1111/j.1541-4337.2009.00105.x

Tran, J.C., Zamdborg, L., Ahlf, D.R., Lee, J.E., Catherman, A.D., Durbin, K.R., Tipton, J.D., Vellaichamy, A., Kellie, J.F., Li, M., Wu, C., Sweet, S.M.M., Early, B.P., Siuti, N., LeDuc, R.D., Compton, P.D., Thomas, P.M., Kelleher, N.L., 2011. Mapping intact protein isoforms in discovery mode using top-down proteomics. Nature 480, 254–258. https://doi.org/10.1038/nature10575

Tu, W., Wang, H., Li, S., Liu, Q., Sha, H., 2019. The Anti-Inflammatory and Anti-Oxidant Mechanisms of the Keap1/Nrf2/ARE Signaling Pathway in Chronic Diseases. Aging Dis 10, 637–651. https://doi.org/10.14336/AD.2018.0513

Twarda-Clapa, A., Olczak, A., Białkowska, A.M., Koziołkiewicz, M., 2022. Advanced Glycation End-Products (AGEs): Formation, Chemistry, Classification, Receptors, and Diseases Related to AGEs. Cells 11, 1312. https://doi.org/10.3390/cells11081312

Tyanova, S., Temu, T., Cox, J., 2016a. The MaxQuant computational platform for mass spectrometry-based shotgun proteomics. Nat Protoc 11, 2301–2319. https://doi.org/10.1038/nprot.2016.136

Tyanova, S., Temu, T., Sinitcyn, P., Carlson, A., Hein, M.Y., Geiger, T., Mann, M., Cox, J., 2016b. The Perseus computational platform for comprehensive analysis of (prote)omics data. Nat Methods 13, 731–740. https://doi.org/10.1038/nmeth.3901

Tyers, M., Mann, M., 2003. From genomics to proteomics. Nature 422, 193–197. https://doi.org/10.1038/nature01510

Verrecchia, F., Mauviel, A., 2002. Transforming growth factor-beta signaling through the Smad pathway: role in extracellular matrix gene expression and regulation. J Invest Dermatol 118, 211–215. https://doi.org/10.1046/j.1523-1747.2002.01641.x

Verzijl, N., DeGroot, J., Oldehinkel, E., Bank, R.A., Thorpe, S.R., Baynes, J.W., Bayliss, M.T., Bijlsma, J.W., Lafeber, F.P., Tekoppele, J.M., 2000. Age-related accumulation of Maillard reaction products in human articular cartilage collagen. Biochem J 350 Pt 2, 381–387.

Viswanathan, S., Unlü, M., Minden, J.S., 2006. Two-dimensional difference gel electrophoresis. Nat Protoc 1, 1351–1358. https://doi.org/10.1038/nprot.2006.234

Vollmer, M., Hörth, P., Nägele, E., 2004. Optimization of two-dimensional off-line LC/MS separations to improve resolution of complex proteomic samples. Anal Chem 76, 5180–5185. https://doi.org/10.1021/ac040022u

Wang, A.S., Dreesen, O., 2018. Biomarkers of Cellular Senescence and Skin Aging. Frontiers in Genetics 9.

Wang, D., Lu, P., Liu, Y., Chen, L., Zhang, R., Sui, W., Dumitru, A.G., Chen, X., Wen, F., Ouyang, H.-W., Ji, J., 2016. Isolation of Live Premature Senescent Cells Using FUCCI Technology. Sci Rep 6, 30705. https://doi.org/10.1038/srep30705

Wang, H., Sun, S., Zhang, Y., Chen, S., Liu, P., Liu, B., 2015. An off-line high pH reversed-phase fractionation and nano-liquid chromatography-mass spectrometry method for global proteomic profiling of cell lines. J Chromatogr B Analyt Technol Biomed Life Sci 974, 90–95. https://doi.org/10.1016/j.jchromb.2014.10.031

Wang, L., Pan, X., Jiang, L., Chu, Y., Gao, S., Jiang, X., Zhang, Y., Chen, Y., Luo, S., Peng, C., 2022. The Biological Activity Mechanism of Chlorogenic Acid and Its Applications in Food Industry: A Review. Frontiers in Nutrition 9.

Wang, M., Carver, J.J., Phelan, V.V., Sanchez, L.M., Garg, N., Peng, Y., Nguyen, D.D., Watrous, J., Kapono, C.A., Luzzatto-Knaan, T., Porto, C., Bouslimani, A., Melnik, A.V., Meehan, M.J., Liu, W.-T., Crüsemann, M., Boudreau, P.D., Esquenazi, E., Sandoval-Calderón, M., Kersten, R.D., Pace, L.A., Quinn, R.A., Duncan, K.R., Hsu, C.-C., Floros, D.J., Gavilan, R.G., Kleigrewe, K., Northen, T., Dutton, R.J., Parrot, D., Carlson, E.E., Aigle, B., Michelsen, C.F., Jelsbak, L., Sohlenkamp, C., Pevzner, P., Edlund, A., McLean, J., Piel, J., Murphy, B.T., Gerwick, L., Liaw, C.-C., Yang, Y.-L., Humpf, H.-U., Maansson, M., Keyzers, R.A., Sims, A.C., Johnson, A.R., Sidebottom, A.M., Sedio, B.E., Klitgaard, A., Larson, C.B., P., C.A.B., Torres-Mendoza, D., Gonzalez, D.J., Silva, D.B., Marques, L.M., Demarque, D.P., Pociute, E., O'Neill, E.C., Briand, E., Helfrich, E.J.N., Granatosky, E.A., Glukhov, E., Ryffel, F., Houson, H., Mohimani, H., Kharbush, J.J., Zeng, Y., Vorholt, J.A., Kurita, K.L., Charusanti, P., McPhail, K.L., Nielsen, K.F., Vuong, L., Elfeki, M., Traxler, M.F., Engene, N., Koyama, N., Vining, O.B., Baric, R., Silva, R.R., Mascuch, S.J., Tomasi, S., Jenkins, S., Macherla, V., Hoffman, T., Agarwal, V., Williams, P.G., Dai, J., Neupane, R., Gurr, J., Rodríguez, A.M.C., Lamsa, A., Zhang, C., Dorrestein, K., Duggan, B.M., Almaliti, J., Allard, P.-M., Phapale, P., Nothias, L.-F., Alexandrov, T., Litaudon, M., Wolfender, J.-L., Kyle, J.E., Metz, T.O., Peryea, T., Nguyen, D.-T., VanLeer, D., Shinn, P., Jadhav, A., Müller, R., Waters, K.M., Shi, W., Liu, X., Zhang, L., Knight, R., Jensen, P.R., Palsson, B.O., Pogliano, K., Linington, R.G., Gutiérrez, M.,

Lopes, N.P., Gerwick, W.H., Moore, B.S., Dorrestein, P.C., Bandeira, N., 2016. Sharing and community curation of mass spectrometry data with GNPS. Nat Biotechnol 34, 828–837. https://doi.org/10.1038/nbt.3597

Wang, Z., Wei, D., Xiao, H., 2013. Methods of cellular senescence induction using oxidative stress. Methods Mol Biol 1048, 135–144. https://doi.org/10.1007/978-1-62703-556-9_11

Washburn, M.P., Wolters, D., Yates, J.R., 2001. Large-scale analysis of the yeast proteome by multidimensional protein identification technology. Nat Biotechnol 19, 242–247. https://doi.org/10.1038/85686

Wilkins, M.R., Sanchez, J.-C., Gooley, A.A., Appel, R.D., Humphery-Smith, I., Hochstrasser, D.F., Williams, K.L., 1996. Progress with Proteome Projects: Why all Proteins Expressed by a Genome Should be Identified and How To Do It. Biotechnology and Genetic Engineering Reviews 13, 19–50. https://doi.org/10.1080/02648725.1996.10647923

Wilm, M., Mann, M., 1996. Analytical properties of the nanoelectrospray ion source. Anal Chem 68, 1–8. https://doi.org/10.1021/ac9509519

Wilm, M.S., Mann, M., 1994. Electrospray and Taylor-Cone theory, Dole's beam of macromolecules at last? International Journal of Mass Spectrometry and Ion Processes 136, 167–180. https://doi.org/10.1016/0168-1176(94)04024-9

Wlaschek, M., Maity, P., Makrantonaki, E., Scharffetter-Kochanek, K., 2021. Connective Tissue and Fibroblast Senescence in Skin Aging. J Invest Dermatol 141, 985–992. https://doi.org/10.1016/j.jid.2020.11.010

Xu, J.-G., Hu, Q.-P., Liu, Y., 2012. Antioxidant and DNA-Protective Activities of Chlorogenic Acid Isomers. J. Agric. Food Chem. 60, 11625–11630. https://doi.org/10.1021/jf303771s

Yates, J.R., Ruse, C.I., Nakorchevsky, A., 2009. Proteomics by mass spectrometry: approaches, advances, and applications. Annu Rev Biomed Eng 11, 49–79. https://doi.org/10.1146/annurev-bioeng-061008-124934

Yuan, Y., Verma, R., 2006. Measuring microelastic properties of stratum corneum. Colloids Surf B Biointerfaces 48, 6–12. https://doi.org/10.1016/j.colsurfb.2005.12.013

Zeleny, J., 1917. Instability of Electrified Liquid Surfaces. Phys. Rev. 10, 1–6. https://doi.org/10.1103/PhysRev.10.1

Zhang, J., Wang, Y., Li, S., 2010. Deuterium isobaric amine-reactive tags for quantitative proteomics. Anal Chem 82, 7588–7595. https://doi.org/10.1021/ac101306x

Zhang, R., Chen, W., Adams, P.D., 2007. Molecular Dissection of Formation of Senescence-Associated Heterochromatin Foci. Mol Cell Biol 27, 2343–2358. https://doi.org/10.1128/MCB.02019-06

Zhang, T., Cooper, S., Brockdorff, N., 2015. The interplay of histone modifications - writers that read. EMBO Rep 16, 1467–1481. https://doi.org/10.15252/embr.201540945

Zhou, X., Ren, L., Meng, Q., Li, Y., Yu, Y., Yu, J., 2010. The next-generation sequencing technology and application. Protein Cell 1, 520–536. https://doi.org/10.1007/s13238-010-0065-3